AD-A073 371 ARMY ENGINEER WATERWAYS EXPERIMENT STATION VICKSBURG MS F/G 13/2
PROPERTIES OF STEADY, VISCOSITY-STRATIFIED FLOW TO A LINE SINK.(U)
JUL 79 T M WALSKI

UNCLASSIFIED WES-TR-EL-79-6 NL

1 OF 3
AD
A073371

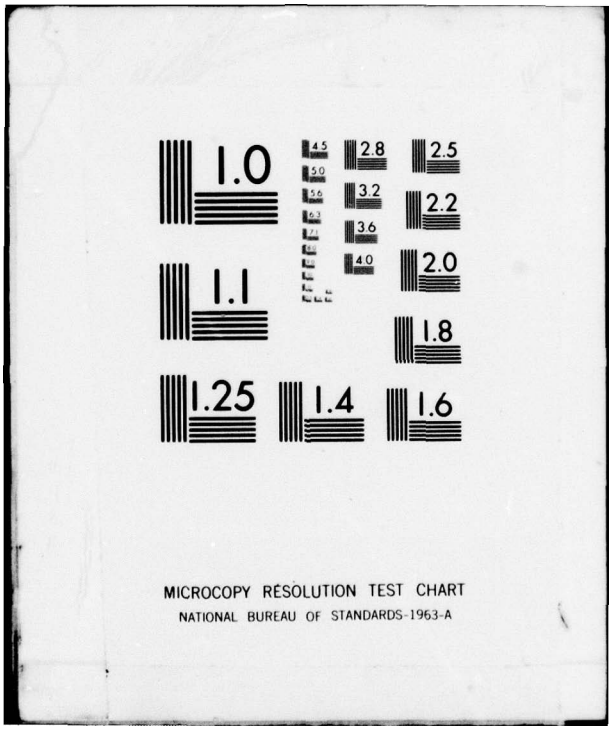
1.0
1.1
1.25
1.4
1.6
1.8
2.0
2.2
2.5
2.8
3.2
3.6
4.0
4.5
5.0
5.6
6.3
MICROCOPY RESOLUTION TEST CHART
NATIONAL BUREAU OF STANDARDS-1963-A

LEVEL II

TECHNICAL REPORT EL-79-6

PROPERTIES OF STEADY VISCOSITY-STRATIFIED FLOW TO A LINE SINK

by

Thomas M. Walski

Environmental Laboratory
U. S. Army Engineer Waterways Experiment Station
P. O. Box 631, Vicksburg, Miss. 39180

July 1979

Final Report

Prepared for Assistant Secretary of the Army (R&D)
Department of the Army
Washington, D. C. 20310

Under Project No. 4A161101A91D, Task 02, Work Unit 112

Destroy this report when no longer needed. Do not return it to the originator.

The findings in this report are not to be construed as an official Department of the Army position unless so designated by other authorized documents.

The contents of this report are not to be used for advertising, publication, or promotional purposes. Citation of trade names does not constitute an official endorsement or approval of the use of such commercial products.

(14) WES-TR-EL-79-6

Unclassified

SECURITY CLASSIFICATION OF THIS PAGE (When Data Entered)

REPORT DOCUMENTATION PAGE

READ INSTRUCTIONS BEFORE COMPLETING FORM

1. REPORT NUMBER: Technical Report EL-79-6
2. GOVT ACCESSION NO.
3. RECIPIENT'S CATALOG NUMBER
4. TITLE (and Subtitle): (6) PROPERTIES OF STEADY, VISCOSITY-STRATIFIED FLOW TO A LINE SINK
5. TYPE OF REPORT & PERIOD COVERED: (9) Final report
6. PERFORMING ORG. REPORT NUMBER
7. AUTHOR(s): (10) Thomas M. Walski
8. CONTRACT OR GRANT NUMBER(s): (16)
9. PERFORMING ORGANIZATION NAME AND ADDRESS:
U. S. Army Engineer Waterways Experiment Station
Environmental Laboratory
P. O. Box 631, Vicksburg, Miss. 39180
10. PROGRAM ELEMENT, PROJECT, TASK AREA & WORK UNIT NUMBERS:
Project No. 4A161101A91D
Task 02, Work Unit 112
11. CONTROLLING OFFICE NAME AND ADDRESS:
Assistant Secretary of the Army (R&D)
Department of the Army
Washington, D. C. 20310
12. REPORT DATE: (11) July 1979
13. NUMBER OF PAGES: 211 (12) 215 p.
14. MONITORING AGENCY NAME & ADDRESS (if different from Controlling Office)
15. SECURITY CLASS. (of this report): Unclassified
15a. DECLASSIFICATION/DOWNGRADING SCHEDULE

16. DISTRIBUTION STATEMENT (of this Report)

Approved for public release; distribution unlimited.

17. DISTRIBUTION STATEMENT (of the abstract entered in Block 20, if different from Report)

18. SUPPLEMENTARY NOTES

19. KEY WORDS (Continue on reverse side if necessary and identify by block number)

Bingham plastic	Stratification	Weirs
Mathematical models	Stratified flow	
Rheology	Viscosity	
Selective withdrawal	Viscous flow	

20. ABSTRACT (Continue on reverse side if necessary and identify by block number)

Viscosity stratification (variation of the viscosity of a fluid with depth) can significantly modify the velocity profiles observed in a fluid being selectively withdrawn from a tank or duct. A mathematical model is developed to predict velocity distribution for steady, Newtonian, slow, laminar, two-dimensional, viscosity-stratified flow to a line sink.

The mathematical model was verified in experiments conducted in three → over

(Continued)

DD FORM 1 JAN 73 1473 EDITION OF 1 NOV 65 IS OBSOLETE

Unclassified

SECURITY CLASSIFICATION OF THIS PAGE (When Data Entered)

20. ABSTRACT (Continued).

flumes using sugar and carboxymethylcellulose to create density and viscosity gradients. Viscosity stratification caused the velocity profile to become skewed in the direction of lower viscosity.

Criteria are presented to determine when velocity profiles are skewed. Existence of skewness depends on three dimensionless parameters: dimensionless viscosity gradient (A or C); ratio of buoyancy to viscous forces (B); and dimensionless distance from sink (X).

The results of the verified model are extended to (a) viscosity-stratified flow over a weir, and (b) flow of a Bingham plastic in which yield stress varies with depth.

PREFACE

The investigation reported herein was conducted under the Department of the Army Project No. 4A161101A91D, In-House Laboratory Independent Research Program (ILIR), sponsored by the Assistant Secretary of the Army (R&D). This investigation was conducted by the U. S. Army Engineer Waterways Experiment Station (WES) in the Environmental Laboratory (EL). The work unit was initiated to provide theoretical background for empirical techniques developed by the author to describe selective withdrawal from dredged material containment areas. This report also served as the doctoral dissertation for the author.

The investigation was performed during the period October 1977 to October 1978 under the general supervision of Dr. John Harrison, Chief, EL, and the direct supervision of Mr. Andrew J. Green, Chief, Environmental Engineering Division (EED), and Dr. Raymond L. Montgomery, Chief, Water Resources Engineering Group (WREG). Dr. Thomas M. Walski, WREG, was the principal investigator and author of this report.

Support in conducting the experiments, reducing data, and preparing the final report was provided by Mr. Donald F. Hayes, Mrs. Cheryl M. Lloyd, Mrs. Patricia B. Hopkins, Mr. Anthony C. Gibson, Mr. E. Keith Ford, Mrs. Jean M. Bishop, Mr. David E. Niederhauser, Mr. Robert J. Wills, and Mr. J. Donald LaGrone of the WREG. Mr. D. B. Larr, Mr. Vessen Magee, and Mr. Thomas L. Guynes, Jr., of the Publications and Graphic Arts Division photographed the experiments.

Many other individuals provided guidance and support on this work unit from its conception to completion of the final report. Most notable among these was Dr. Montgomery.

Commander and Director of WES during the conduct of the study and the preparation of this report was COL John L. Cannon, CE. Technical Director was Mr. F. R. Brown.

CONTENTS

LIST OF TABLES

LIST OF ILLUSTRATIONS

CONVERSION FACTORS, NONSTANDARD METRIC TO SI UNITS OF MEASUREMENT

Nonstandard metric units of measurement used in this report can be converted to SI units as follows:

Multiply	By	To Obtain
centimetres	0.01	metres
square centimetres per second	0.000001	square metres per second
cubic centimetres	0.000001	cubic metres
tonne	1000.	kilogram
grams per litre	1.	kilograms per cubic metre
grams per cubic centimetre	1000.	kilograms per cubic metre
cubic centimetres per gram	0.001	cubic metre per kilogram
dyne per square centimetre	0.1	pascal
dyne-centimetre	0.0000001	newton-metre
dynes-second per square centimetres	0.1	pascal-second
centipoise	0.001	pascal-second
poise	0.1	pascal-second
micromhos per centimetre	0.0001	siemens per metre

PROPERTIES OF STEADY, VISCOSITY-STRATIFIED FLOW TO A LINE SINK

CHAPTER I

INTRODUCTION

Background

A fluid in which the viscosity varies in the vertical direction is defined as being "viscosity stratified." The effects of viscosity stratification are investigated in this report using a two-dimensional, non-diffuse, laminar flow mathematical model which was developed for low Reynolds numbers.

Flows in which density stratification exist have been of considerable engineering interest. Examples of these flows include selective withdrawal from reservoirs, density currents in reservoirs, and salt wedges in estuaries. In these instances, the variation in viscosity of the fluid has been ignored in mathematically modeling the flow of the fluid to a sink with negligible error.

In some fluids large variations of the rheological properties of the fluid with depth can exist. Walski and Schroeder (1978), in attempting to model the behavior of dredged material flowing over a weir at a dredged material containment area, speculated that some of the differences between observed and predicted velocity profiles were due to the increased viscosity in the lower layers of material in the containment area. The ability to better describe the behavior of fluids which are viscosity stratified could result in more efficient

design of weirs at these containment areas or in any separation process in which viscosity gradients exist.

The problem is complicated by the fact that viscosity gradients are usually accompanied by density gradients. The literature does not contain solutions of the equations of motion for two-dimensional flow to a sink with both viscosity and density gradients existing. There are no criteria to predict when viscosity stratification affects velocity profiles, nor has the magnitude of these effects been quantified.

Objectives

The objectives of this study are to experimentally determine the magnitude of the effect of viscosity stratification on two-dimensional flow to a line sink and to develop a technique for mathematically modeling such flow. (Note that in the above objective a weir is considered a special case of a line sink, i.e., surface sink.) This study develops not only criteria for predicting when viscosity stratification is significant but also for predicting the velocity profiles in those cases.

Overview of Report

In order to adequately cover this topic, a fairly lengthy report is necessary. The chapters have been written so that they may be read individually. The only exceptions to this are that Chapter III (Basic Equations and Concepts) is a prerequisite for Chapters IV, VI,

VII, VIII, and IX, and Chapter V is similarly a prerequisite for Chapters VI through IX.

The literature review outlines state-of-the-art at the time this study was done. Chapter III, Basic Equations and Concepts, begins with a list of assumptions used in the mathematical model development. The horizontal and vertical momentum equations, continuity equation, and species continuity equation are then simplified and nondimensionalized to yield the equations to be solved in later parts of the report. The boundary conditions and numerical techniques used are also discussed.

One-dimensional models are developed in Chapter IV for a variety of viscosity gradients and boundary conditions to illustrate the effect of viscosity stratification. Skewness of velocity profiles is defined as an indicator of the effect of viscosity stratification on velocity profiles in Chapter V.

Chapter VI, Linear Viscosity Gradients Neglecting Buoyancy Forces, contains solutions to the equations developed in Chapter III first considering only viscous forces, then, later inertial forces. The equations are first solved for duct boundary conditions, then for boundary conditions corresponding to a fixed upstream wall.

In Chapter VII, Model for a Linear Gradient with Buoyancy Forces, the equations are solved with the buoyancy force term included. Criteria for the existence of viscosity stratification are developed. Chapter VIII addresses the same problem as the previous chapter except that the viscosity gradient increases logarithmically with depth. The concept of "incipient skewness" is introduced to describe cases in which buoyancy forces predominate near the top of the fluid while

viscous forces predominate below.

Chapter IX contains a discussion of the effect of some of the simplifications made on the previous solutions. These include the effects of the uniform upstream velocity assumption, the fixed back wall, and neglecting inertial forces.

Laboratory procedures are presented in Chapter X, including a discussion of equipment, fluids, and procedures. Experiment results are then presented in Chapter XI. First, data for the runs are given. This is followed by a discussion of the agreement between the mathematical model and experimental results and an analysis of errors.

In Chapter XII, the model is then applied to weirs. The effect of viscosity stratification on concentrations of a fluid flowing over a weir is discussed.

The properties of non-Newtonian flow, in particular a Bingham plastic with yield stress increasing with depth, are presented in Chapter XIII. The implications of this on design are discussed for yield stress increasing linearly and logarithmically with depth.

CHAPTER II

LITERATURE REVIEW

Existing literature in several areas of fluid mechanics was surveyed to locate solutions to the problems of selective withdrawal from a line sink in a two-dimensional, continuously stratified fluid with varying viscosity. While no papers could be found which directly addressed the problem, a large number were available on areas closely related to the problem. These papers are grouped into the eight categories presented below.

General Reviews

One of the earliest reviews on stratified flow through the late 1950's was prepared by Harleman (1961). The selective withdrawal work at this time was limited generally to two-layer systems.

Yih (1965, 1967, 1970) published a number of works on stratified flow. In general, Yih's work on selective withdrawal is limited to the inviscid flows with a linear density gradient far upstream.

Brooks and Koh (1968) presented an excellent overview of the state-of-the-art of selective withdrawal models in the late 1960's. They dealt chiefly with reservoir stratification, and did not consider variations in viscosity.

Turner's (1973) text, Buoyancy Effects in Fluids, does not dwell on the subject of selective withdrawal, but it does include a

discussion of the differences between solutions ignoring diffusion, which rely on the Richardson and Reynolds number, and those that account for diffusion, which rely on a Rayleigh number.

Early Research

Most early research on stratified fluids was concerned with the problem of stability, e.g., Taylor (1931). When viscosity was considered as in Keulegan (1949), it was treated as being constant.

The problem of selective withdrawal was first approached by Gariel (1949) and Craya (1949). Craya pointed out that viscous forces will predominate as one moves away from the sink. Gariel was first to show the shape of the velocity profile in this zone.

Harleman, Gooch, and Ippen (1958) studied withdrawal from a sluice gate and found the withdrawal layer thickness to be dependent on the densimetric Froude number. Harleman, Morgan, and Purple (1959) then extended this work to different types of withdrawal structures.

Huber (1960) produced a solution for a two-layer fluid flowing through a line sink using a relaxation technique and found the flow to be governed by the densimetric Froude number.

Martin and Schuster (1956) produced the first study of stratified flow over a weir. They were the first to speculate: "The effect of increasing viscosity with depth, although not a predominant factor of withdrawal, would be to lessen the contribution of the lower strata to the total outflow." They modeled thermal stratification with salt solutions. They speculated on using glycerol to model the viscosity but abandoned the idea since they could not achieve the

desired density and viscosity gradients simultaneously. They therefore ignored viscosity in the analysis.

Schlag (1965) did the most thorough study of two-layer flow over a weir. He was first to study the case in which the weir did not extend completely across the channel. He produced a set of nomograms to determine withdrawal depth.

The above studies were concerned primarily with predicting the thickness of the withdrawal layer. No attempt was made to predict velocity profiles except to indicate average velocity in each layer of a two-layer fluid.

Empirical Studies

In a series of studies produced at the U. S. Army Engineer Waterways Experiment Station (WES), Grace (1971) and Bohan and Grace (1973) produced an empirical model which predicted both depth of withdrawal layer and velocity profiles for flow over sharp- and broad-crested weirs. The model has been tested for a wide range of cases both in the laboratory and, to a lesser extent, in the field.

The model was later used to model turbidity in an impoundment by Fontane, Bohan, and Grace (1973). This application did not consider the effect of turbidity on viscosity, and the model does not account for the effect of viscosity on the velocity profile.

Johnson (1974) produced a model very similar to that of Bohan and Grace. It also neglected viscous forces.

Walski and Schroeder (1978) applied the WES selective withdrawal to flow over a weir in a dredged material containment area. They found

the model after some empirical corrections could describe the observed velocity profiles measured at several containment areas. They speculated that the corrections to the model were due to the fact that the suspended solids did not only create a density gradient but a significant viscosity gradient.

Several models of flow in sedimentation tanks have been prepared by Ingersoll, McKee, and Brooks (1956) and Clements (1966). These did not consider the effects of stratified flow.

Inviscid Flow Models

Debler (1959), working with Yih (1958), showed that selective withdrawal would occur for densimetric Froude numbers less than $1/\pi$. Debler's technique for filling the flume served as a model for later researchers, including this study.

Yih's solution was invalid for values of the densimetric Froude number less than $1/\pi$. Kao (1965) was able to solve the problem using a free streamline solution to model this case. His theoretical results roughly agreed with Debler's. The differences could be explained by the fact that Kao ignored viscous effects.

Trustrum (1964) showed the relationship between blocked flows in stratified and rotating fluids. Later Janowitz (1973) showed that introduction of viscosity could have a significant impact on flow over a vertical barrier in an unbounded case.

In a series of studies at the University of Canterbury, Wood (1968), Wood and Lai (1972a, 1972b), and Lust and Wood (1974) solved a two- (or multi-) layer energy equation for flow through a gradually

tapered weir, sluice gate and orifice. They determined the discharge from each layer.

Armi (1975) solved the inviscid energy and momentum equations for flows through contractions and over broad-crested weirs for the two-layer case. The solutions were dependent on the Froude numbers. He ignored viscous forces.

Viscous Flow Models

Koh (1964, 1966a) was first to solve the problem of viscous, diffuse flow toward a line sink. He used Boussinesq and boundary layer assumptions and the slow flow assumption to simplify his equation. (Boussinesq assumption states $\rho_o + \Delta\rho \sim \rho_o$* if stratification is small.) Similar assumptions are used in this study. Koh then was able to define a similarity transformation to reduce the equation which he solved using a perturbation scheme.

His solution showed that the flow would be symmetric about the elevation of the sink. His solution predicted a large forward flowing zone with a small backflow.

Koh made the assumption that the stratification is small which permitted neglecting derivatives of density with depth in inertial terms. At the same point in his development he eliminated derivatives of viscosity with depth, using the implicit argument that since the density stratification is small, the viscosity stratification must also be small. While this assumption is valid for some fluids, especially salt stratification which Koh and others used, it does not follow that it will be true for all fluids.

---

* For convenience, symbols and unusual abbreviations are listed and defined in the Notation (Appendix E).

The same reasoning has been used by all later researchers. Among the advances presented in this study are criteria stating when this assumption is no longer true.

In contrast to most other researchers, Koh carried the term

$$\frac{\partial}{\partial y}\left(\mu \frac{\partial u}{\partial y}\right) = \frac{\partial \tau_{yx}}{\partial y} \tag{1}$$

where

μ = viscosity

y = vertical distance

u = horizontal velocity

through most of his development before eliminating it with what is essentially a Boussinesq assumption for viscosity. (Most other researchers begin their development using $\mu\nabla^2 u$ to represent the viscous stress tensor.) Koh writes this assumption as

$$|\Delta\mu| << \mu_o \tag{2}$$

where

$\Delta\mu$ = change in viscosity due to stratification

μ_o = characteristic viscosity

For a fluid with a linear temperature gradient from 4 to 20°C, μ_o is 1.235 cp and $\Delta\mu$ is 0.565 cp. Koh's assumption, therefore, is not always true. The results are even more dramatic when stratified fluids with widely varying viscosities are used.

The techniques for measuring velocity developed by Koh for this study have been used by a large number of later researchers, including this study, with some modification. It consisted of dropping dye pellets into the fluid and photographing them at later times. The

displacement of the streaks indicates the velocity.

Gelhar and Mascolo's (1966) work in selective withdrawal, and Long's (1962) work in "jets," used assumptions similar to Koh (1964) except that they ignored the effect of diffusion which in most cases is small. They found velocity profiles which were virtually identical to Koh's, which indicates that the effect of diffusion was probably small in Koh's experiment.

Gelhar and Mascolo developed the differential equation:

$$\frac{\partial^4 \Psi}{\partial Y^4} + \frac{f}{\nu} \frac{\partial \Psi}{\partial X} = 0 \qquad (3)$$

where

Ψ = stream function

X,Y = horizontal and vertical distances, respectively

$f = \frac{-g}{\rho_o} \frac{\partial \rho}{\partial \Psi}$

ρ = density

ν = kinematic viscosity

which, except for the fact that it assumes constant viscosity, is the equation to be solved in this study.

Imberger (1970) and Imberger and Fischer (1970) showed that several zones governed by different force balances exist in stratified flow to a sink. While they defined several zones, the two most critical are the outer zone in which a viscous-buoyancy balance predominates, and an inner zone in which the inviscid inertia-buoyancy balance predominates.

Unlike Koh (1964, 1966a) and Gelhar and Mascolo (1966),

Imberger (1970) used a finite duct model instead of a semi-infinite fluid model, although he did allow slip along the duct wall. He found the most important parameters to be the Raleigh number $\left(\sqrt{\nu D/\varepsilon g \ell^2}\right)$ and the Schmidt number $\left(\sqrt{\nu/D}\right)$, where D = molecular diffusion coefficient.

While he was able to solve the outer equations using a Fourier series technique, he needed an approximate integral technique for the inner layer. His laboratory results showed excellent agreement with the integral solution.

Imberger and Fischer (1970) criticize Gelhar and Mascolo (1966) for ignoring diffusion, especially since they were solving the problem in an infinite domain. They criticize Koh's (1964, 1966a) solution near the sink since it ignores inertia and far from the sink since the linear density profile is inconsistent with an infinite domain.

In a series of papers prepared at the University of Wisconsin, Walesh and Monkmeyer (1973), Ho (1973), and Clark (1974) studied slow, viscous, stratified flow to line sinks for several reservoir geometries. Their solution method was similar to Gelhar and Mascolo (1966) although they did extend the method to axisymmetric cases in cylindrical coordinates. They also analyzed shear stress in stratified flow. They developed an empirical relationship for the f term in Gelhar and Mascolo's model. Their model has a realistic boundary condition of no flow at solid boundaries although they treat viscosity as a constant.

King, Norton, and Orlob (1973) developed a finite element model which solves the Reynolds equation for variable stratification over a broad-crested weir. They replaced viscosity with eddy viscosity which they determined empirically. They only reported the results for two

cases, homogeneous flow and a two-layer system with a large density gradient. The model agreed reasonably well with the data provided by Bohan and Grace. Since the solution was developed for high Reynolds numbers, it was more closely related to the inviscid case than the viscous. The authors reported difficulty in applying the model for low Reynolds numbers.

One source which contains some examples of steady one-dimensional flow in the form of example problems is Bird, Stewart, and Lightfoot's (1960) Transport Phenomena. While it does not contain any two-dimensional problems with varying viscosity, its example served as a guide to one-dimensional solutions presented later in this report.

For the case of steady seepage, with Peclet number ($\ell u/D$) greater than one, Yih (1961) showed that the problem of varying viscosity can be solved in a straightforward manner. The technique involved solving the problem of potential flow in a porous media for a homogeneous fluid. The velocity determined by this solution, which Yih called the velocity of associated flow, can then be transformed to the velocity at any point by multiplying by the ratio of the reference viscosity to the viscosity at that point. This approach could also apply to flows in Hele-Shaw cells. In this study, the derivatives in the direction of flow and vertical direction are at least the size of derivatives normal to the flow so the above transformation is of little use.

Unsteady Flow Models

Koh (1966b), and later Imberger and Fischer (1970), solved the

initial value problem for the inviscid case. By matching the solution to a steady-state solution, they determined the time for a withdrawal layer to form. This result is used in this study to check to see if steady-state conditions were reached in the model tests.

In a series of articles, Kao, Pao, and Wei (1972), Pao and Kao (1974), Kao, Pao, and Wei (1974), and Kao (1976) developed a numerical model to more closely study the mechanisms involved in the establishment of stratified flow in an infinite duct. They showed that steady-state develops as a series of columnar disturbances propagating out from the sink. They found viscous forces to be unimportant for Reynolds numbers greater than 1000.

Fandry (1974), Imberger and Fandry (1975), and Imberger, Thompson, and Fandry (1976) extended unsteady-state solutions from the infinite duct problem to a tank with a back wall. They showed that reflection of the disturbances from the back wall can result in a secondary collapse of the withdrawal layer depending on the Prandtl number (ν/D) and a parameter relating inertial and buoyancy forces ($q(\varepsilon g \ell^2 \nu^2)^{-1/3}$).

Numerical Methods

This study does not involve any major, new developments in numerical solution of fluid mechanics problems. The basic reference used was Carnahan, Luther, and Wilkes (1969), Applied Numerical Methods. Another reference used was a state-of-the-art paper on simulation of viscous flows by Orszag and Israeli (1974).

Imberger, Thompson, and Fandry (1976) point out that for flows in

which large density differences develop, an Eulerian solution is not appropriate. They used a mixed Eulerian-Lagrangian solution in their study similar to "cloud in cell" techniques in which particles of constant density are tracked through an Eulerian field. They implied that this technique was expensive.

Rheological References

Significant viscosity gradients in fluids can be achieved by the presence of colloidal suspensions. There is a linear relationship between concentration and viscosity for dilute suspensions as given by Einstein's Law of Viscosity. This relationship becomes non-linear at higher concentrations and non-Newtonian effects predominate at even higher concentrations. Reviews of these models of the effect of suspensions on viscosity have been prepared by Frisch and Simha (1956) and Jeffrey and Acrivos (1976).

Sediments were found to have Bingham plastic behavior at concentrations greater than 30 g/ℓ by Krone (1963a, 1963b) and Migniot (1968). Krone found the yield stress to be a function of concentration to the 2.5 power while Migniot determined it to be to the fourth power.

The basic references used for determining the rheological properties of model fluids used in this study were Metzner (1956), Reiner (1960), and Van Wazer et al. (1963).

Summary

No solution could be found to the problem of two-dimensional, stratified, non-Newtonian flow to a line sink.

In general, the effects of a viscosity gradient on the velocity distribution in stratified flow have been ignored, since in the cases studied thus far the effects of a density gradient are more dramatic than those caused by the viscosity gradient. In particular, in the case of slow, viscous flow to a line sink, previous researchers have made the assumption that the density stratification is small, which allows them to invoke the Boussinesq assumption ($\rho_o \sim \rho_o + \Delta\rho$).

They have then concluded that since the density stratification is small, then the viscosity stratification must also be small ($\mu_o \sim \mu_o + \Delta\mu$). In this report, criteria are developed to determine when the assumption of small viscosity stratification is not true and techniques for predicting the velocity distribution are presented for that case.

CHAPTER III

BASIC EQUATIONS AND CONCEPTS

In this chapter, the scope of the study is precisely defined by listing the assumptions used in the study. The equation of motion to be solved is presented with special emphasis on the $\partial\tau_{yx}/\partial y$ term in the horizontal momentum equation which accounts for viscosity stratification (τ is viscous stress tensor). Notational conventions and dimensionless groups are discussed and the equations are presented in a manner so that it is unnecessary to repeat these preliminaries in later chapters of the report.

Assumption

The following assumptions are used to define the scope of the study. The first set of assumptions are true in a large number of practical cases for laminar flow.

1. Flow is laminar (no turbulent momentum transfer terms in equation);
2. Stratification is Boussinesq ($\rho_o \sim \rho_o + \Delta\rho$);
3. Flow is non-diffuse ($D \sim 0$);
4. Flow is steady in duct models and quasi-steady in tank models (derivatives with respect to time are neglected);
5. Flow is incompressible ($\nabla \cdot \bar{u} = 0$);
6. Inertial terms in vertical motion equation are neglected (accelerations are only important in horizontal direction);

7. Density is a linear function of concentration of species affecting density (density can be used in place of concentration in species continuity equation);

8. There are no body forces in horizontal direction ($g_x = 0$);

9. Viscosity is independent of pressure, ($\partial\mu/\partial p = 0$);

10. Flow is two-dimensional (derivatives in the lateral direction can be ignored).

A second set of assumptions may not generally be true in practical problems. Nevertheless, the assumptions are useful in making the mathematics tractable. Each of these assumptions will be relaxed during the study to determine its effects.

1. Flow is Newtonian (Newton's Law of Viscosity can be applied);

2. Flow is slow ($\bar{u} \cdot \nabla\bar{u} = 0$);

3. Density gradient is linear ($\partial\rho_s/\partial y = \varepsilon\rho_o$ = constant);

4. Line sink is located at mid-depth in the model (horizontal boundaries have equal impact on solution);

5. Boundary layer type assumptions can be used ($\partial u/\partial y >> \partial u/\partial x$).

Development of Basic Equations

The following equations are a direct result of the first set of assumptions. The terms are defined in Figure 1.

x-momentum

$$\rho_o \left(u \frac{\partial u}{\partial x} + v \frac{\partial u}{\partial y} \right) + \frac{\partial p}{\partial x} = -\mu \left(\frac{\partial \tau_{xx}}{\partial x} + \frac{\partial \tau_{yx}}{\partial y} \right) \tag{4}$$

y-momentum

$$\frac{\partial p}{\partial y} = -\rho g \tag{5}$$

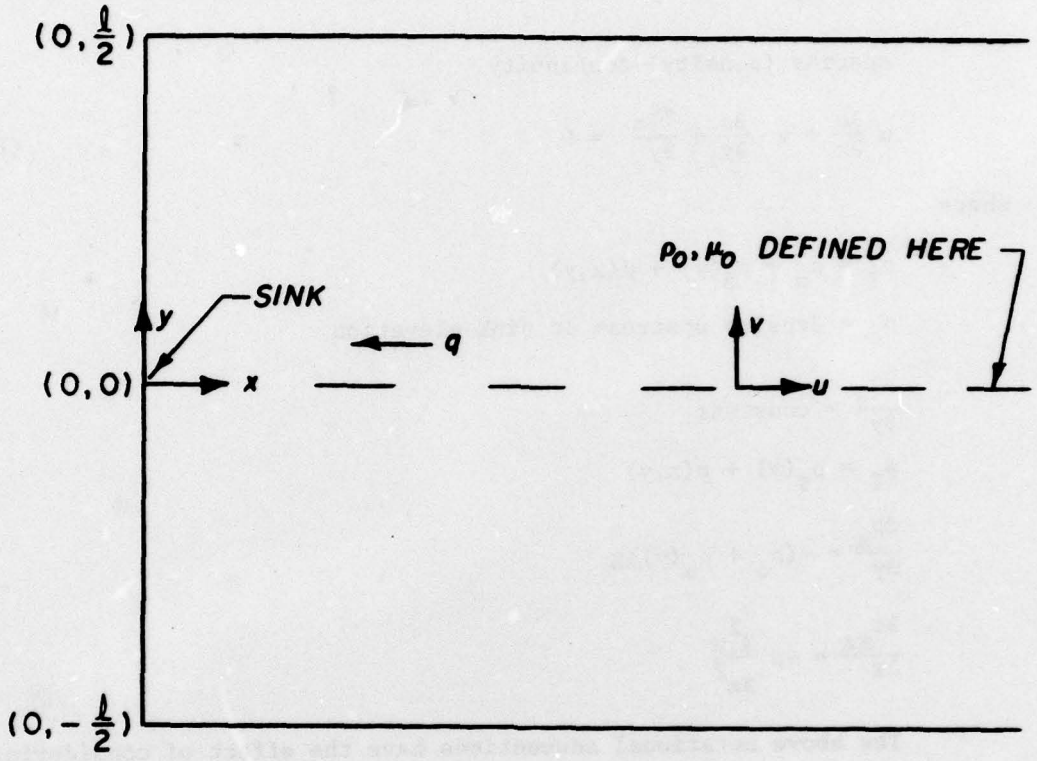

Fig. 1. Definition sketch

continuity

$$\frac{\partial u}{\partial x} + \frac{\partial v}{\partial y} = 0 \tag{6}$$

species (density) continuity

$$u \frac{\partial \rho}{\partial x} + v \frac{\partial \rho}{\partial y} + \frac{\partial \rho_s}{\partial y} = 0 \tag{7}$$

where

$\rho_T = \rho_o + \rho_s(y) + \rho(x,y)$

ρ_o = density upstream at sink elevation

$\frac{\partial \rho_s}{\partial y}$ = constant

$p_T = p_s(y) + p(x,y)$

$\frac{dp_s}{dy} = -(\rho_o + \rho_s(y))g$

$\frac{\partial \tau_{xx}}{\partial x} = -\mu \frac{\partial^2 u}{\partial x^2}$

The above notational conventions have the effect of considering density and pressure only as they are affected by motion, i.e., subtracting out static pressure gradient. The above equations are essentially the same as those used by Imberger (1970) with the exception that viscosity is now allowed to vary and time derivatives are neglected in this study.

In the past studies the τ_{yx} term has been treated as the τ_{xx} term and replaced by

$$\frac{\partial \tau_{yx}}{\partial y} = -\mu \frac{\partial^2 u}{\partial y^2} \tag{8}$$

based on Newton's Law of Viscosity for fluids with constant viscosity.

To allow for varying viscosity

$$\frac{\partial \tau_{yx}}{\partial y} = \frac{\partial}{\partial y}\left[-\mu\left(\frac{\partial u}{\partial y} + \frac{\partial v}{\partial x}\right)\right]$$

$$= -\mu \frac{\partial^2 u}{\partial y^2} - \frac{\partial \mu}{\partial y}\frac{\partial u}{\partial y} - \frac{\partial \mu}{\partial x}\frac{\partial v}{\partial x} - \mu \frac{\partial^2 v}{\partial x \partial y} \tag{9}$$

The last two terms can be eliminated with a boundary layer type assumption. It is because of the term $\partial\mu/\partial y$ $(\partial u/\partial y)$ and the fact that μ is not constant in $\mu\ \partial^2 u/\partial y^2$ that viscosity stratification can affect flow.

This study will examine the effect of retaining the $\partial\mu/\partial y$ term, which will be called the viscosity stratification term. Two special cases will be studied extensively. The first is a linear viscosity gradient

$$\mu = \mu_o + \frac{\partial \mu}{\partial y}\, y \tag{10}$$

where μ_o = viscosity at sink elevation.

The second is a logarithmic increase of viscosity with depth

$$\mu = \mu_o\, e^{c_1 y} \tag{11}$$

where c_1 = slope of log viscosity curve.

Allowing for this viscosity stratification, the x-momentum equation becomes

$$\rho_o\left(u\frac{\partial u}{\partial x} + v\frac{\partial u}{\partial y}\right) + \frac{\partial p}{\partial x} = \mu\left(\frac{\partial^2 u}{\partial x^2} + \frac{\partial^2 u}{\partial y^2}\right) + \frac{\partial \mu}{\partial y}\frac{\partial u}{\partial y} \tag{12}$$

Note that the $\partial^2 u/\partial x^2$ term will be eliminated from most equations by the boundary layer assumption.

Non-Dimensionalizing

Throughout this report the equations are solved in their

dimensionless form. The equations are non-dimensionalized using a characteristic two-dimensional flow at the sink (q), length (ℓ), and viscosity (μ_o) with units L^2/T, L, and M/LT, respectively. When the substitutions

$$U = u\ell/q,\ V = v\ell/q,\ X = \frac{x}{\ell},\ Y = \frac{y}{\ell}$$

are made, equations 4, 6 and 7 become:

x-momentum

$$\frac{q\rho_o}{\mu_o}\left(U\frac{\partial U}{\partial X} + V\frac{\partial U}{\partial Y}\right) + \frac{\ell^3}{q\mu_o}\frac{\partial p}{\partial x} = \frac{\mu}{\mu_o}\left(\frac{\partial^2 U}{\partial X^2} + \frac{\partial^2 U}{\partial Y^2}\right) + \frac{\ell}{\mu_o}\frac{\partial \mu}{\partial y}\frac{\partial U}{\partial Y} \tag{13}$$

continuity

$$\frac{\partial U}{\partial Y} + \frac{\partial V}{\partial Y} = 0 \tag{14}$$

species continuity

$$U\frac{\partial \rho}{\partial x} + V\left(\frac{\partial \rho}{\partial Y} + \frac{\partial \rho_s}{\partial y}\right) = 0 \tag{15}$$

The y-momentum equation is unchanged.

Note that capital letters will be used to designate the dimensionless value of the variables. No attempt was made above to non-dimensionalize the pressure and buoyancy terms since these will be handled differently in the various cases.

The above equations will be used as a starting point for many of the following chapters. Note that the equations contain the Reynolds number ($q\rho_o/\mu_o$). In most cases this will be considered small and can be eliminated from the equations.

The most important parameter for the purposes of this study is

$$\frac{\ell}{\mu_o}\frac{\partial u}{\partial y}$$

which is an indicator of the strength of the viscosity stratification. It will give rise to two dimensionless groups depending on whether $\partial u/\partial y$ is constant, i.e., gradient is linear.

Simplification of Equations

To solve the system of equations, a single equation with one unknown (Ψ) was constructed from the four coupled equations (5, 13, 14, 15) with four unknowns (U, V, ρ, P). This is done below for the case in which the Reynolds number is small and

$$\frac{\partial^2 U}{\partial X^2} << \frac{\partial^2 U}{\partial Y^2} \tag{16}$$

First, pressure can be eliminated from the momentum equations by differentiating the x-momentum equation by y and the y-momentum equation by x to give

$$\frac{\ell^3}{q\mu_o}\frac{\partial^2 p}{\partial x \partial y} = \frac{\mu}{\ell\mu_o}\frac{\partial^3 U}{\partial Y^3} + \frac{2}{\mu_o}\frac{\partial \mu}{\partial y}\frac{\partial^2 U}{\partial Y^2} + \frac{\ell}{\mu_o}\frac{\partial^2 \mu}{\partial y^2}\frac{\partial U}{\partial Y} = -\frac{\ell^3 g}{q\mu_o}\frac{\partial \rho}{\partial x} \tag{17}$$

The continuity equation implies the existence of a stream function Ψ such that

$$\frac{\partial \Psi}{\partial y} = U \ , \ \frac{\partial \Psi}{\partial x} = -V \tag{18}$$

Substituting this into the above equation and rearranging terms gives

$$\frac{\partial^4 \Psi}{\partial Y^4} + 2\frac{\ell}{\mu}\frac{\partial \mu}{\partial y}\frac{\partial^3 \Psi}{\partial Y^3} + \frac{\ell^2}{\mu}\frac{\partial^2 \mu}{\partial y^2}\frac{\partial^2 \Psi}{\partial Y^2} = -\frac{\ell^4}{q\mu}\frac{\partial \rho}{\partial x} \tag{19}$$

The species continuity equation can be rearranged (for $U \neq 0$) as

$$\frac{\partial \rho}{\partial x} = -\frac{V}{U}\frac{\partial}{\partial y}(\rho + \rho_s) \tag{20}$$

While $\partial/\partial y\ (\rho + \rho_s)$ is not known, it is known that the fluid is non-diffuse (density constant on a streamline) so that

$$\frac{\partial(\rho + \rho_s)}{\partial \Psi} \frac{\partial \Psi}{\partial y} = \frac{\partial}{\partial y} (\rho + \rho_s) \tag{21}$$

At some point very far from the sink, the density field is not affected by flow and it is possible to write

$$\frac{\partial \rho_s}{\partial \Psi} = \frac{\partial(\rho + \rho_s)}{\partial \Psi} \quad , \quad \frac{\partial \Psi}{\partial y} = \frac{1}{\ell} \left(\frac{\partial \Psi}{\partial Y} \right) \Bigg|_\infty \tag{22}$$

$\frac{\partial(\rho + \rho_s)}{\partial \Psi}$ is a constant, and

$$\frac{\partial(\rho + \rho_s)}{\partial \Psi} = \ell \left(\frac{\partial Y}{\partial \Psi} \right) \frac{\partial}{\partial y} (\rho + \rho_s) = \ell \varepsilon \rho_o \left(\frac{\partial Y}{\partial \Psi} \right) \Bigg|_\infty \tag{23}$$

where

$$\varepsilon = \frac{1}{\rho_o} \frac{d\rho}{dy}$$

Equation 23 can be rearranged (noting $\partial \Psi/\partial Y = U$) and inserted into equation 21 to give

$$\frac{\partial}{\partial y} (\rho + \rho_s) = \frac{-\varepsilon \rho_o U}{U_\infty} \tag{24}$$

Substituting back into equation 20 gives

$$\frac{\partial \rho}{\partial x} = \frac{V}{U_\infty} \varepsilon \rho_o \tag{25}$$

Substituting for $\partial \rho/\partial x$ in the motion equation gives

$$\frac{\partial^4 \Psi}{\partial Y^4} + 2 \frac{\ell}{\mu} \frac{\partial \mu}{\partial y} \frac{\partial^3 \Psi}{\partial Y^3} + \frac{\ell^2}{\mu} \frac{\partial^2 \mu}{\partial y^2} \frac{\partial^2 \Psi}{\partial Y^2} + \frac{\ell^4 \varepsilon \rho_o g}{q \mu_o U_\infty} \frac{\mu_o}{\mu} \frac{\partial \Psi}{\partial X} = 0 \tag{26}$$

The above equation is the model for stratified flow that is used in the remainder of the report whenever buoyancy forces are important.

This equation is used as the starting point for the models developed in Chapters VII, VIII, IX, XI, and XII.

The solutions are shown not to be very sensitive to the term $\mu U_\infty/\mu_o$ since it deals with upstream boundary conditions which are of only minor importance since the equation is solved as an initial value problem in x. U_∞ is usually set to one to simplify the solution procedure.

Similarly, μ/μ_o is replaced by the appropriate $\mu(Y)$ for that model. Note that since the flow is non-diffuse, μ is constant on a streamline and is a function of Ψ not Y. Using μ as a function of Y implies that the viscosity field is fixed. The effect of this assumption is small and is discussed in Chapter IX.

Boundary Conditions

Each of the cases studied in this report requires a slightly different set of boundary or initial conditions. These conditions are categorized in this chapter and are developed in greater detail as each case is analyzed.

In the one-dimensional models the only question is whether the fluid is allowed to slip at the boundaries. In general, it will not. In two-dimensional flow problems, the distinction between duct and tank models must be made. The flow originates at $x = \infty$ for the duct model, while for tank models there is a fixed back wall and the flow originates at $y = \ell/2$ ($Y = 1/2$). These cases are shown in Figure 2.

A much more important question, especially in the duct model, is whether the fluid is allowed to slip along the wall. Most earlier

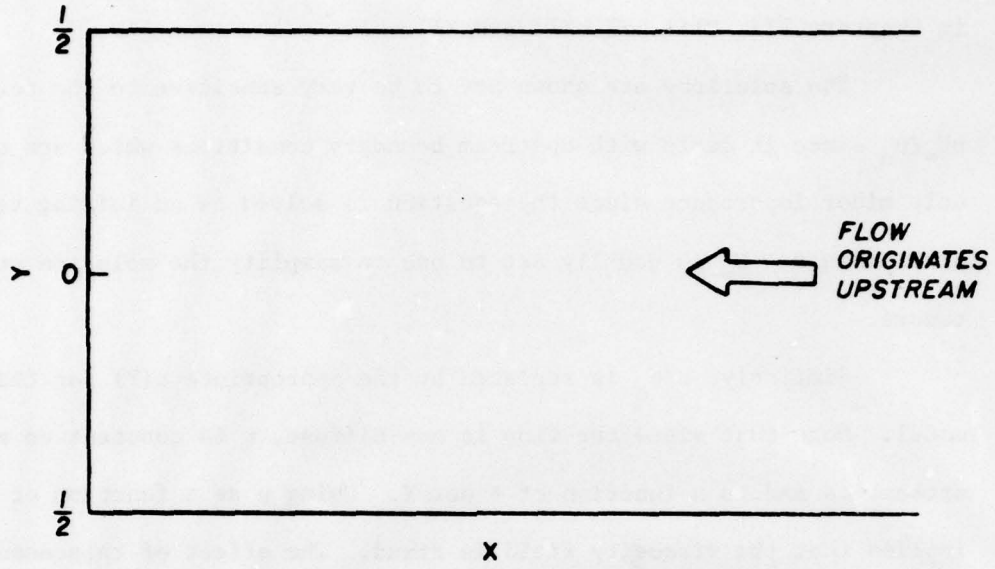

a. DUCT MODEL

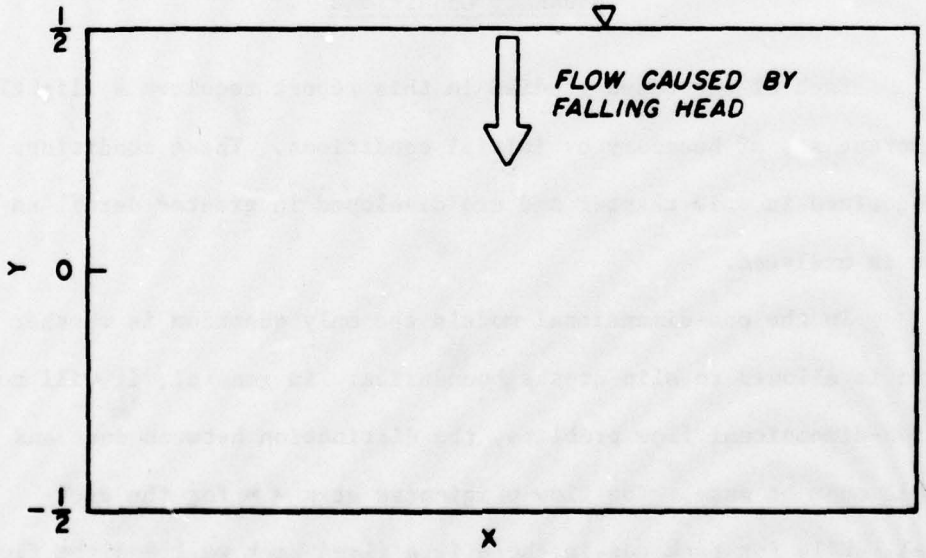

b. TANK MODEL

Fig. 2. Boundary conditions

researchers were interested in withdrawal layers much smaller than the height of the duct and hence allowed the flow to slip. For viscosity stratification to become important, it is important that the fluid not be allowed to slip.

In general, the problem is a boundary value problem in the y-direction. In the x-direction, it is a boundary value problem in the tank model and an initial value problem in the duct model. The boundary conditions for the duct model are given in Figure 3.

Numerical Techniques

Numerical methods for solving differential equations are required for a number of problems in this study. Finite difference methods are used to reduce the problem to a system of algebraic equations which are solved by the Gauss-Seidel Iterative Method.

The numbering convention for the grids is shown in Figure 4. The finite difference approximations for derivatives used in this study are listed below using U as the dependent variable and Y as the independent variable.

First derivative (boundary value problem)

$$\frac{\partial U}{\partial Y} = \frac{U_{j+1} - U_{j-1}}{2\Delta Y} \tag{27}$$

First derivative (initial value problem)

$$\frac{\partial U}{\partial Y} = \frac{U_j - U_{j-1}}{\Delta Y} \tag{28}$$

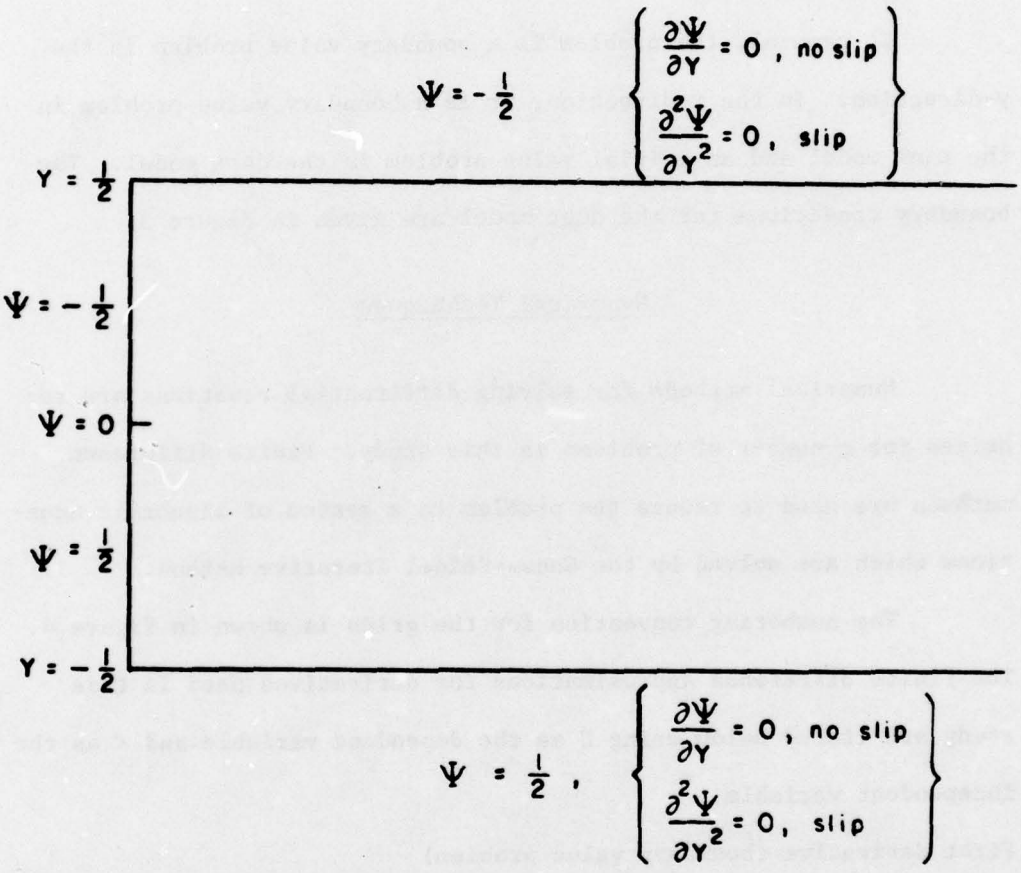

Fig. 3. Boundary conditions for duct model

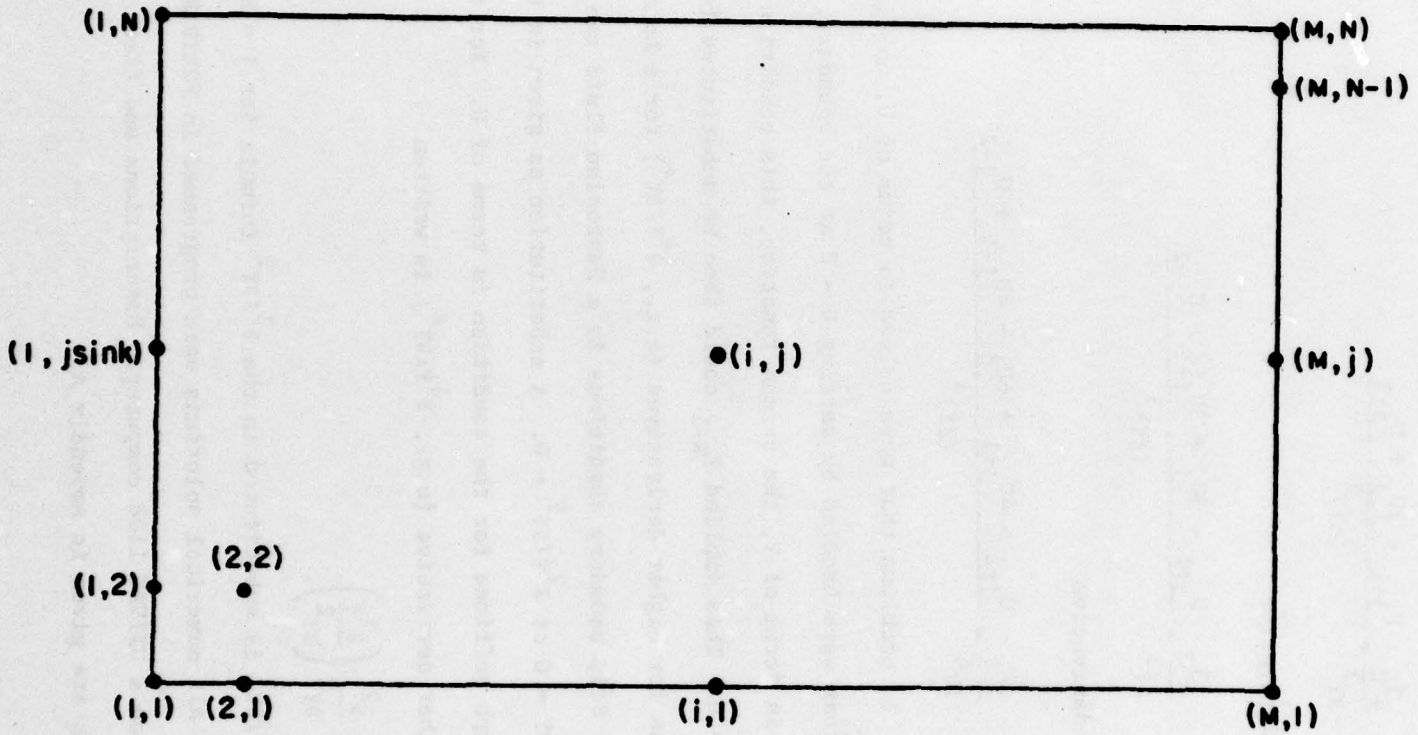

Fig. 4. Layout of grid cells

Second derivative

$$\frac{\partial^2 U}{\partial Y^2} = \frac{U_{j+1} - 2U_j + U_{j-1}}{(\Delta Y)^2} \tag{29}$$

Third derivative

$$\frac{\partial^3 U}{\partial Y^3} = \frac{U_{j+1} - 3U_j + 3U_{j-1} - U_{j-2}}{(\Delta Y)^3} \tag{30}$$

Fourth derivative

$$\frac{\partial^4 U}{\partial Y^4} = \frac{U_{j+2} - 4U_{j+1} + 6U_j - 4U_{j-1} + U_{j-2}}{(\Delta Y)^4} \tag{31}$$

In problems that were solved in terms of U, no slip boundary conditions were handled by setting U = 0 at the boundary. In problems solved in terms of Ψ, the stream function, this condition became $\partial\Psi/\partial Y = 0$. This implied Ψ_{N-1} could then be substituted for Ψ_{N+1} in formulas for higher derivatives (e.g., $\partial^4\Psi/\partial Y^4$) for a boundary at j = N.

Slip boundary conditions in a Newtonian fluid can be interpreted as $\partial U/\partial Y = 0$ or $\partial^2\Psi/\partial Y^2 = 0$. A substitution as given in the preceeding paragraph suffices for the condition in terms of U. For the case of Ψ, the higher derivative (e.g., $\partial^4\Psi/\partial Y^4$) is written

$$\frac{\partial^2}{\partial Y^2}\left(\frac{\partial^2 \Psi}{\partial Y^2}\right)$$

and $\partial^2\Psi/\partial Y^2$ is substituted in the $\partial^2/\partial Y^2$ formula for j = N.

All numerical solutions were programmed in FORTRAN IV and solved on a UNIVAC 1108 computer. Descriptions and flow chart of the programs are given in Appendix A.

CHAPTER IV

ONE-DIMENSIONAL MODELS

Velocity profiles are developed in this part of the report for some simple one-dimensional flows. The profiles developed here are used to demonstrate the effect of viscosity gradients on velocity, to illustrate the concept of skewness in the following chapter, and to serve as a check for the two-dimensional models far from the sink.

The form of the x-momentum equation solved in this chapter is

$$\frac{\partial p}{\partial x} = - \frac{\partial \tau_{yx}}{\partial y} \tag{32}$$

which corresponds to laminar one-dimensional flow with no body forces. The solutions are fairly simple, since the pressure gradient $\partial p/\partial x$ is constant (and is represented by p_x). The equations are solved first for a two-layer stratified system, then, for a linear viscosity gradient, and finally, for a log viscosity gradient. The effect of a slip boundary condition is then studied.

Two-Layer Flow

The solution to the stable, two-layer flow of immiscible fluids problem has been presented by Bird, Stewart, and Lightfoot (1960) as

$$U_T = \frac{p_x \ell^3}{8\mu_T q} \left[\frac{\partial \mu_T}{\mu_T + \mu_B} + \frac{\mu_T - \mu_B}{\mu_T + \mu_B} (2Y) - 4Y^2 \right] \tag{33}$$

$$U_B = \frac{p_x \ell^3}{3\mu_B q}\left[\frac{2\mu_B}{\mu_T + \mu_B} + \frac{\mu_T - \mu_B}{\mu_T + \mu_B}(2Y) - 4Y^2\right] \tag{34}$$

where

U_T = velocity in top layer

U_B = velocity in bottom layer

μ_T = viscosity in top layer

μ_B = viscosity in bottom layer

Since p_x is usually not known, it can be eliminated by integrating the velocity profile and solving for p_x in terms of q, ℓ, and μ.

$$p_x = \frac{96(\mu_B + \mu_T)q}{\ell^3}\left[\frac{\mu_B \mu_T}{\mu_B^2 + 14\mu_B\mu_T + \mu_T^2}\right] \tag{35}$$

Substituting back into the velocity equation gives

$$U = \frac{12(\mu_B + \mu_T)\mu^*}{\mu_k}\left[\frac{2\mu_k}{\mu_B + \mu_T} + \left(\frac{\mu_B - \mu_T}{\mu_B + \mu_T}\right)2Y - 4Y^2\right] \tag{36}$$

where

$$\mu^* = \frac{\mu_B\mu_T}{\mu_B^2 + 14\mu_B\mu_T + \mu_T^2}$$

$$\mu_k = \begin{cases}\mu_B, & \text{for bottom layer}\\ \mu_T, & \text{for top layer}\end{cases}$$

A plot of this solution for values of $2(\mu_B - \mu_T)/(\mu_B + \mu_T) = \frac{\Delta\mu}{\mu}$ which corresponds to $\frac{\ell}{\mu_o}\frac{\partial\mu}{\partial y}$ for this problem is given in Figure 5.

The important thing to note is that as the viscosity difference

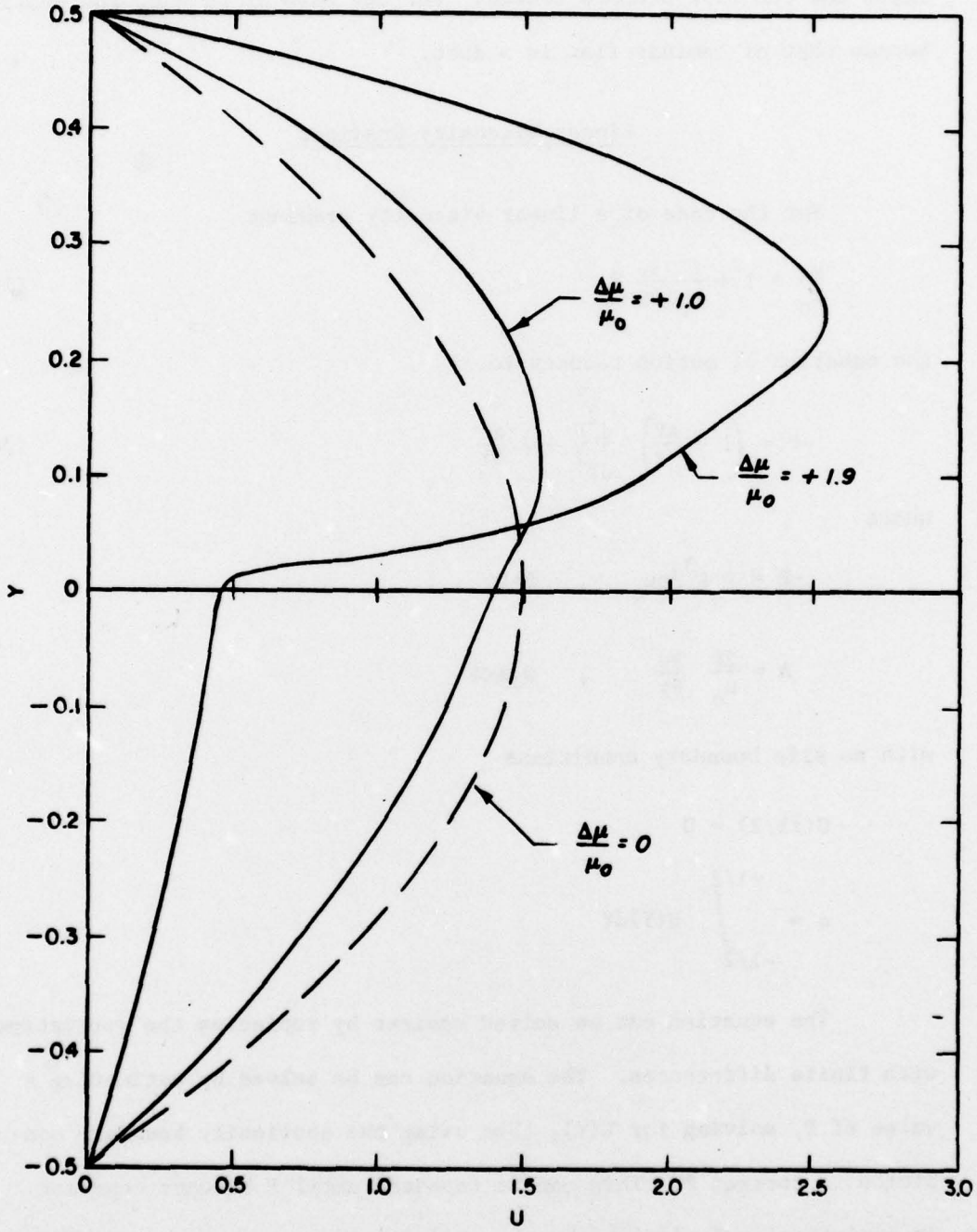

Fig. 5. Velocity profiles, two-layer flow

between layers becomes larger more fluid is withdrawn from the top layer and the flow becomes skewed. For the case of $\Delta\mu = 0$, the profile became that of laminar flow in a duct.

Linear Viscosity Gradient

For the case of a linear viscosity gradient

$$\frac{\mu}{\mu_o} = 1 + \frac{\ell}{\mu_o}\frac{\partial \mu}{\partial y} Y \tag{37}$$

the equation of motion reduces to

$$-P = \left(1 + \frac{AY}{2}\right) \frac{d^2U}{dY^2} + A\frac{dU}{dY} \tag{38}$$

where

$$-P = p_x \ell^3/q\mu_o \quad , \quad P>0$$

$$A = \frac{2\ell}{\mu_o}\frac{\partial \mu}{\partial y} \quad , \quad 0 \leq A < 4$$

with no slip boundary conditions

$$U(\pm 1/2) = 0$$

$$q = \int_{-1/2}^{+1/2} U(Y)dY$$

The equation can be solved easiest by replacing the derivatives with finite differences. The equation can be solved by estimating a value of P, solving for U(Y), then using the continuity boundary condition to correct P. This can be repeated until P becomes constant. An analytical solution can be obtained for the case when A = 0 (constant viscosity). In this case P = 12. This is used as an initial

estimate of P.

The finite difference equation becomes

$$U_j = \left[\left(\frac{1}{\Delta Y^2} + \frac{A}{(2+AY)\Delta Y}\right) U_{j+1} + \left(\frac{1}{\Delta Y^2} - \frac{A}{(2+AY)\Delta Y}\right) U_{j-1} + \left(\frac{P}{1+AY}\right)\right] \frac{\Delta Y^2}{2} \qquad (39)$$

$$P = Pq / \sum_{j=1}^{N} (U_j \Delta Y)$$

The solution is plotted for three values of A (.002, 2., 3.98) to show the effect of A on the velocity profiles in Figure 6. Figure 7 shows that P will remain constant for small values of A but as A becomes large, P decreases rapidly.

Log Viscosity Gradient

Some runs in the laboratory portion of the study were found to have viscosity gradients given by

$$\mu = \mu_o e^{-c_1 y} \qquad (40)$$

which will be called the "log" viscosity gradient. Substituting for μ and

$$\frac{\partial \mu}{\partial y} = -c_1 \mu_o e^{-c_1 y} \qquad (41)$$

gives

$$\frac{d^2U}{dY^2} - C \frac{dU}{dY} = -P e^{CY} \qquad (42)$$

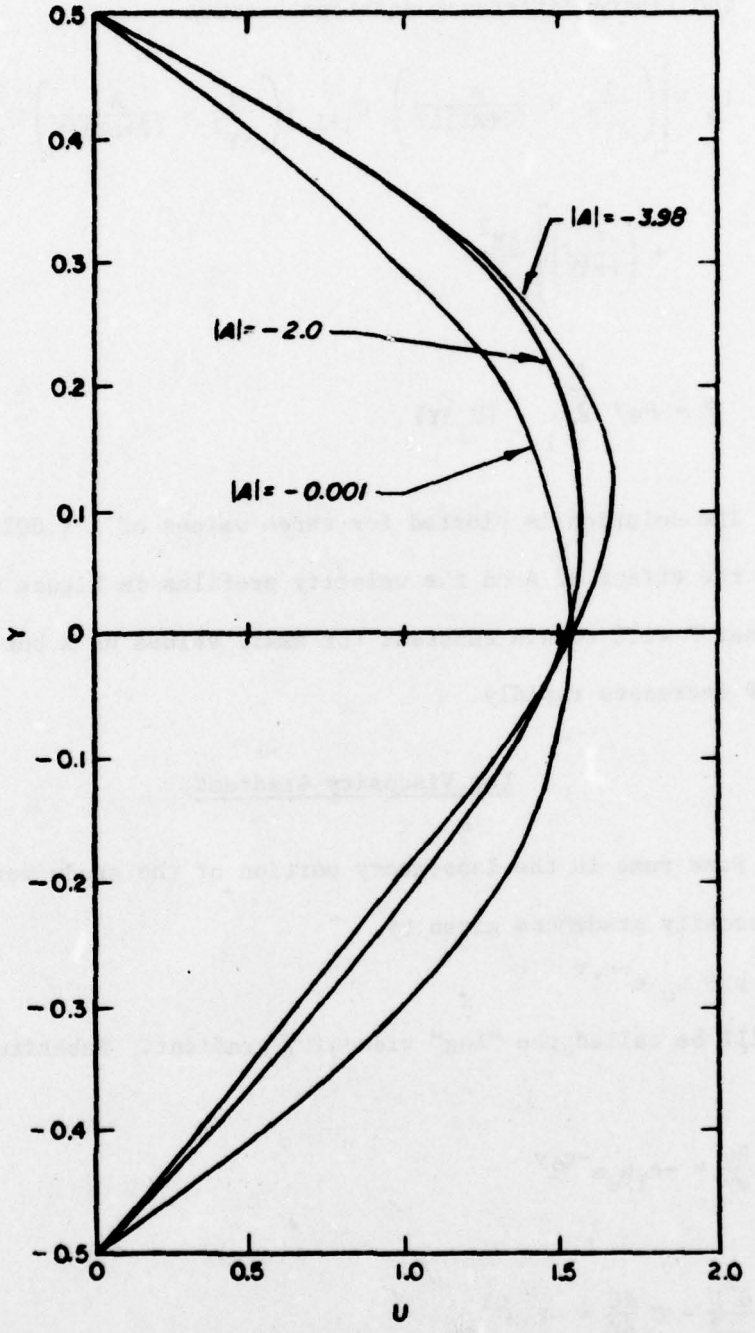

Fig. 6. Velocity profiles, linear viscosity gradient

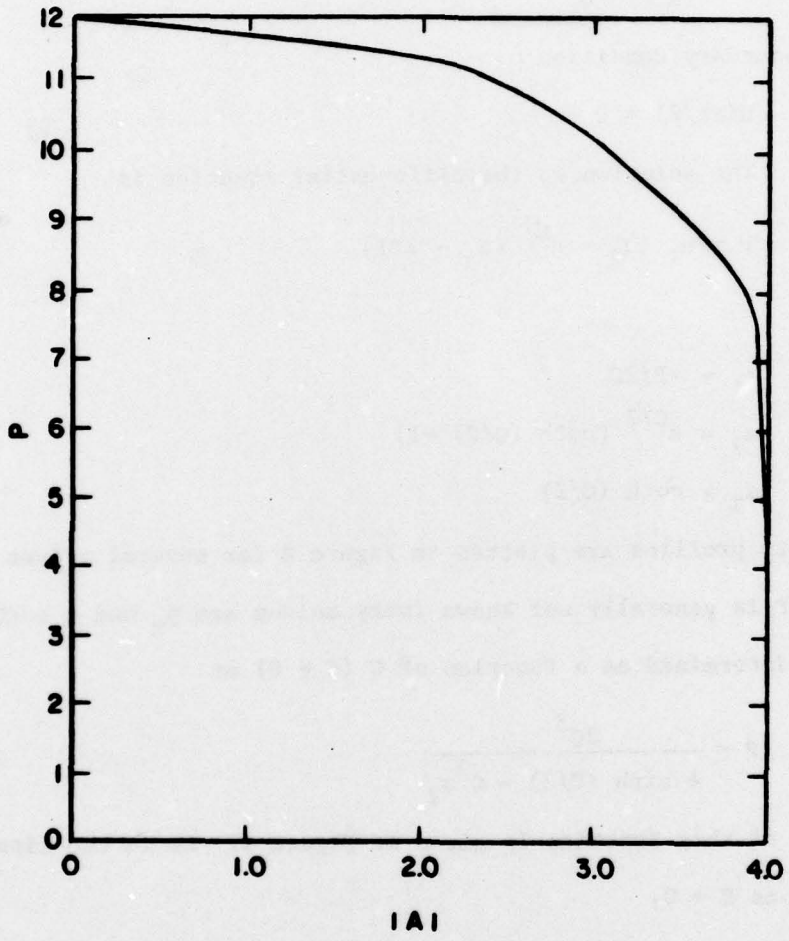

Fig. 7. Effect of A on P

where

$$C = c_1 \ell$$

$$P = p_x \ell^3 / q\mu_o$$

with boundary condition

$$U(\pm 1/2) = 0$$

The solution to the differential equation is

$$U = a_1 \left[a_2 - e^{CY} (a_3 - 2Y)\right] \tag{43}$$

where

$$a_1 = -P/2C$$

$$a_2 = e^{C/2} \left[\coth (C/2) - 1\right]$$

$$a_3 = \coth (C/2)$$

Velocity profiles are plotted in Figure 8 for several values of C. Since P is generally not known (very seldom are p_x and q both known), P was determined as a function of C ($C \neq 0$) as

$$P = \frac{2C^3}{4 \sinh (C/2) - C^2 a_2} \tag{44}$$

A plot of this function is given in Figure 9. As in the linear case, $P \to 12$ as $C \to 0$.

Slip Along Surface Boundary

A boundary condition which may be of some practical value is that in which the flow slips along a top boundary while having no slip on the bottom. This type of boundary condition might characterize flow upstream of a weir.

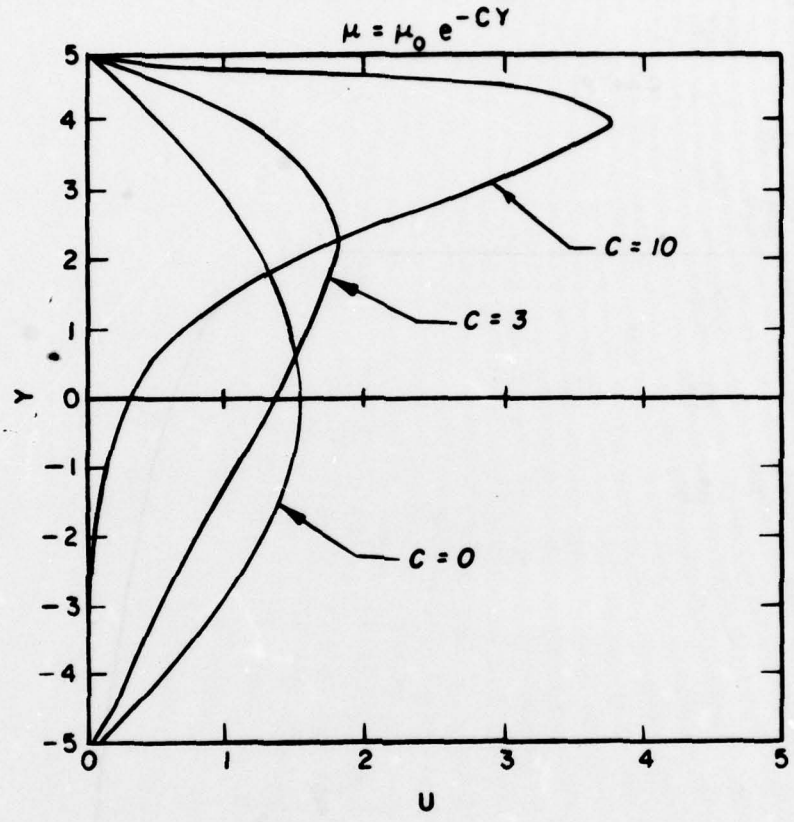

Fig. 8. Velocity profiles, log viscosity gradient

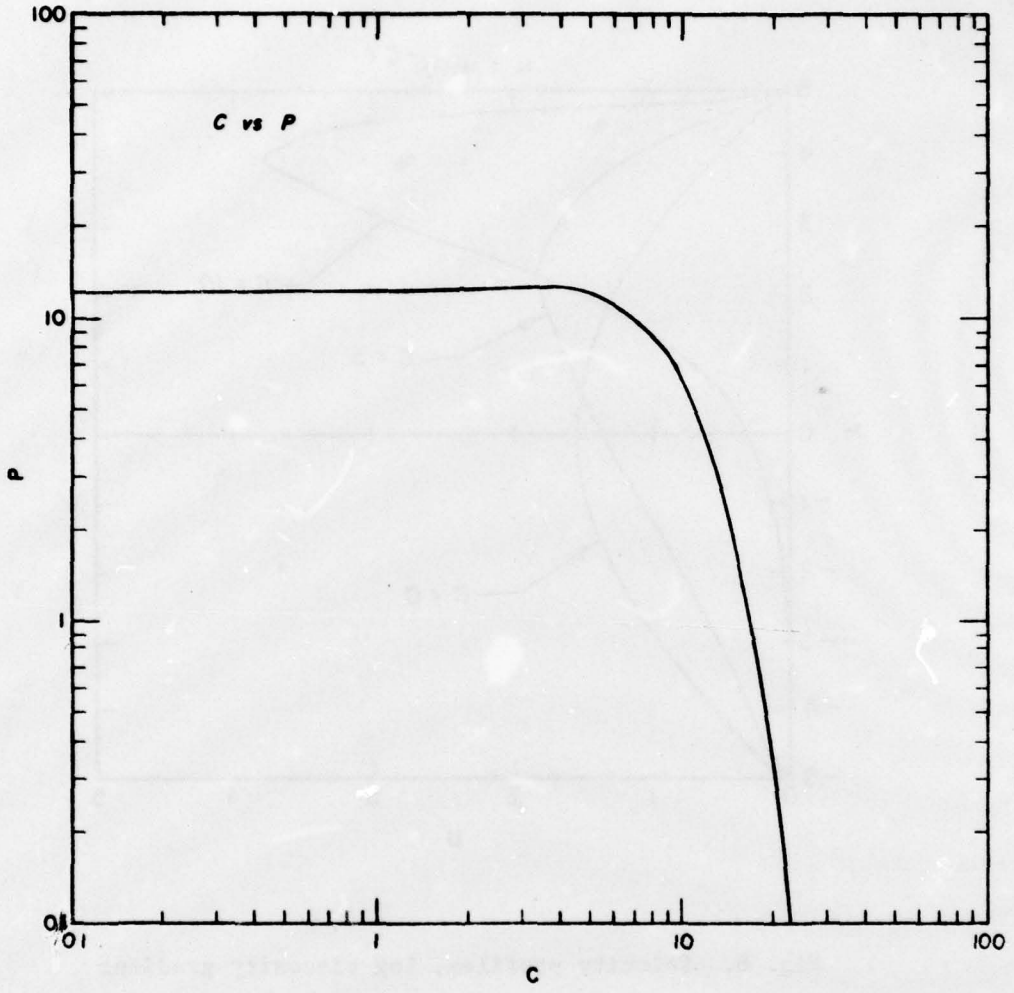

Fig. 9. Effect of C on P

The x-momentum equation can be written

$$\frac{d\tau_{yx}}{dy} = p_x \tag{45}$$

with boundary conditions

$$\frac{dU}{dY}(+1/2) = 0 = \tau_{yx}(+1/2) \tag{46}$$

which is equivalent to the equation solved earlier with the substitution of the dimensionless Newton's Law of Viscosity

$$\tau = \frac{-\mu}{\mu_o}\frac{dU}{dY} \tag{47}$$

The dimensionless shear stress is related to shear stress by

$$\tau = \frac{\ell^2}{q\mu_o}\ \tau_{yx} \tag{48}$$

The differential equation for τ can be solved with the top boundary condition to give

$$\tau = -P/2(2Y - 1) \tag{49}$$

At this point, Newton's Law of Viscosity can be substituted to give

$$-\frac{\mu}{\mu_o}\frac{dU}{dY} = P\left(\frac{1 - 2Y}{2}\right) \tag{50}$$

which can be solved with $\mu/\mu_o = e^{-cy}$ and the bottom boundary condition to give

$$U = \frac{Pe^{CY}}{2C^2}(2YC - C - 2) + \frac{Pe^{-C/2}}{C^2}(1 + C) \tag{51}$$

A condition for continuity can be used to derive an expression for P

$$\int_{-1/2}^{1/2} U dY = 1 \tag{52}$$

The above condition implies

$$P = C^2\left[\cosh (C/2) - \left(\frac{4 + C}{C}\right)\sinh (C/2) + (1 + C)\right.$$
$$\left. e^{-c/2}\right]-1 \tag{53}$$

The solution to this problem is given in Figure 10 for C = 5, 1 and 0. The solution for C = 0 was

$$U = -1.5(Y^2 - Y - .75) \tag{54}$$

Figure 10 indicates that the effect of C on the profile is not large until C becomes greater than one. The profile changes significantly after that point.

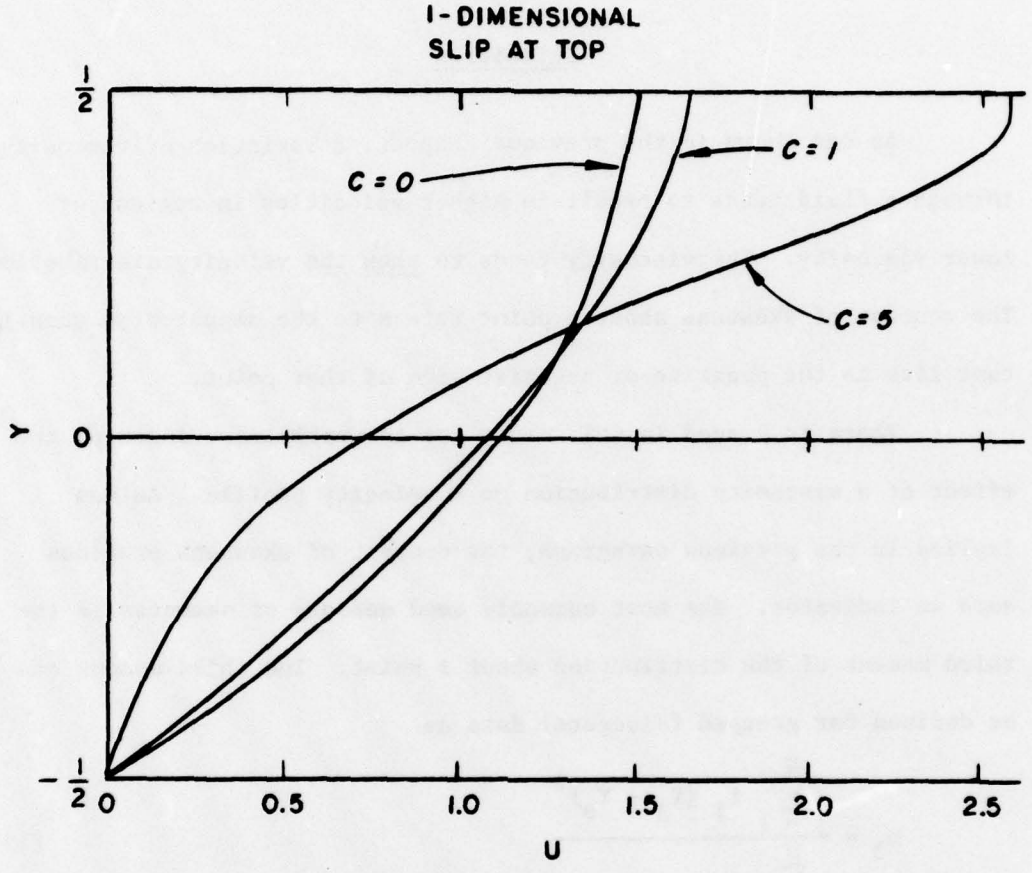

Fig. 10. Velocity profiles, log gradient, slip at top boundary

CHAPTER V

SKEWNESS OF VELOCITY PROFILES

Definition

As was shown in the previous chapter, a variation of viscosity through a fluid tends to result in higher velocities in regions of lower viscosity. The viscosity tends to skew the velocity distribution. The concept of skewness about a point refers to the amount of a quantity that lies to the positive or negative side of that point.

There is a need in this study for an unarbitrary index of the effect of a viscosity distribution on a velocity profile. As was implied in the previous paragraph, the concept of skewness provides such an indicator. The most commonly used measure of skewness is the third moment of the distribution about a point. The third moment can be defined for grouped (discrete) data as

$$m_3 = \frac{\sum_{j=1}^{N} f_j (Y_j - Y_o)^3}{\sum_{j=1}^{N} f_j} \tag{55}$$

where Y_o is the point about which the moment is taken and f_j is the frequency (intensity) of whatever is distributed about Y_o. In this study f represents velocity. Y_o is taken as the centroid of the velocity profile when the profile is symmetric. This corresponds to the elevation Y = 0 throughout this study. Skewness has dimensions of

length cubed. To avoid problems caused by scaling, the third moment is calculated only for dimensionless profiles in this study.

With the above conventions, the formula for calculating skew is given as

$$\text{skew} = \frac{\sum_{j=1}^{N} U_j Y_j^3}{\sum_{j=1}^{N} U_j} \tag{56}$$

where

U_j = horizontal velocity at elevation Y_j

N = number of points at which velocity is calculated

When the velocity profile is available as a continuous function U(Y), the skew can be defined

$$\text{skew} = \frac{\int_{-1/2}^{1/2} U(Y)Y^3 dY}{\int_{-1/2}^{1/2} U(Y) dY} \tag{57}$$

Since the integral in the denominator represents dimensionless flow, which will always be one since $U = u\ell/q$, the definition becomes

$$\text{skew} = \int_{-1/2}^{1/2} U(Y)Y^3 dY \tag{58}$$

Since most of the solutions presented in this report are reached using numerical methods, the skew formula using discrete values for U is used most often.

Application to One-Dimensional Velocity Profiles

The velocity profiles developed in the previous chapter all showed increasing skew as the viscosity stratification $\ell/\mu_o(\partial\mu/\partial y)$ term increased. The dimensionless skewness is plotted vs. a parameter that indicates the magnitude of the viscosity stratification for two-layer, linear and log viscosity gradients in Figures 11, 12, and 13.

The figures show that skewness increases with the appropriate viscosity stratification parameter. There exists an upper bound for the parameter in both the two-layer and linear case since the change in viscosity cannot exceed twice the average viscosity. The reader can gain an appreciation for skewness from Figure 14 which gives the skewness for several velocity profiles.

Application to Two-Dimensional Velocity Profiles

In two-dimensional flow to a line sink, the skew increases as one moves away from the sink where skewness is zero. It is therefore, necessary to specify the dimensionless location in the flume at which the skewness is measured in the two-dimensional case.

In the problems which require upstream boundary conditions, these conditions will also play a role in determining skewness. Most of the two-dimensional problems are formulated as initial value problems so that upstream boundary conditions are not usually required.

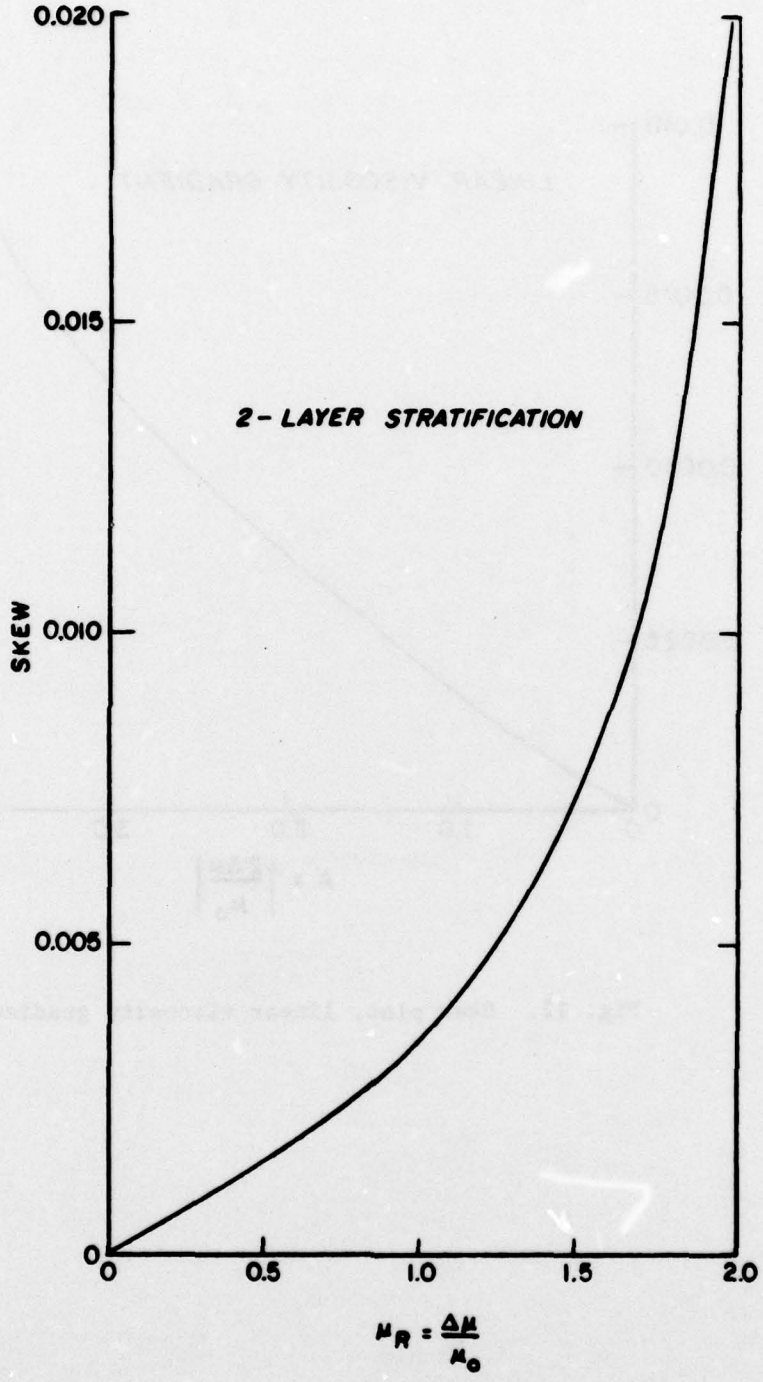

Fig. 11. Skew plot, two-layer stratification

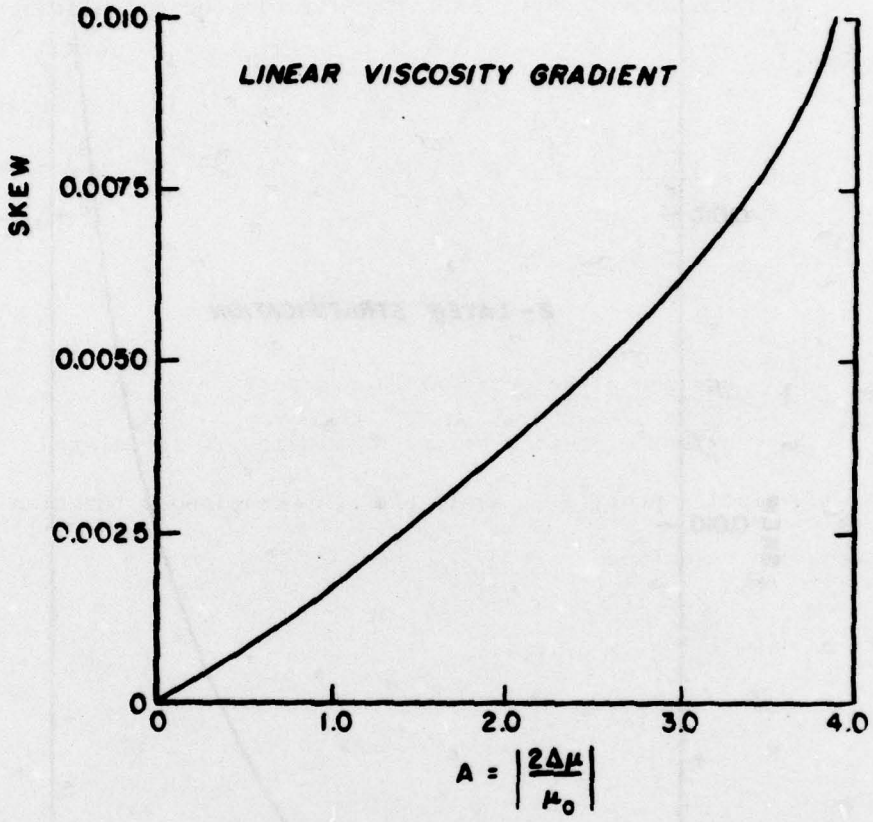

Fig. 12. Skew plot, linear viscosity gradient

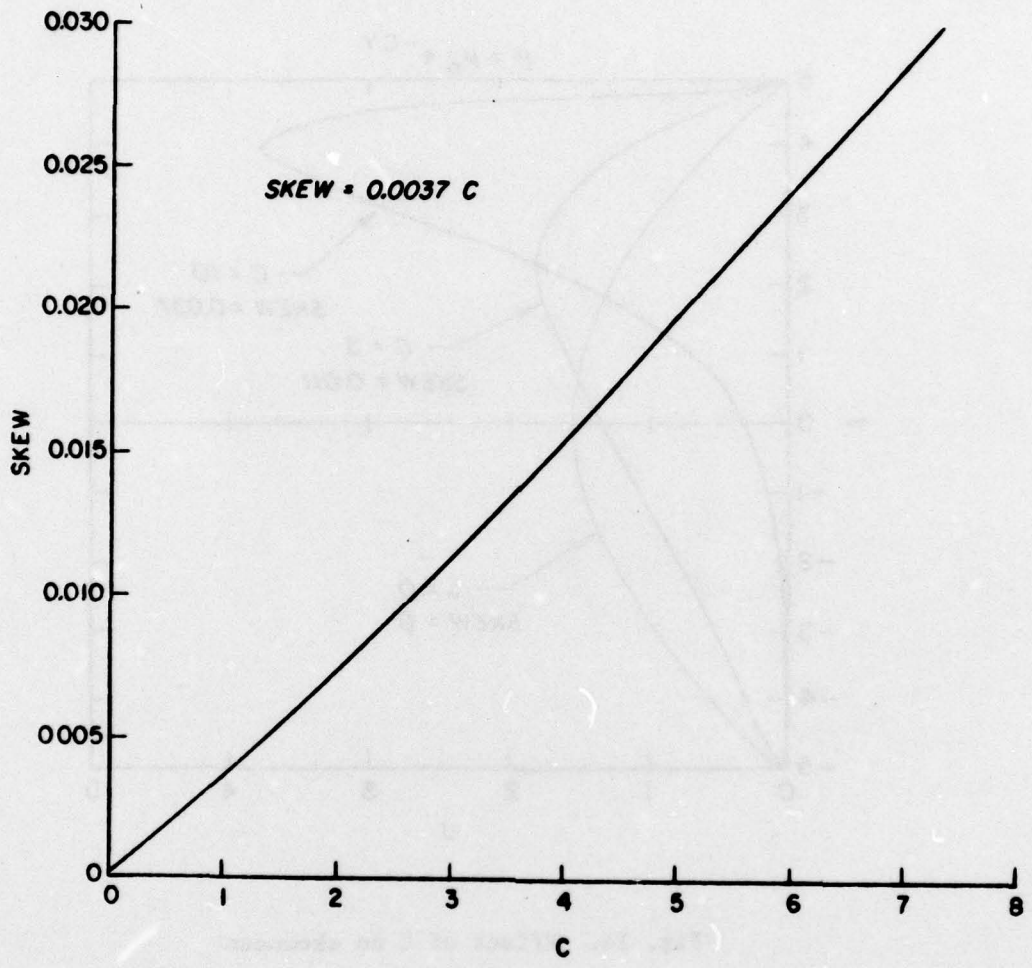

Fig. 13. Skew plot, log viscosity gradient

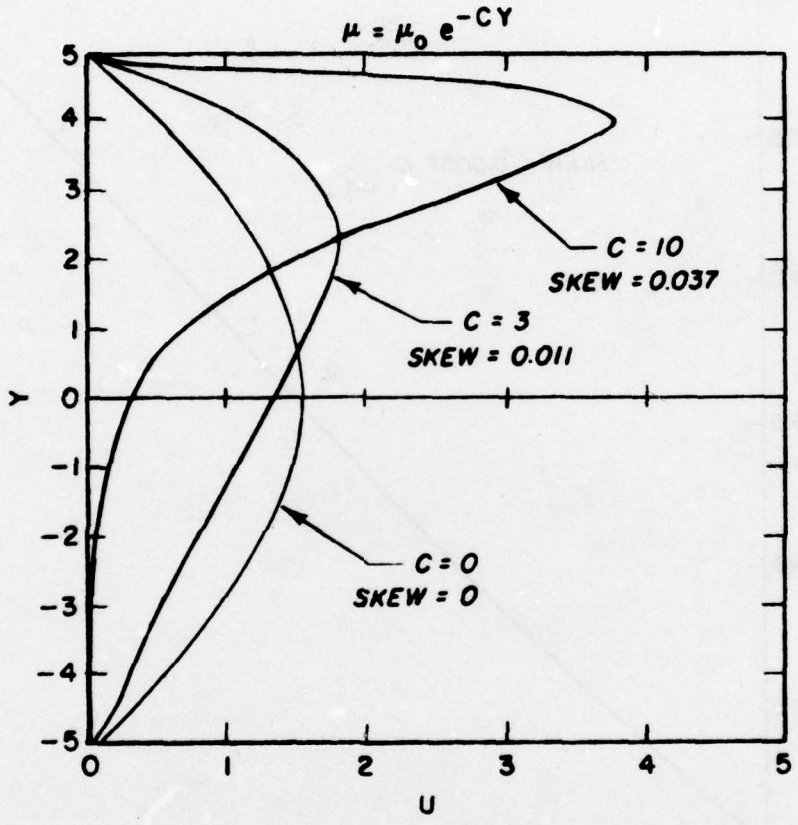

Fig. 14. Effect of C on skewness

CHAPTER VI

LINEAR VISCOSITY GRADIENT NEGLECTING BUOYANCY FORCES

Two models for describing viscosity stratified flow are presented in this chapter. The first model is a duct model which is used to illustrate some concepts for two-dimensional flow, to demonstrate the importance of the viscosity stratification term in the x-momentum equation, and to study the effect of including inertia terms in the model. The second model is a tank model which is used to investigate the effects of a fixed back wall on the flow.

Duct Flow

This model uses the boundary layer type assumption and the assumption that buoyancy forces and vertical velocity are negligible to reduce equations 13 and 5 to

$$\frac{\ell^3}{\mu_o}\frac{\partial p}{\partial x} = \frac{\mu}{\mu_o}\left(\frac{\partial^2 U}{\partial X^2} + \frac{\partial^2 U}{\partial Y^2}\right) + \frac{\ell}{\mu_o}\frac{\partial \mu}{\partial y}\frac{\partial U}{\partial Y} - \frac{q\rho_o}{\mu_o} U \frac{\partial U}{\partial Y} \tag{59}$$

$$\frac{\partial p}{\partial y} = 0 \tag{60}$$

Two-dimensionless groups are apparent in the above equation, the Reynolds number ($q\rho_o/\mu_o$) which indicates the magnitude of the inertial forces and the viscosity stratification number ($\ell/\mu_o\ \partial\mu/\partial y$) which indicates the importance of viscosity stratification. To be consistent with its uses later in the report, this number is defined as

$$\frac{A}{2} = \frac{\ell}{\mu}\frac{\partial \mu}{\partial y} \tag{61}$$

The equation becomes

$$P = 1 + \frac{A}{2} Y \left(\frac{\partial^2 U}{\partial X^2} + \frac{\partial^2 U}{\partial Y^2} \right) + \frac{A}{2}\frac{\partial U}{\partial Y} - PU \frac{\partial U}{\partial X} \tag{62}$$

where

$$P = \frac{\ell^3}{\mu_o}\frac{\partial p}{\partial x}$$

with boundary conditions

$$U(X, \pm 1/2) = 0 \tag{63}$$

$$U(0, Y) = \delta(0) = \text{Dirac delta function} \tag{64}$$

$$U(X_{max}, Y) = 1 \tag{65}$$

$$\int_{-1/2}^{1/2} U(X, Y)dY = 1 \tag{66}$$

The flow starts as uniform flow upstream and flows out through a sink at Y = 0. While the upstream boundary conditions and the neglect of buoyancy forces are somewhat unrealistic, this makes the model easy to use.

Note that there is no skewness at either the upstream or downstream boundary. With the lack of skew upstream, the skewness appears to die off near the upstream boundary. This is an anomoly of this model which is dealt with later.

Creeping Flow Results

The model was first solved with the inertial terms omitted using the techniques described earlier; that is, solving equation 59

for U(Y) then using the continuity boundary condition to get a new value for P.

The first effect studied was that of omitting the A/2 $\partial U/\partial Y$ term and allowing the varying viscosity to be accounted for in the $(1 + AY/2)$ $\nabla^2 U$ term. The results are shown for $x/x_{max} = \bar{X} = 1/2$ in Figure 15. Note that the skew is almost twice as large for the case in which the viscosity stratification is accounted for using both terms. The A/2 $\partial U/\partial Y$ term will be retained for the remainder of the study.

The relationship of skew vs. distance from sink is shown for two values of A in Figure 16. The skewness increases with A much as in the one-dimensional cases except that very near the sink the profile becomes symmetric. This accounts for the decreased skew near the sink.

The model was also run for a variety of length to depth aspect ratios. The profile for different values of X were virtually identical as long as they were calculated away from the upstream boundary. For the remaining model runs in this section the aspect ratio x_{max}/ℓ will be set to 10, since this is consistent with the assumption $V \ll U$ and yet should not require numerous or large grid cells.

The velocity profile development from the uniform flow upstream to the narrow withdrawal layer at the sink is shown in Figure 17. Note that once the flow is away from the symmetric upstream and downstream boundary condition, skewness arises. In Figure 17 the upstream boundary is at x = 10.

Effect of Reynolds Number

The Reynolds number was increased in the model to account for

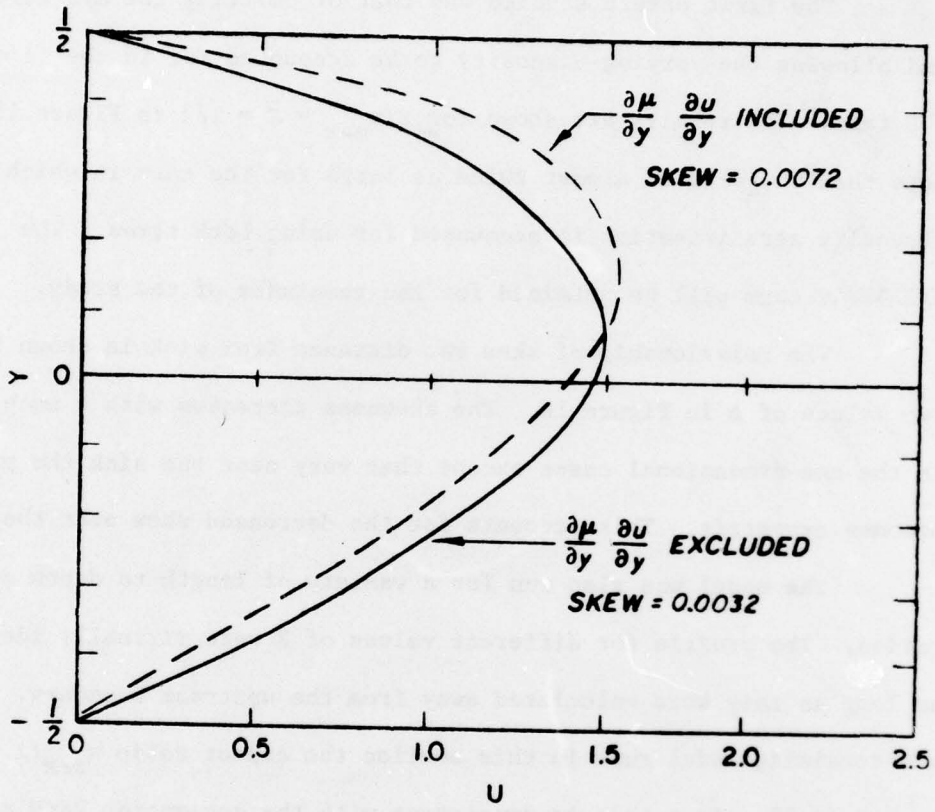

Fig. 15. Effect of ∂u/∂y term

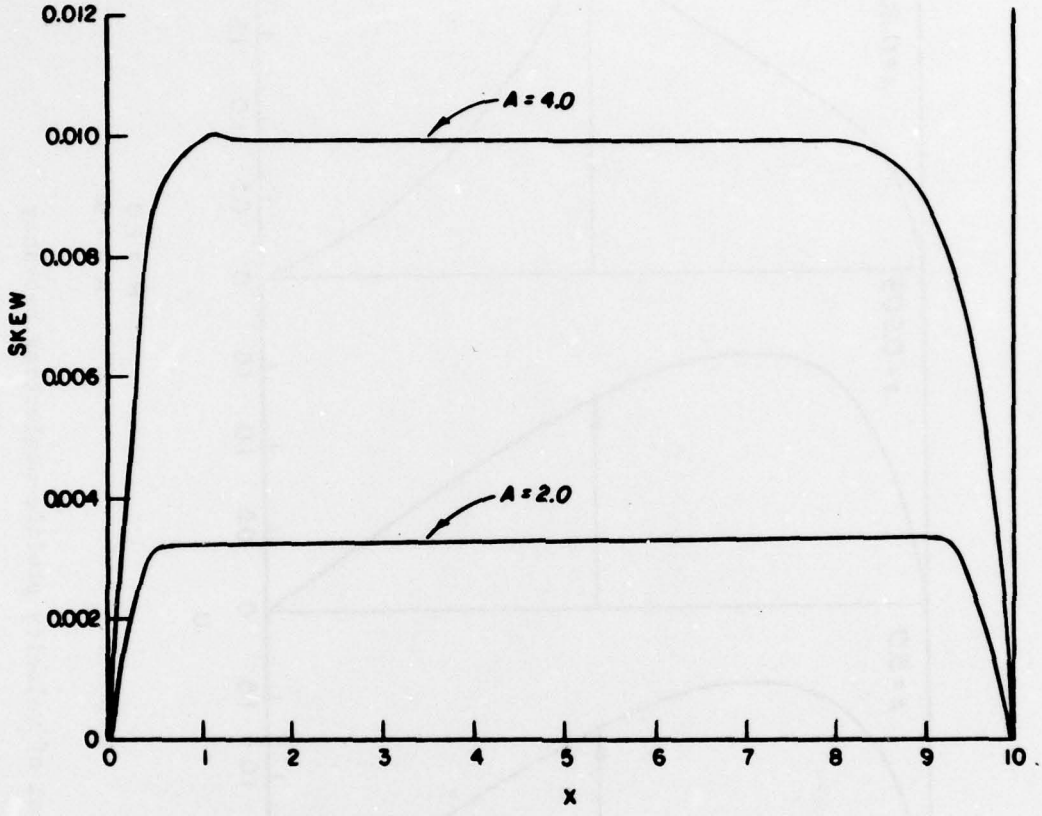

Fig. 16. Effect of x-coordinate on skew

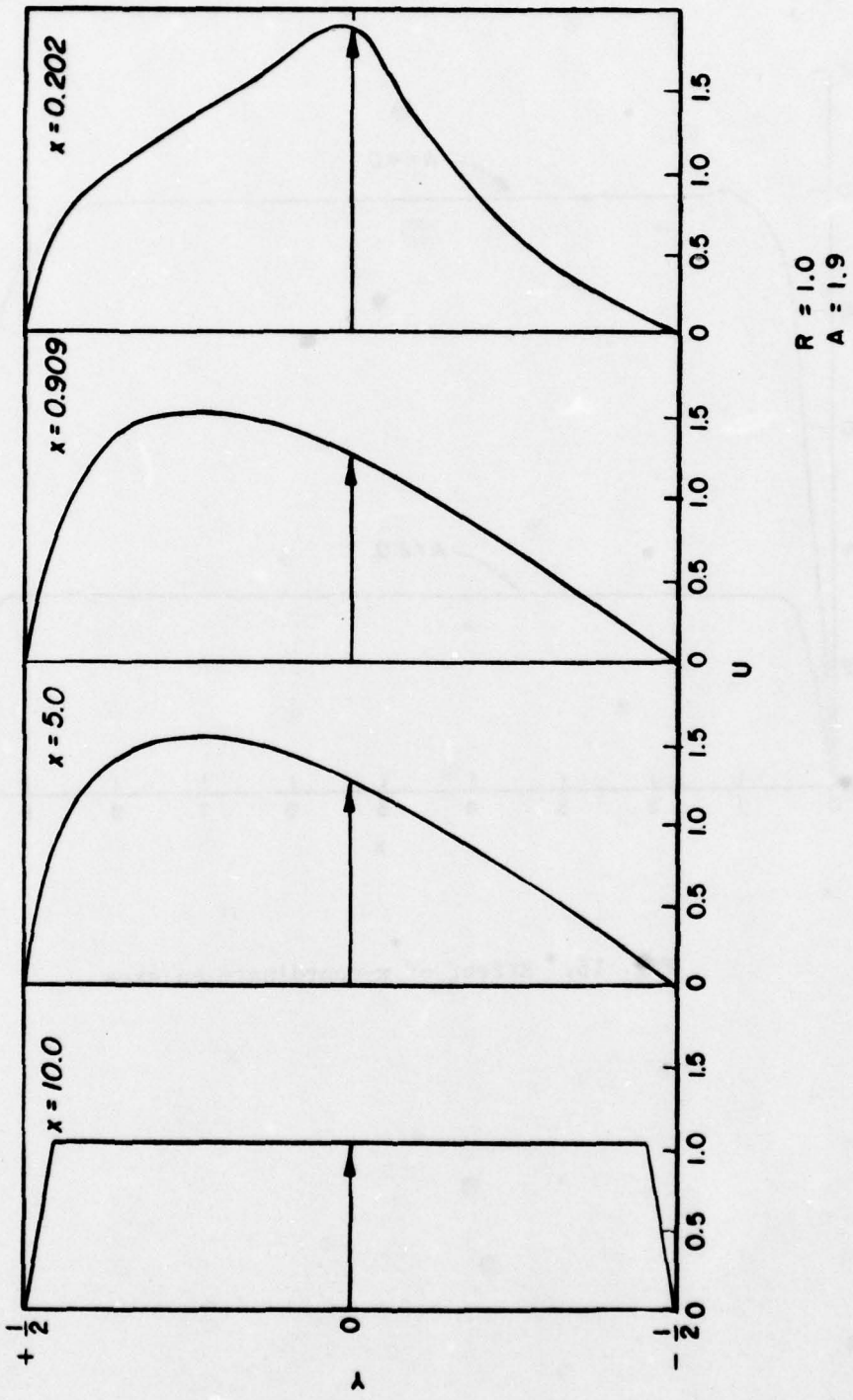

Fig. 17. Development of velocity profile-neglecting buoyancy

inertial forces. It was found that for Reynolds numbers less than 100, inertial forces had no effect on the flow. It was only as the Reynolds number approached 1000 that the profiles began to change dramatically. The velocity profile became blunter and the skewness decreased dramatically. Because of this result, it was concluded that the Reynolds numbers to be investigated in this study would be 0(100) or less. In general, the laboratory runs would be for Reynolds number between 10 and 0.1.

Tank Boundary Conditions

The equations were then solved with boundary conditions corresponding to that of a closed end tank with fixed back wall. In this case the boundary conditions were

$$U(0,Y) = \delta(0) \tag{67}$$

$$U(X, \pm 1/2) = 0 \tag{68}$$

$$U(X_{max}, Y) = 0 \tag{69}$$

$$q_x = \int_{-1/2}^{1/2} U(X,Y)dX = 1 - \frac{x}{x_{max}} \tag{70}$$

The solution in terms of streamlines is shown in Figure 18. The growth of the velocity profile is shown in Figure 19. The profiles show more skew in the tank case since the artificial upstream boundary condition of uniform flow was not imposed.

This indicates that there should be skew even when the flow was virtually zero at the back wall. The importance of the back wall was investigated at this point in the study because it is impossible to

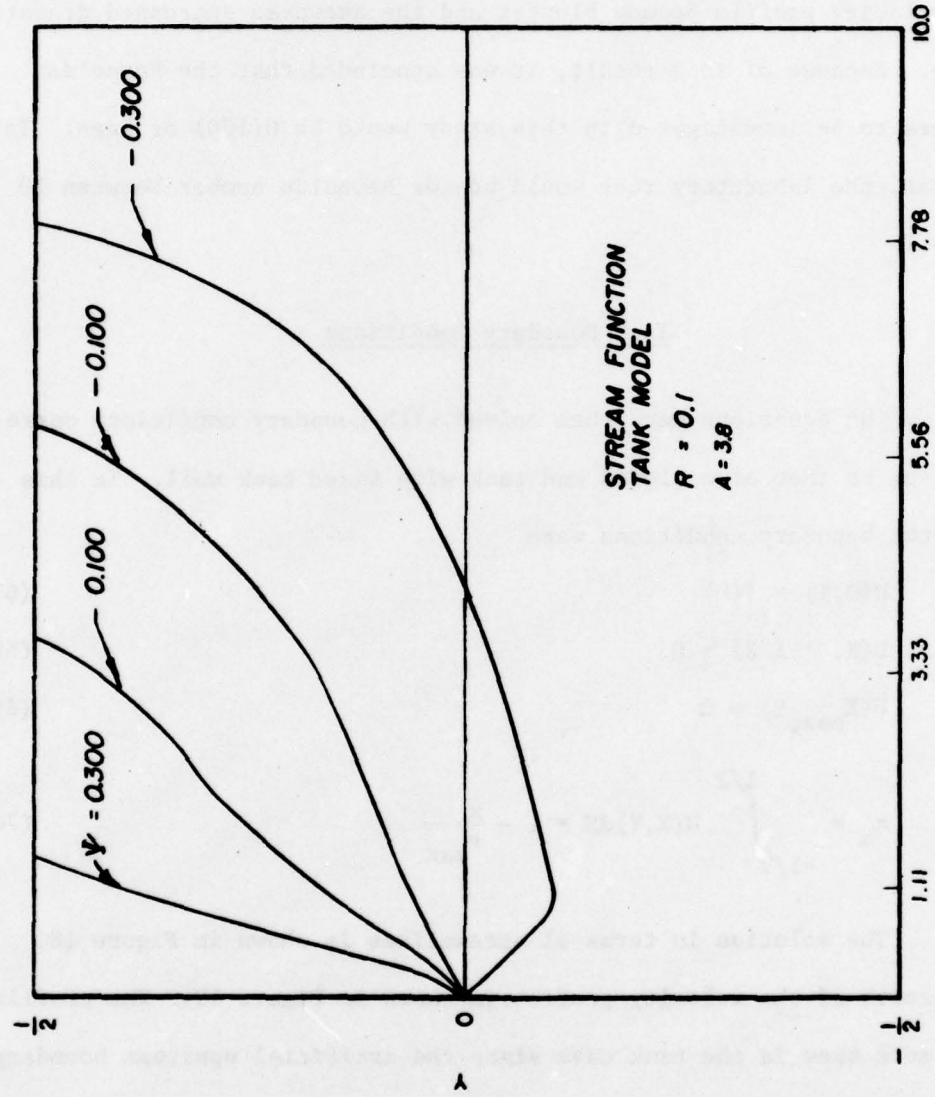

Fig. 18. Streamlines for tank model

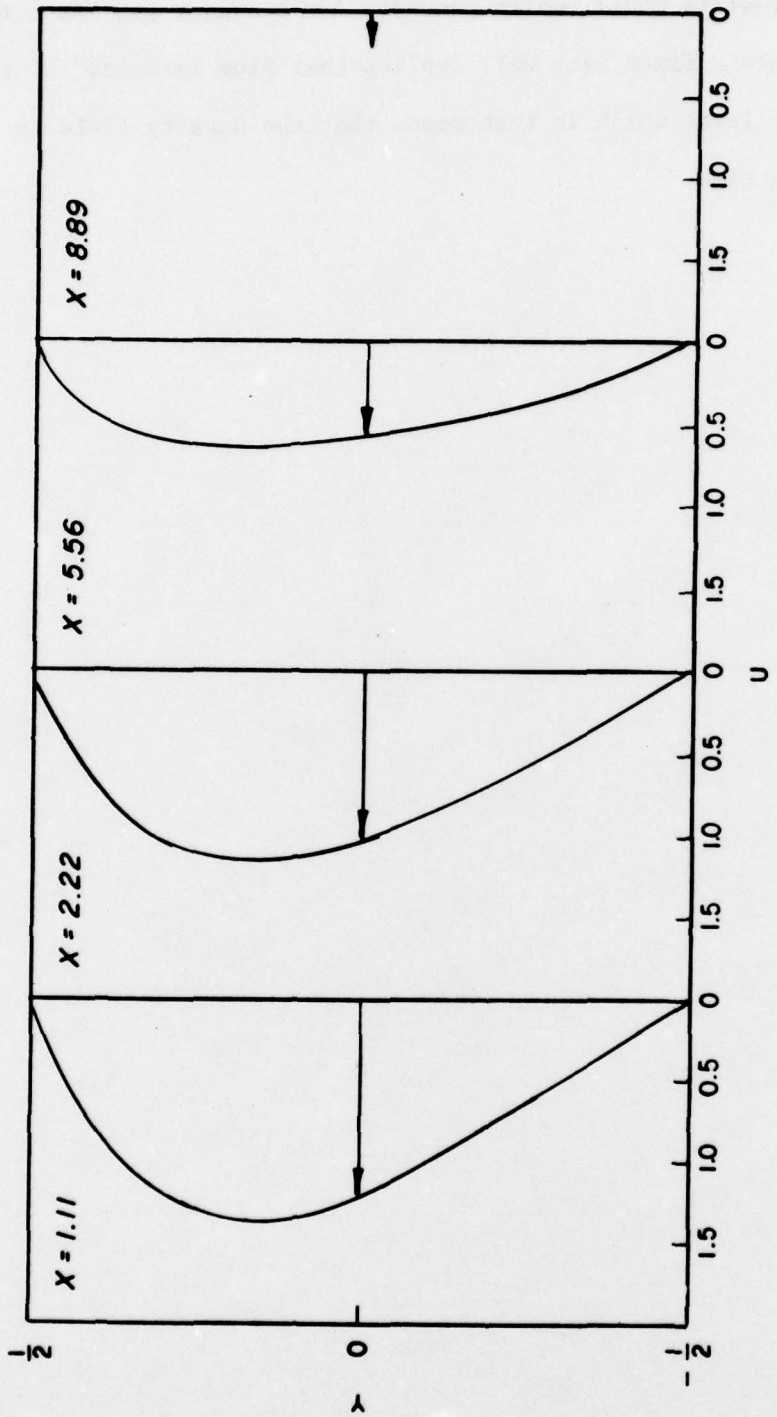

Fig. 19. Development of velocity profile - tank model

have a steady-state model, which accounts for buoyancy and has a fixed back wall since a fixed back wall implies that flow is caused by the falling water level which in turn means that the density field is changing with time.

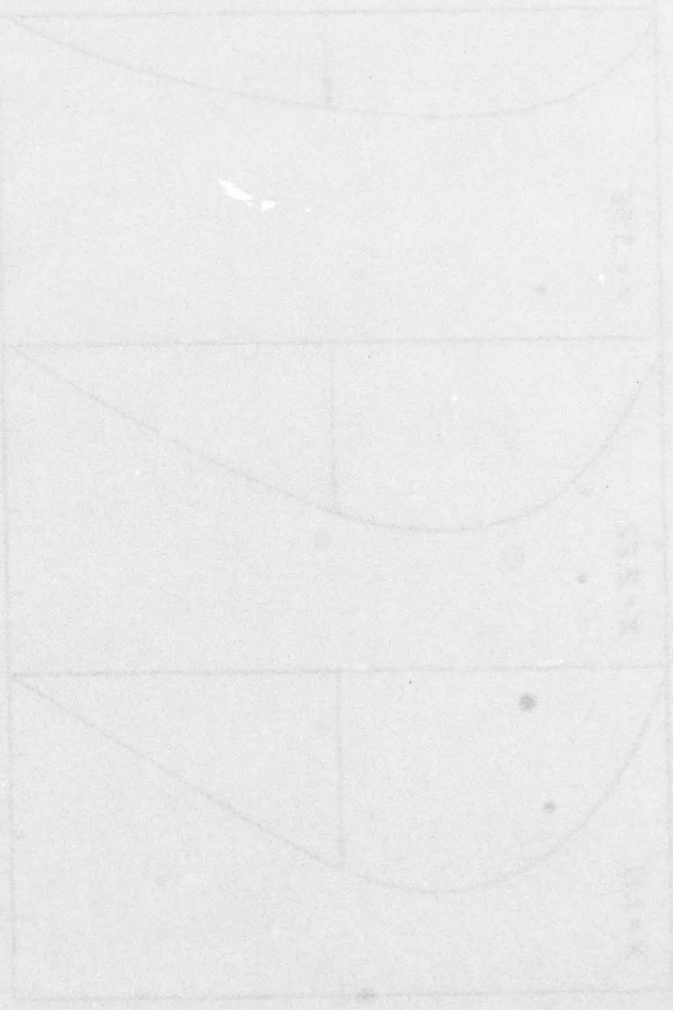

CHAPTER VII

LINEAR VISCOSITY GRADIENT WITH BUOYANCY FORCES

Buoyancy forces have not been accounted for in the velocity profiles determined in Chapters IV and VI. The equations developed in Chapter III are solved below and the skewness is given for an array of viscosity and density gradients. Criteria for existence of skewness are then derived.

Model Development

Equation 26 can be rearranged to give (for $\partial^2\mu/\partial y^2 = 0$)

$$\frac{\mu}{\mu_o}\frac{\partial^4\psi}{\partial Y^4} + A\frac{\partial^3\psi}{\partial Y^3} + B\frac{\partial\psi}{\partial X} = 0 \qquad (71)$$

where

$$A = \frac{2\ell}{\mu_o}\frac{\partial\mu}{\partial Y}$$

$$B = \frac{g\ell^4\varepsilon\rho_o}{q\mu_o}$$

The first term in the above equation represents viscous forces, the second viscosity stratification and the third buoyancy. The dimensionless group A represents the ratio of viscosity stratification to viscous forces. The group B can be written

$$\left(\frac{q\rho_o}{\mu_o}\right)\left(\frac{\ell^4 g\varepsilon\rho_o}{q^2}\right) = \frac{\text{Reynolds Number}}{(\text{Densimetric Froude Number})^2} \qquad (72)$$

which is actually a balance between buoyancy and viscous forces.

To solve the above equation, four boundary conditions on Y and one on X must be specified. The boundary condition on X is that all flow passes through the origin

$$\Psi(0,Y) = \begin{cases} -1/2 & , \quad Y>0 \\ 0 & , \quad Y=0 \\ 1/2 & , \quad Y<0 \end{cases} \tag{73}$$

Two conditions on Y are used to insure continuity

$$\Psi(X, \pm 1/2) = \mp 1/2 \tag{74}$$

The other two boundary conditions on Y will be used to indicate whether or not the flow is slipping along the top and bottom of the duct. They are

$$\frac{\partial^2 \Psi}{\partial Y^2}(X, \pm 1/2) = 0 \quad , \text{ slip}$$

$$\frac{\partial \Psi}{\partial Y}(X, \pm 1/2) = 0 \quad , \text{ no slip} \tag{75}$$

The above equations are solved numerically as described in Chapter III.

Figures 20, 21, and 22 give the solution to the slip problem for different values of B. Note that as B increases, the withdrawal layer becomes smaller as buoyancy forces tend to inhibit viscous momentum transport. This can be deduced from the equations by noting that as B becomes large, the solution reduces to

$$\frac{\partial \Psi}{\partial X} = 0 \tag{76}$$

which corresponds to an infinitely thin withdrawal layer with infinite velocity.

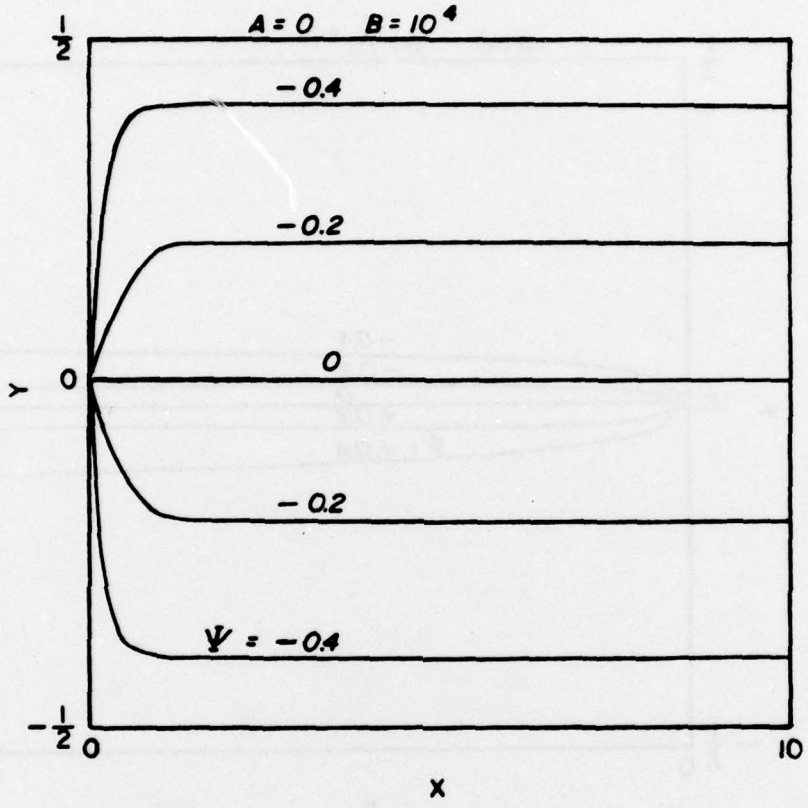

Fig. 20. Viscosity-dominant solution

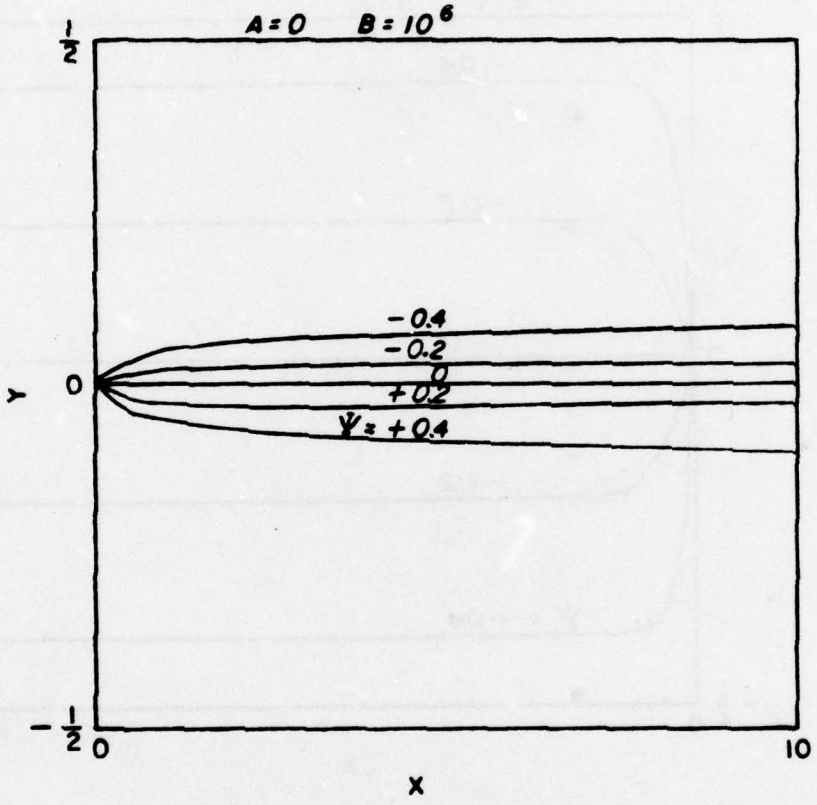

Fig. 21. Viscosity-buoyancy of similar magnitude

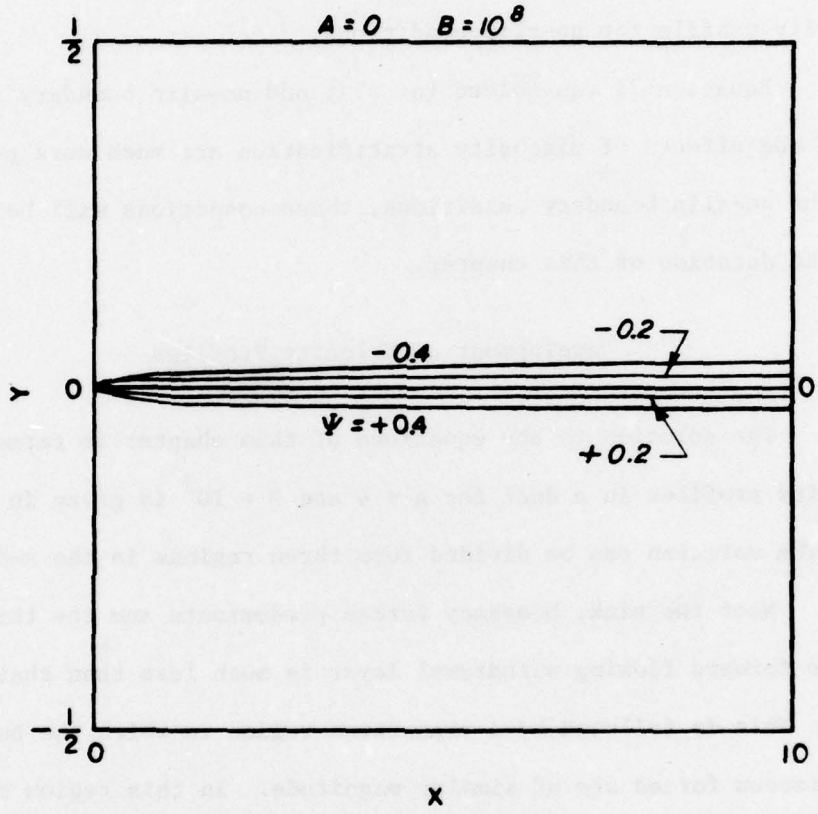

Fig. 22. Buoyancy-dominant solution

As B becomes small, the solutions approach those of the previous chapter. As B becomes small for A = 0, the solution corresponds to uniform flow upstream for slip boundary conditions and to a parabolic velocity profile for no-slip conditions.

Equation 71 was solved for slip and no-slip boundary conditions. Since the effects of viscosity stratification are much more pronounced for the no-slip boundary conditions, those conditions will be employed for the duration of this chapter.

Development of Velocity Profiles

The solution to the equations of this chapter in terms of velocity profiles in a duct for A = 4 and B = 10^3 is given in Figure 23. The solution can be divided into three regions in the x-direction.

Near the sink, buoyancy forces predominate and the thickness of the forward flowing withdrawal layer is much less than that of the duct. This is followed by a transition region in which the buoyancy and viscous forces are of similar magnitude. In this region the velocity profile begins to drag along the boundaries.

Far from the sink the viscous forces predominate. The streamlines become parallel, the pressure gradient becomes hydrostatic, and the velocity profiles approach those given in the one-dimensional solutions.

Skewness of Velocity Profiles

The skewness of the velocity profile is somewhat irrelevant in the buoyancy region since it represents the importance of viscosity

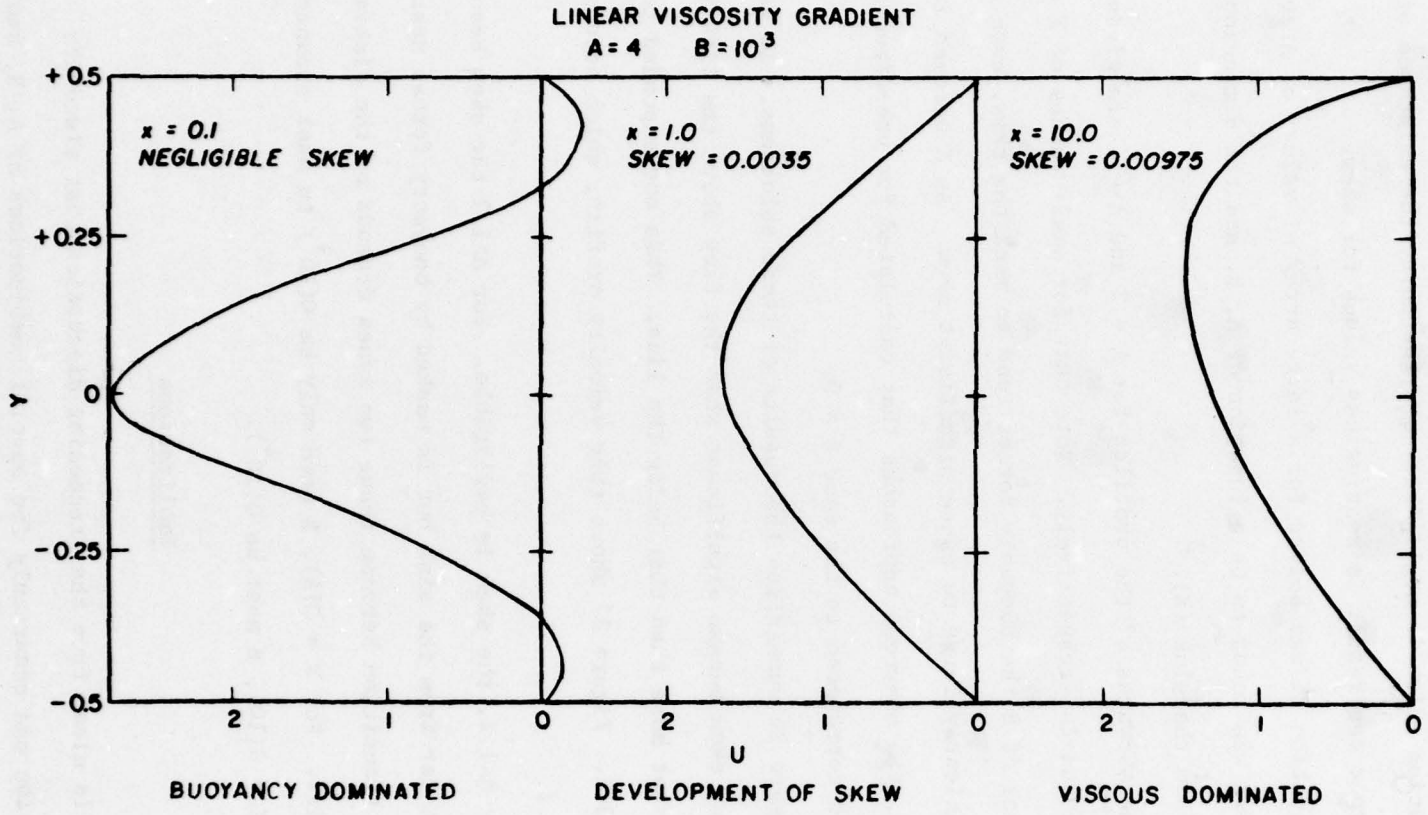

Fig. 23. Development of velocity profile-linear gradient

stratification which is negligible. Furthermore, the existence of a backflow zone can result in meaningless values for skew.

Equation 71 was solved for a large array of values of A and B. The skewness was found to be a function of A, B, and the dimensionless distance from the sink (X).

The skewness of the profiles for A = 2 and A = 4 are given in Figures 24 and 25, respectively. Note that for small values of X and large values of B the buoyancy forces tend to mask the skew, even though A is sufficiently large to cause significant skew. As X becomes large or B small, the skewness approaches that calculated for one-dimensional flows which correspond to the case B = 0.

Figure 26 summarizes the results of these solutions. It was decided that skew became significant when the flow above the line Y = 0 was 20 percent more than that below the line. This corresponded to skew of 0.002. Figure 27 shows this velocity profile, which occurs when A = 1.2.

For A<1.2, the skew is negligible. For A>1.2 the skew becomes significant far from the sink but is masked by buoyancy forces near the sink. The transition between these two zones depends on the distance from the sink. For X = O(1), B need only be $O(10^3)$ to mask skewness, while for X = O(10), B must be $O(10^4)$.

Implications

It is clear from the preceeding discussion that viscosity stratification can occur only for special combinations of A, B, and X. In order to derive a simple formula to determine if skew is greater than

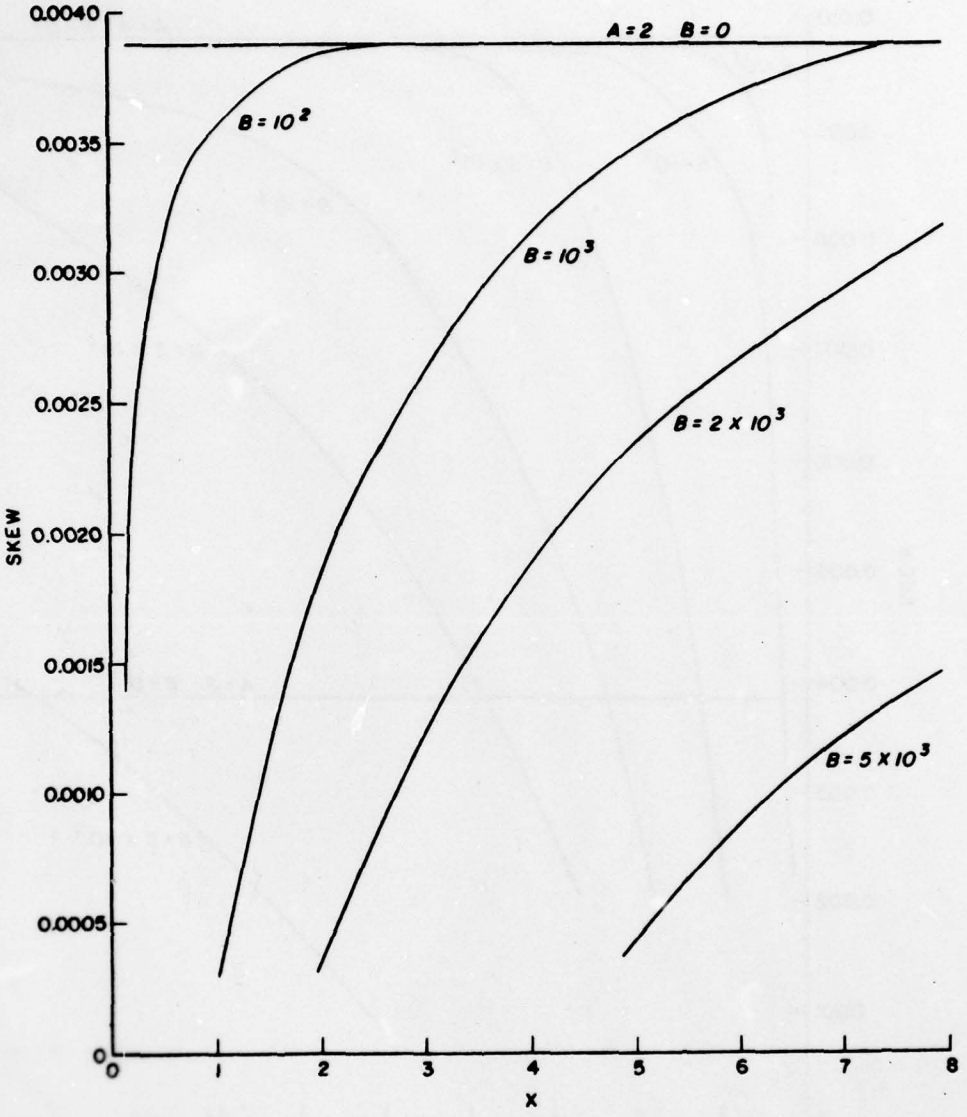

Fig. 24. Skew plot, A = 2

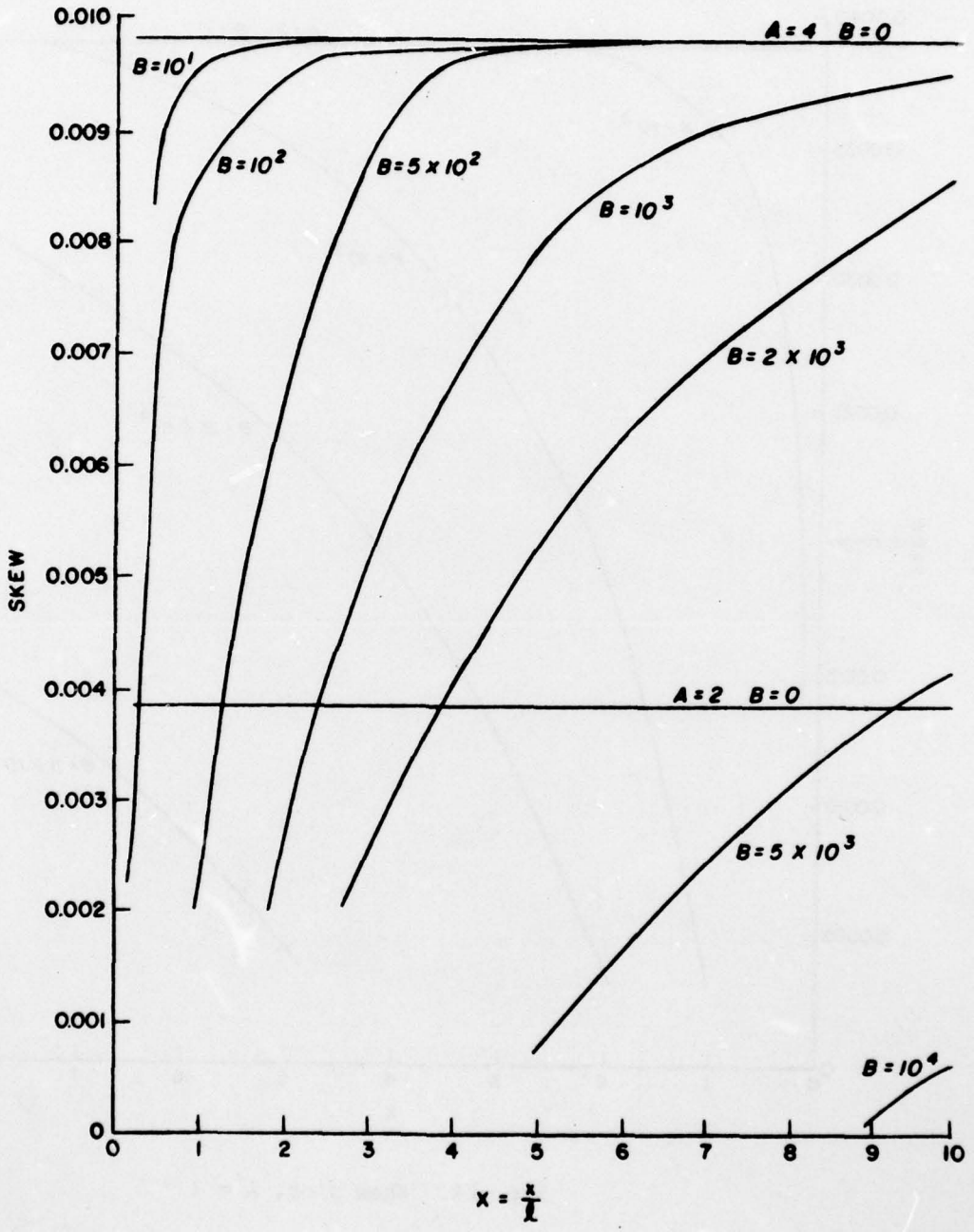

Fig. 25. Skew plot, A = 4

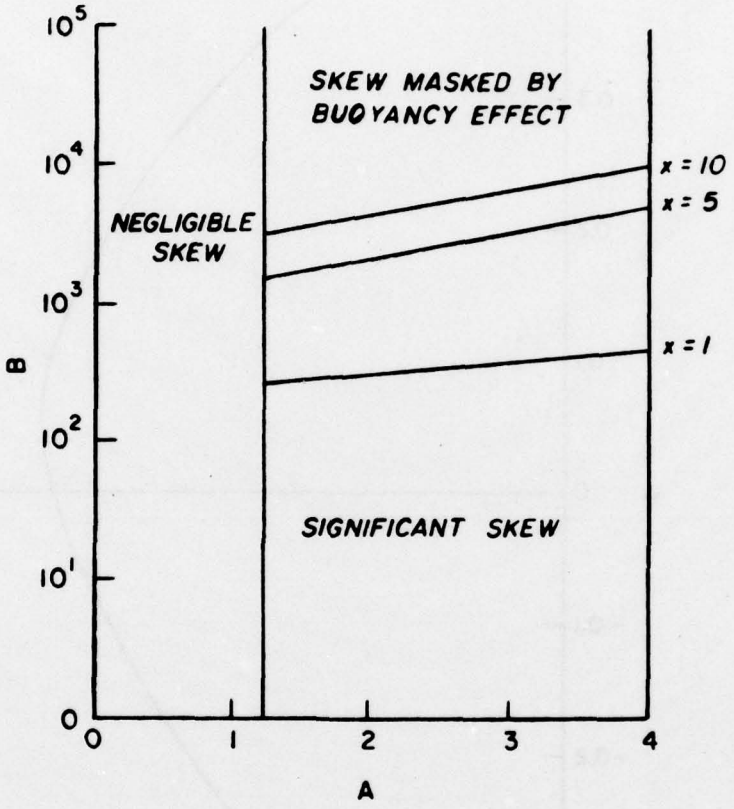

Fig. 26. Criteria for skewness, linear viscosity gradient

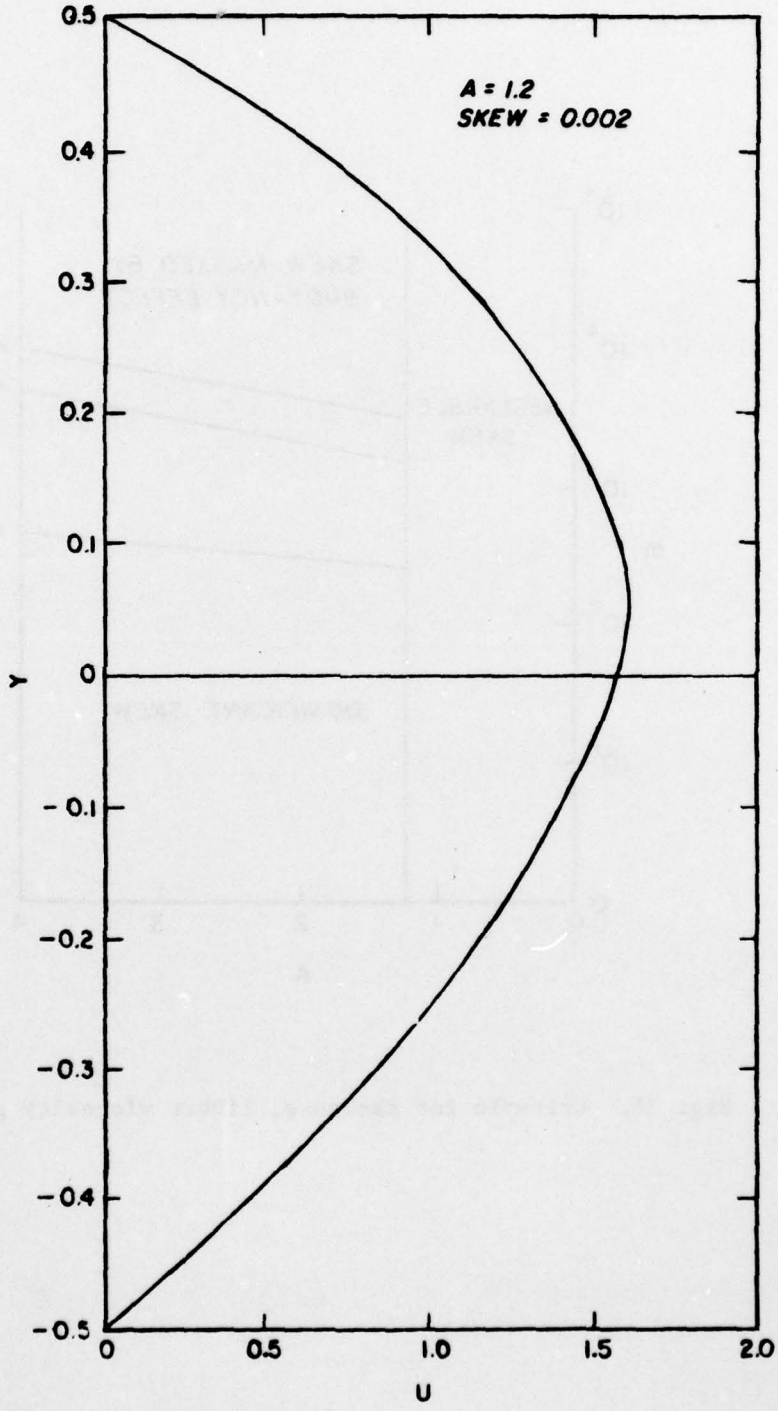

Fig. 27. Example of skew = 0.002

0.002, A, B, and X were plotted to gain insight into their interrelationship for the critical value of skew.

For a constant value of A, both B and X are plotted as straight lines on log-log paper. A multiple regression program was used to determine the equation for these lines and it was found that

$$B = 0.572(A-1.2)^{1/2}X^{3/4} \tag{77}$$

fit the data with index of determination 0.895.

To give additional insight into the criteria for viscosity stratification, the definitions of A, B, and X were substituted into equation 77 and the equation was solved for $\partial\mu/\partial y$. The criteria for viscosity stratification to occur is

$$\left|\frac{\partial\mu}{\partial y}\right| > 3 \times 10^{-6} \frac{\ell^{17/2}}{x^{3/2}\mu_o} \left(\frac{g\varepsilon\rho_o}{q}\right)^2 + \frac{6\mu_o}{\ell} \tag{78}$$

The above relation shows that viscosity stratification will occur for small values of the density gradient, and small ducts or at large distances upstream of the sink, as is shown in the laboratory results in Chapter XI.

CHAPTER VIII

LOG VISCOSITY GRADIENT WITH BUOYANCY FORCES

In this chapter, the motion equations are solved for the log viscosity gradient. From the solution, criteria for the existence of viscosity stratification are developed.

Model Development

As described earlier, the viscosity gradient for the log viscosity profile can be given by

$$\mu = \mu_o e^{-c_1 y} \tag{79}$$

where c_1 is the "slope" of the gradient on semi-log graph paper, and μ_o is the viscosity at $y = 0$. Defining the dimensionless number $C = c_1 \ell$, the dimensionless viscosity and its derivatives become

$$\mu/\mu_o = e^{-CY} \tag{80}$$

$$\frac{\ell}{\mu_o}\frac{\partial \mu}{\partial y} = -Ce^{-CY} \quad \text{or} \quad C = -\frac{\ell}{\mu}\frac{\partial \mu}{\partial y} \tag{81}$$

$$\frac{\ell^2}{\mu_o}\frac{\partial^2 \mu}{\partial y^2} = C^2 e^{-CY} \tag{82}$$

Substitution of the above derivatives into equation 26 from Chapter III yields, after multiplying through by e^{CY}

$$\frac{\partial^4 \Psi}{\partial Y^4} - 2C\frac{\partial^3 \Psi}{\partial Y^3} + C^2\frac{\partial^2 \Psi}{\partial Y^2} + B\, e^{CY}\frac{\partial \Psi}{\partial X} = 0 \tag{83}$$

As in the case of the linear viscosity gradient, the first term represents viscous forces, the next two viscosity stratification and the final term buoyancy.

Equation 83 was solved with the no-slip boundary conditions

$$\frac{\partial \Psi}{\partial Y}(X, \pm 1/2) = 0 \tag{84}$$

$$\Psi(X, \pm 1/2) = \mp 1/2 \tag{85}$$

$$\Psi(0,Y) = \begin{cases} -1/2 & , \quad Y>0 \\ 0 & , \quad Y=0 \\ 1/2 & , \quad Y<0 \end{cases} \tag{85}$$

The velocity profiles behaved similarly to those with linear gradients (i.e., buoyancy forces predominating near sink, viscous forces predominating far from sink). For B = 0, the solution approached that obtained for the one-dimensional case. This is shown in Figure 28.

Skewness of Profiles

The skew of the velocity profiles were calculated for an array of values for B, C, and X. These are presented in Figures 29, 30, and 31. The skewness approached that of the one-dimensional solution for large values of X and small values of B.

A plot of B vs. C showing zones in which viscosity stratification can occur is given in Figure 32. Combinations of C, B, and X that yield values of critical skew (0.002) were related by

$$B = 555(C - 0.54)^{0.30} X^{1.03} \tag{87}$$

with index of determination 0.988. Approximating the exponent on X as

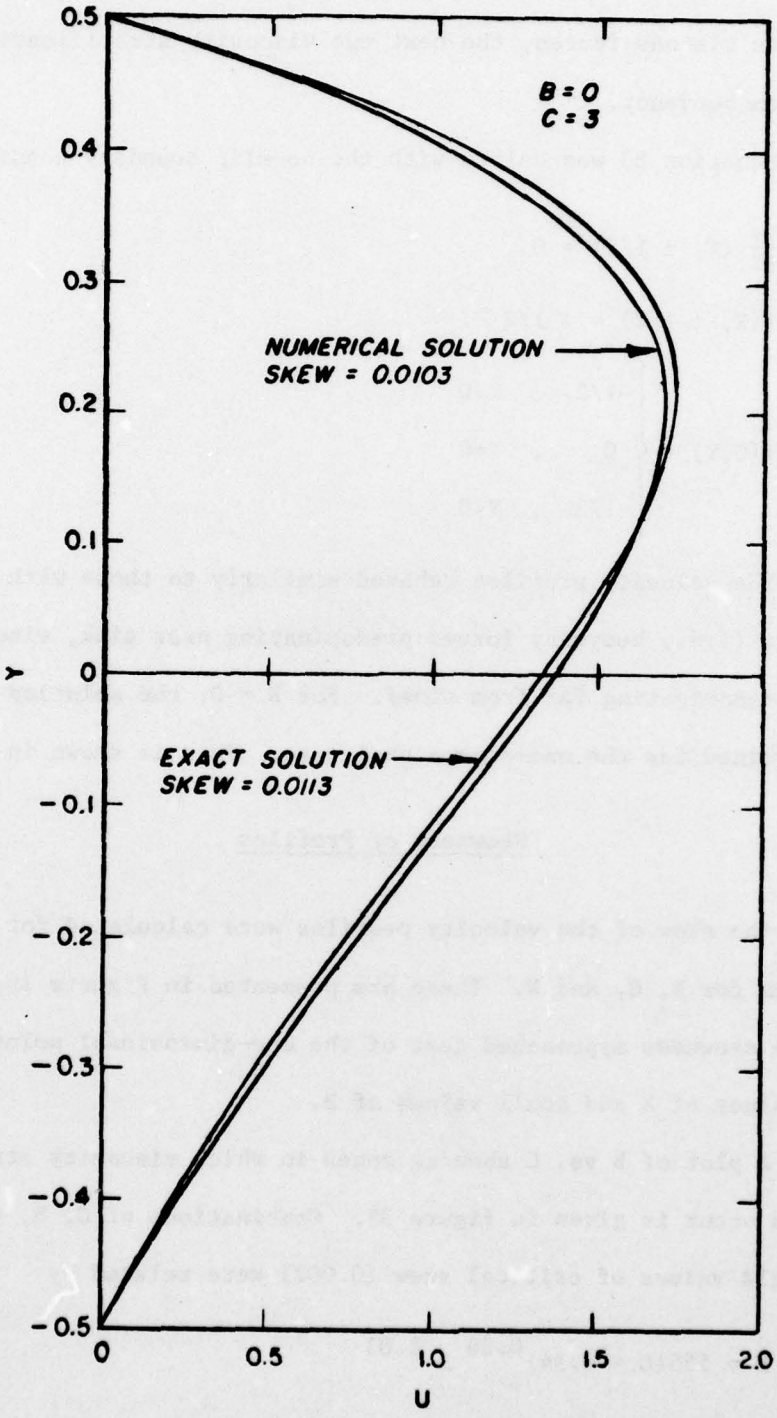

Fig. 28. Exact one-dimensional vs. two-dimensional solution

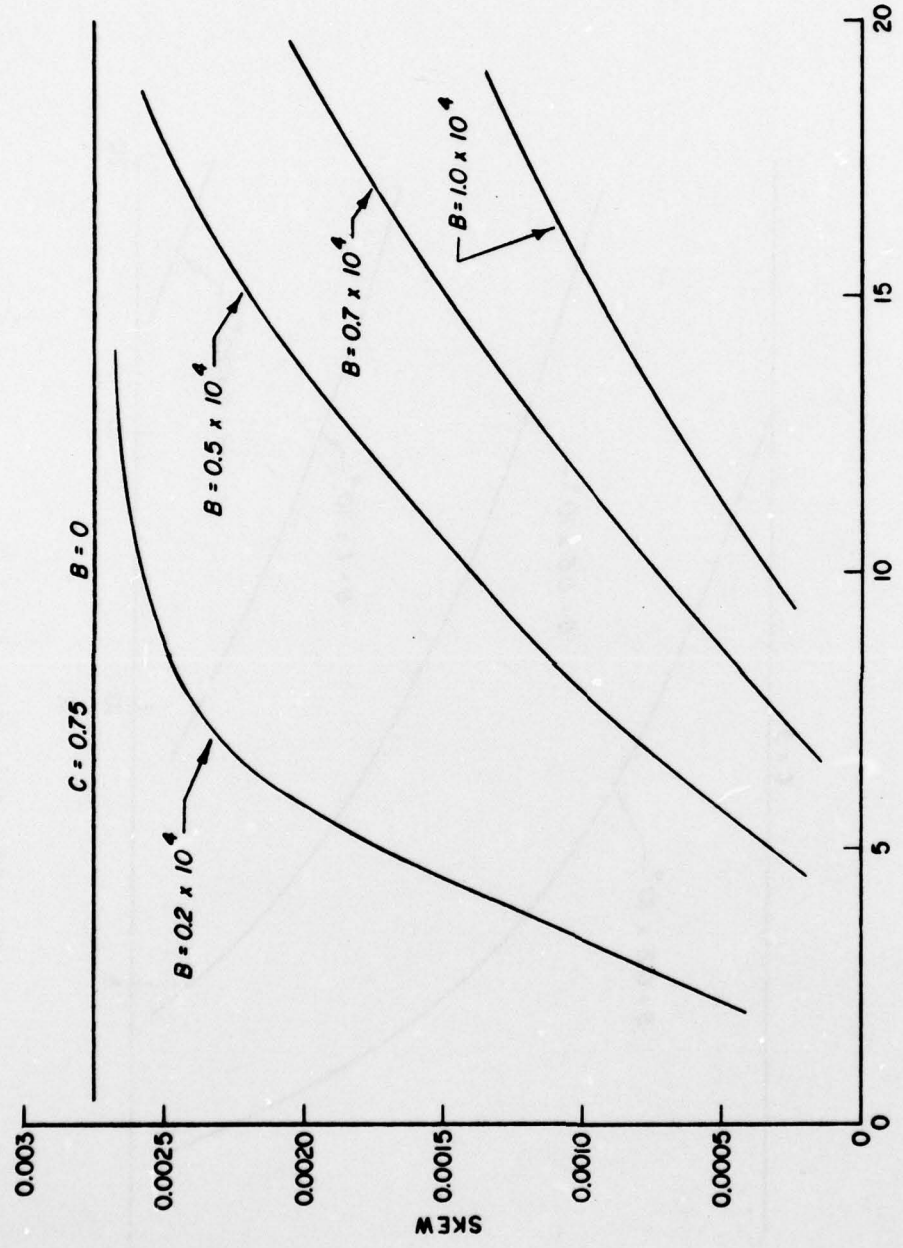

Fig. 29. Skew plot, C = 0.75

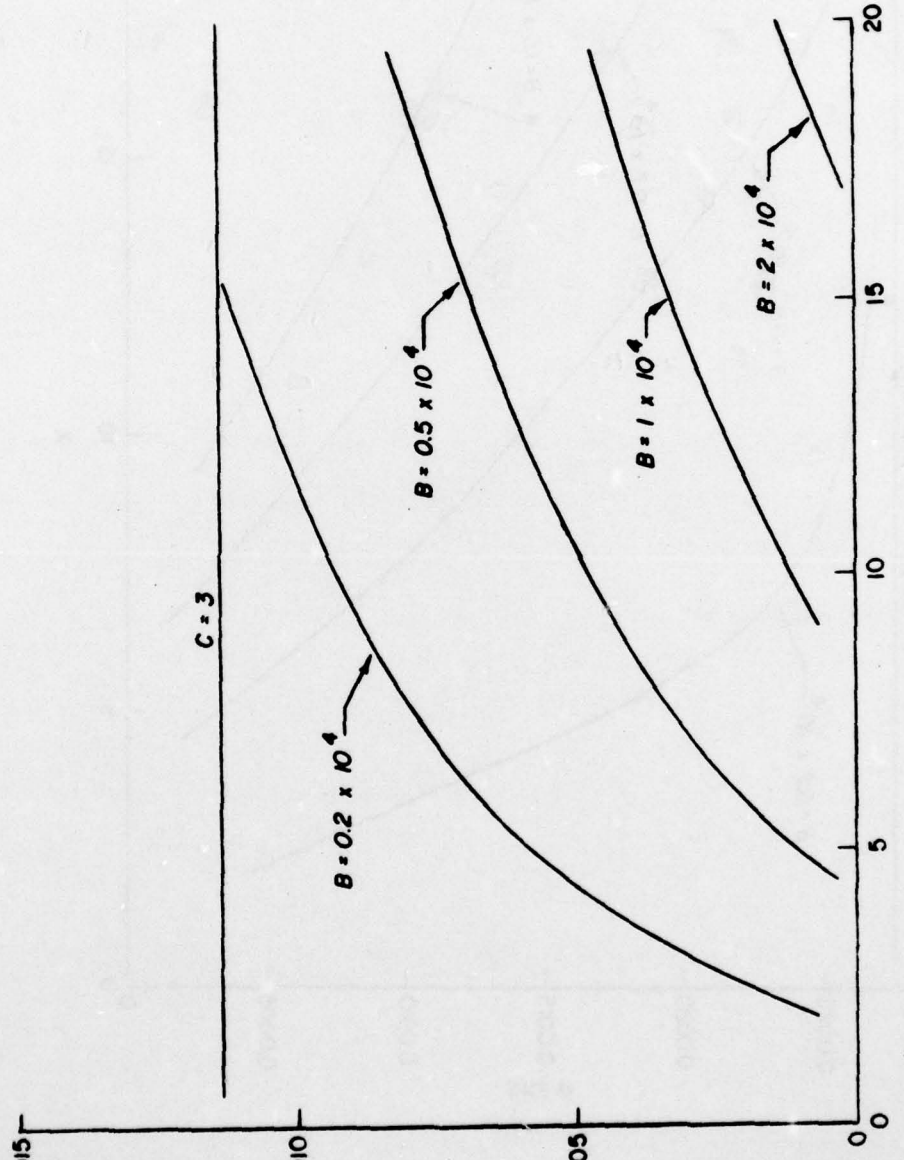

Fig. 30. Skew plot, C = 3.0

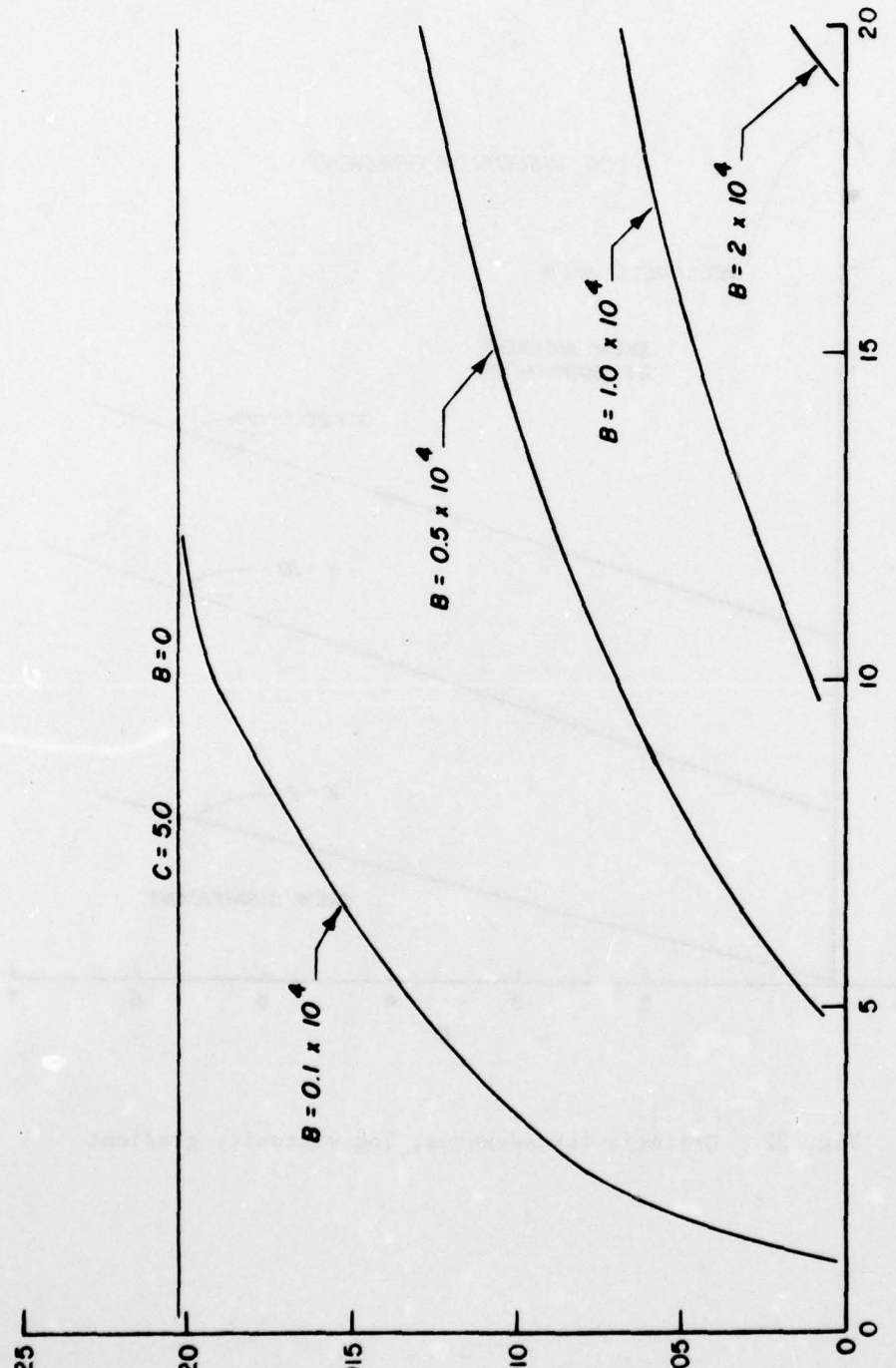

Fig. 31. Skew plot, C = 5.0

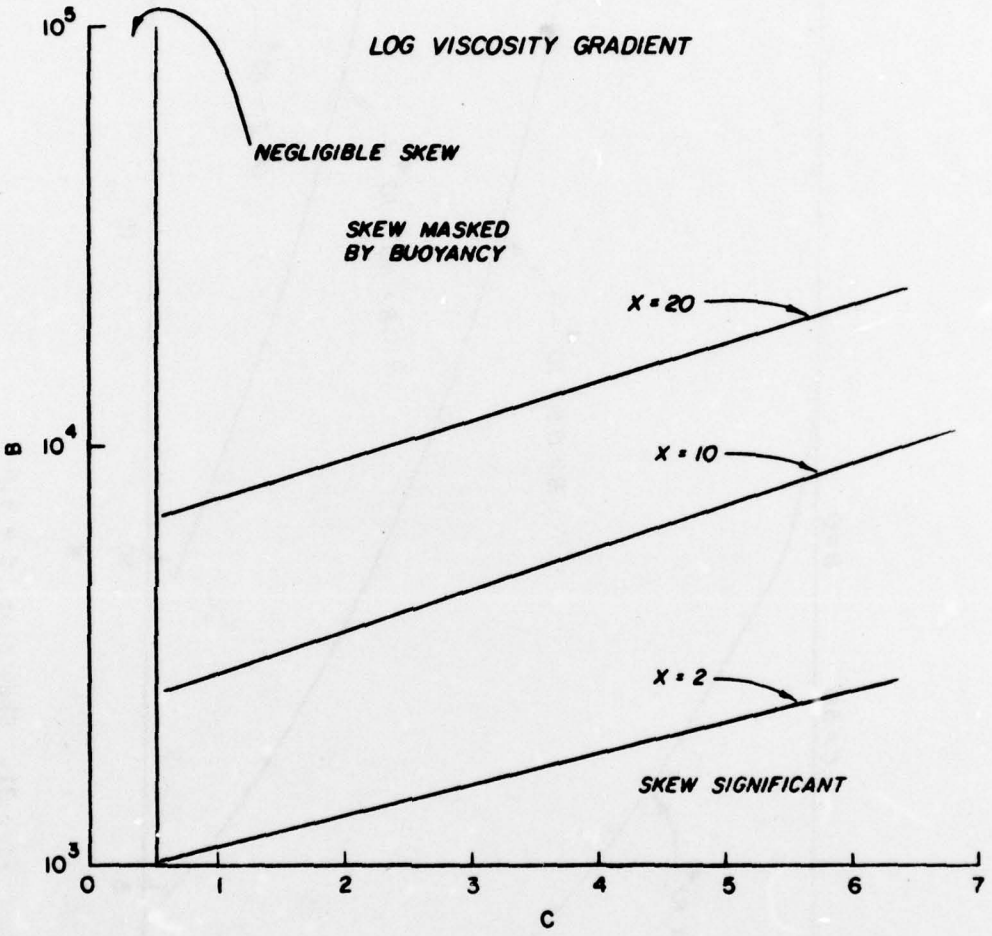

Fig. 32. Criteria for skewness, log viscosity gradient

1.0 and substituting for the definitions of B, C, and X gives the criteria for skewness as

$$\left|\frac{\partial \mu}{\partial y}\right| > \frac{\mu}{\ell}\left[\left(\frac{\ell^5 g\varepsilon\rho_o}{555\ q\mu_o x}\right)^{3.3} + 0.54\right] \tag{88}$$

Significant skewness will therefore occur for large distances from the sink when the viscosity gradient is large.

Incipient Skewness

In the case of the linear viscosity gradients, the flow developed from being buoyancy dominated to viscous dominated over a fairly short transition region. In the case of a log viscosity gradient this transition zone is much larger.

The existence of the transition zone is due partly to the fact that the fluid, being more viscous near the bottom, "grabs onto" the bottom boundary much sooner than it grabs onto the top boundary. There is still backflow in the transition zone so the skewness coefficient is not a good indicator of the effects of the viscosity stratification.

This skewing of the profile in the transition zone where viscous forces dominate in the bottom of the flume and buoyancy forces dominate in the top will be defined as "incipient skewness." The four graphs in Figure 33 show how the flow develops from buoyancy dominated with no skewness, to incipient skewness and finally fully developed skewness.

Figure 34 shows schematically how the zone of incipient skewness relates to the buoyancy and viscous zones. The boundaries between the zones are not intended to imply that this is their actual shape.

Streamlines are plotted in Figure 35 to illustrate the

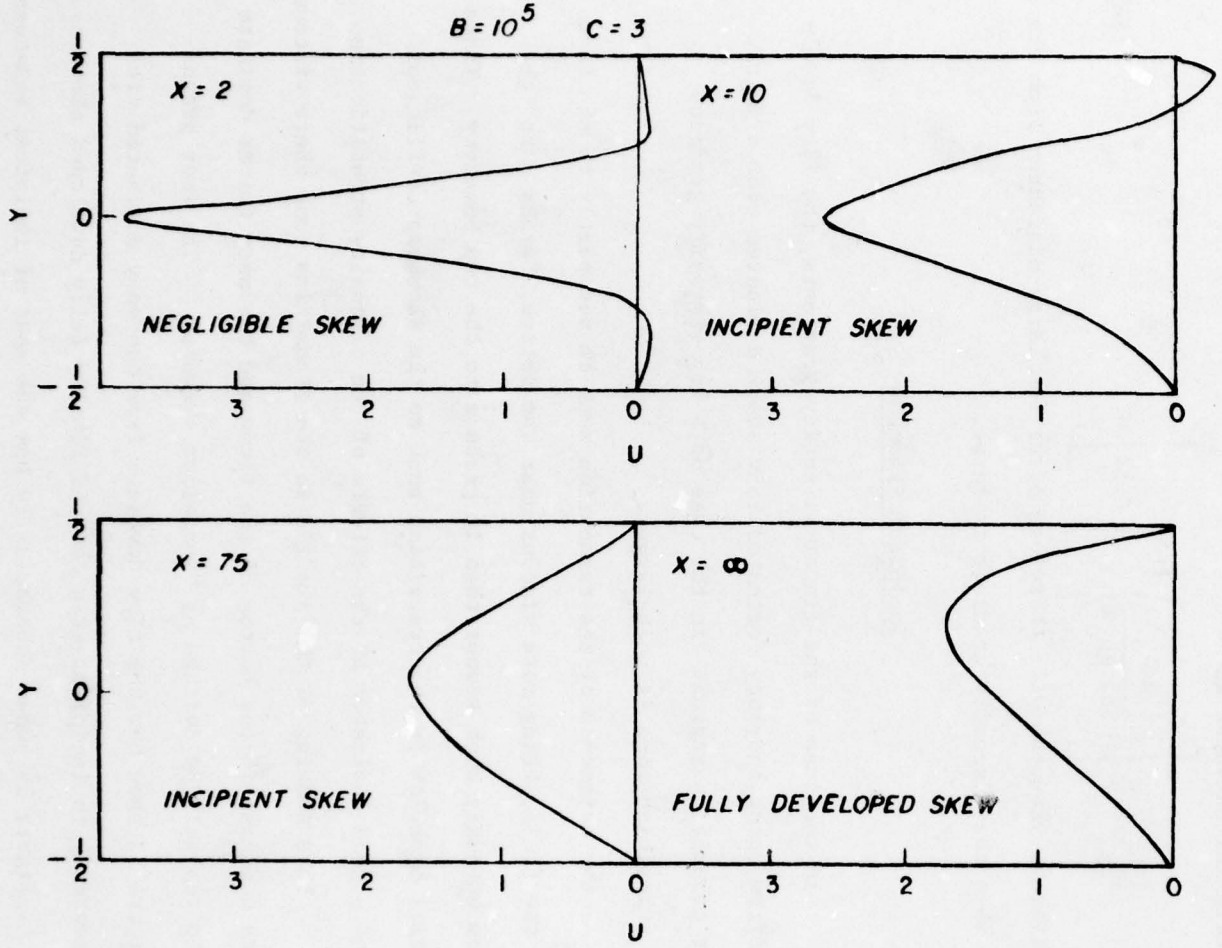

Fig. 33. Development of velocity profile-log gradient

AD-A073 371 ARMY ENGINEER WATERWAYS EXPERIMENT STATION VICKSBURG MS F/G 13/2
PROPERTIES OF STEADY, VISCOSITY-STRATIFIED FLOW TO A LINE SINK.(U)
JUL 79 T M WALSKI

UNCLASSIFIED WES-TR-EL-79-6 NL

2 OF 3
AD
A073371

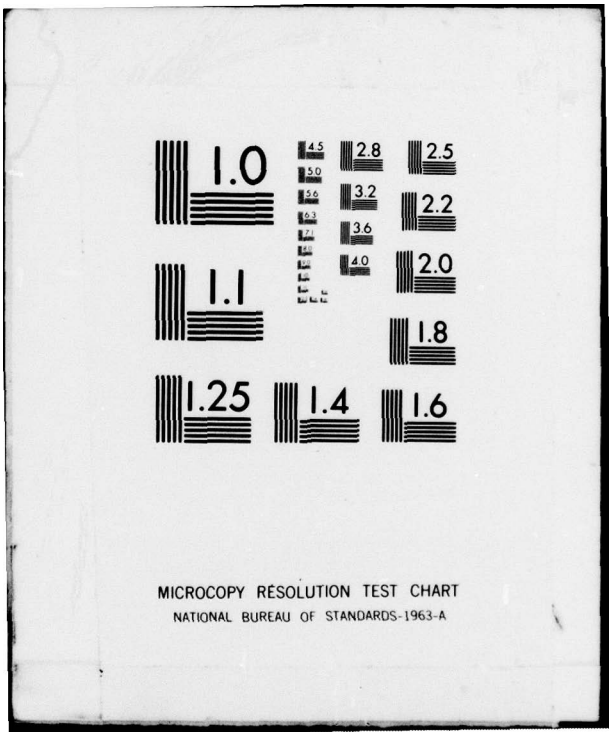
1.0
1.1
1.25
1.4
1.6
1.8
2.0
2.2
2.5
2.8
3.2
3.6
4.0
4.5
5.0
5.6
6.3
7.1
MICROCOPY RESOLUTION TEST CHART
NATIONAL BUREAU OF STANDARDS-1963-A

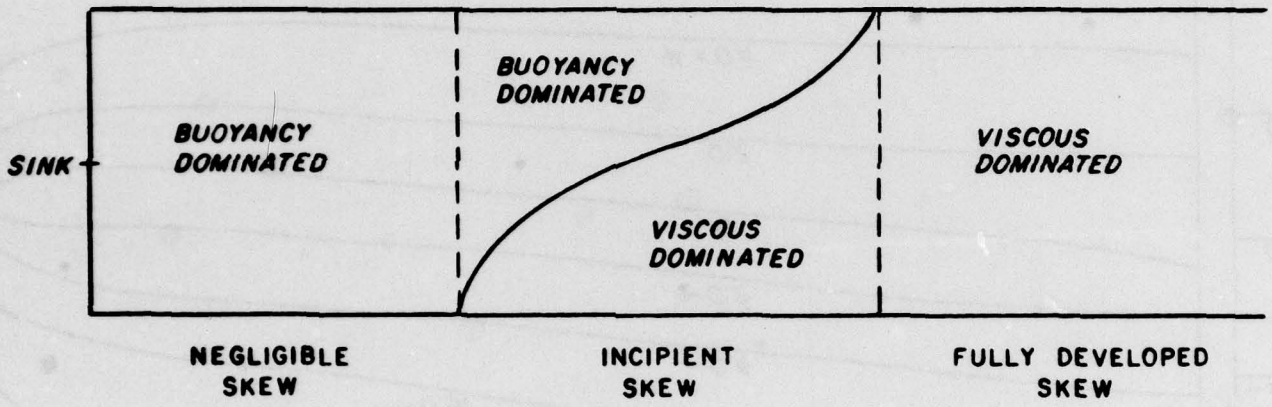

Fig. 34. Zones for viscosity-stratified flow

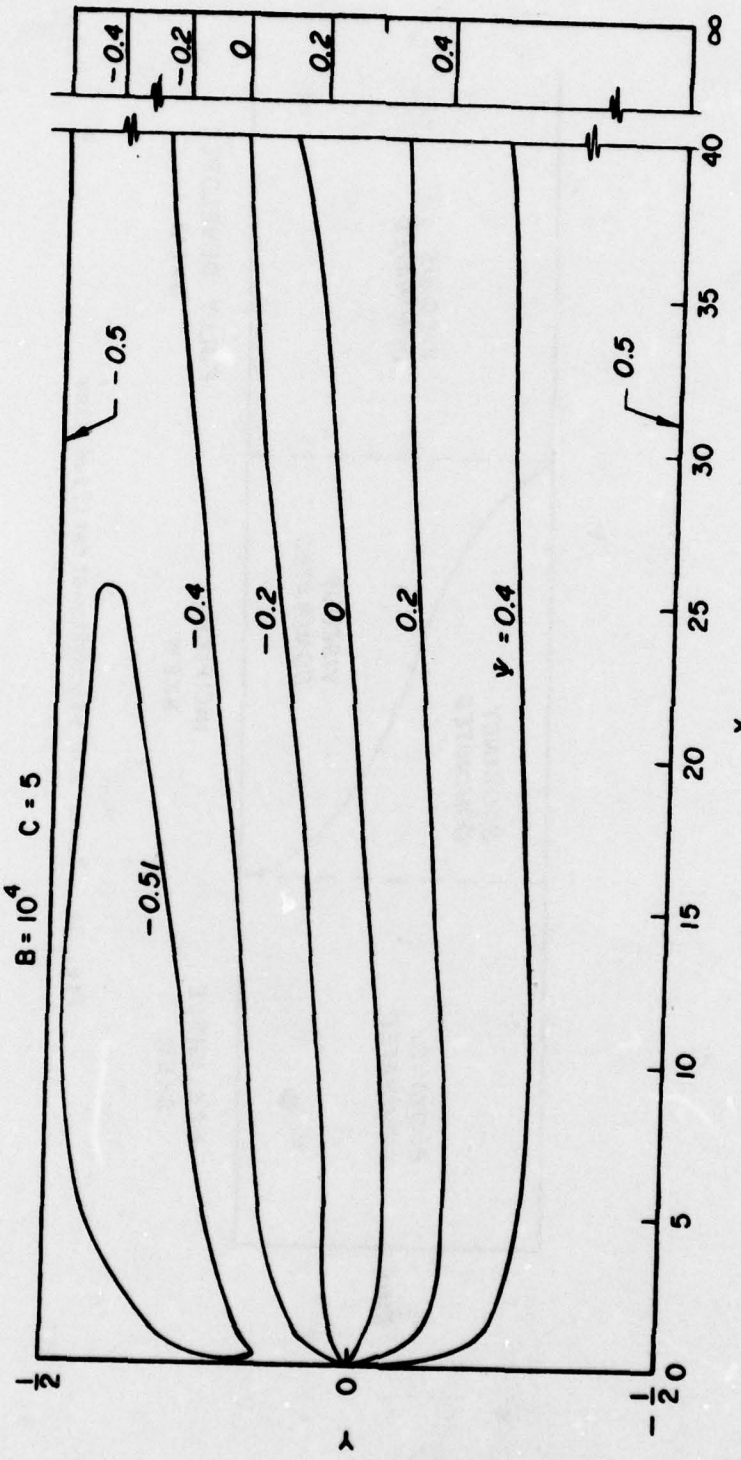

Fig. 35. Streamlines for incipient skewness

transition from incipient skewness to fully developed skewness. The eddy at the surface represents the backflow that occurs in the buoyancy dominated zone. The streamlines become horizontal for large values of X. The values which they approach are shown at $X = \infty$.

Incipient skew begins once the 0.5 streamline reaches the bottom boundary. Using this as an indicator of incipient skew, Figure 36 was prepared. It gives the value of X at which this occurs for an array of values for B and C.

The multiple regression equation which fits the data in Figure 36 is

$$X = B \cdot e^{-0.4C} (3.7 \times 10^{-5}) \tag{89}$$

Substituting for X, B, and C gives

$$x = 3.7 \times 10^{-5} e^{-0.4C} (\ell^5 g\epsilon\rho_o / q\mu_o) \tag{90}$$

x can be interpreted as the distance upstream of the sink at which separation of the 0.5 streamline from the wall occurs.

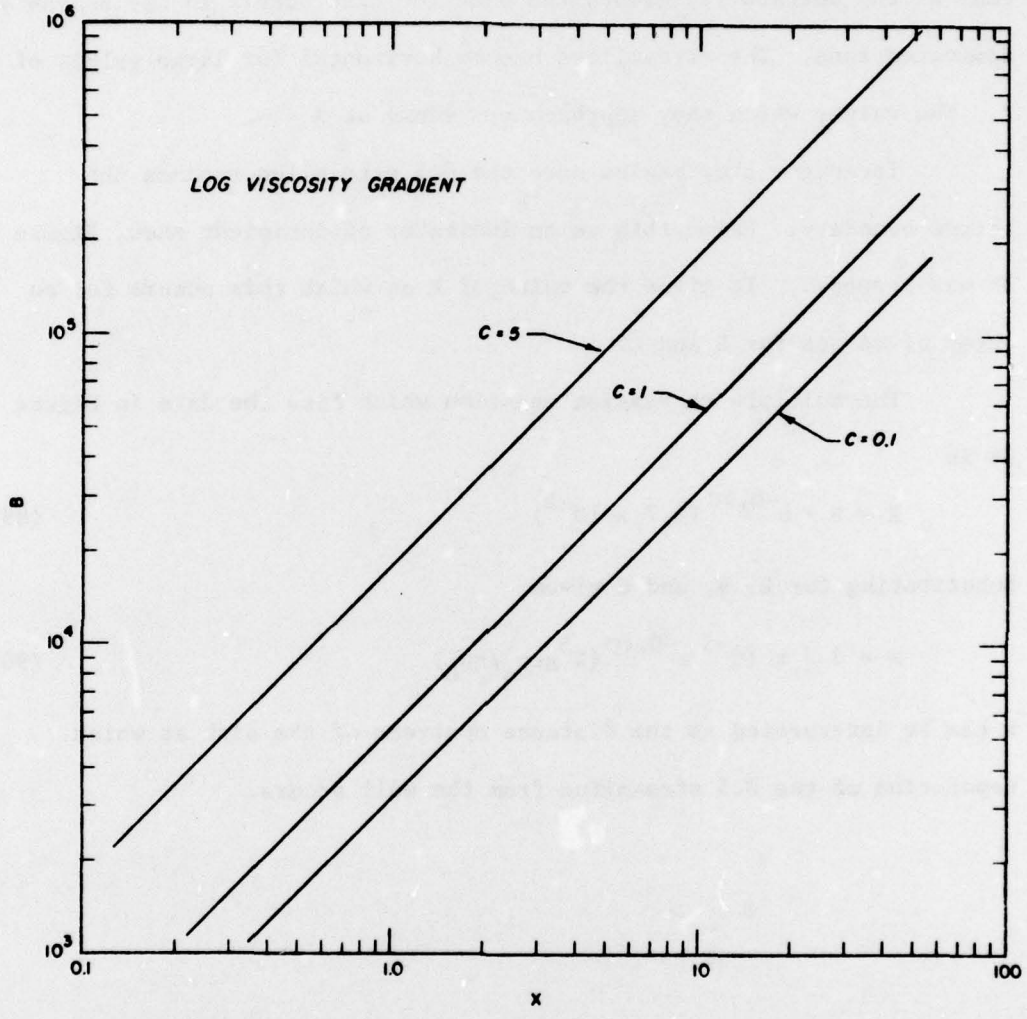

Fig. 36. Criteria for incipient skewness

CHAPTER IX

EFFECT OF UPSTREAM BOUNDARY CONDITIONS AND INERTIA ON VELOCITY

In developing the mathematical model in Chapter III, it was assumed that $U_\infty \mu/\mu_o$ could be replaced by

$1 + AY/2$ for linear gradient

or

e^{-CY} for log gradient

This involved two assumptions: $U_\infty = 1$ and the viscosity field is fixed in space. The effect of these assumptions and of the existence of a fixed back wall in the experiments conducted are discussed in this chapter.

Viscosity Constant on Streamline

While in a non-diffuse model, viscosity is strictly a function of the stream function (Ψ); the viscosity has been modeled thus far as a function of depth. This type of assumption makes mathematical modeling of the system much easier, but may make the results inaccurate. The correct approach to modeling the viscosity is to treat the viscosity as constant on a streamline ($\mu = f(\Psi)$ only).

To find the viscosity at a point, it is necessary to know the stream function at that point. The problem there is to set up a relationship between Ψ and μ. All that is known is that when the fluid

is at rest, $\mu/\mu_o = e^{-CY}$. (The log gradient will be used here to illustrate the implications of using the fixed viscosity field.)

When steady-state is reached, there should be some point at which the relationship below is true. This is taken as $x = \infty$

$$\mu/\mu_o \ (x = \infty) = e^{-CY} \tag{91}$$

even when flow is occurring.

It is necessary then to derive a relationship between Ψ and Y at $X = \infty$. Ideally, the relationship is the solution for one-dimensional flow. Unfortunately, those equations cannot be solved for $Y = f(\Psi)$. So to simplify matters, a uniform upstream velocity profile is used

$$\frac{\partial \Psi}{\partial Y} = -1.0 \tag{92}$$

which implies

$$\Psi = -Y \tag{93}$$

for the boundary condition $\Psi(0) = 0$.

The viscosity at any point in the fluid can be given as

$$\mu/\mu_o(Y) = \begin{cases} e^{C\Psi}, & -5 \leq \Psi \leq 0.5 \\ e^{C(\pm 0.5)}, & \Psi \gtrless \pm 0.5 \end{cases} \tag{94}$$

Equation 26 with this new expression for viscosity becomes

$$\frac{\partial^4 \Psi}{\partial Y^4} - 2C \frac{\partial^3 \Psi}{\partial Y^3} + C^2 \frac{\partial^2 \Psi}{\partial Y^2} + B\, e^{-C\Psi} \frac{\partial \Psi}{\partial Y} = 0 \tag{95}$$

This equation was solved numerically and the solution is plotted in Figure 37, along with the solution from the previous chapter.

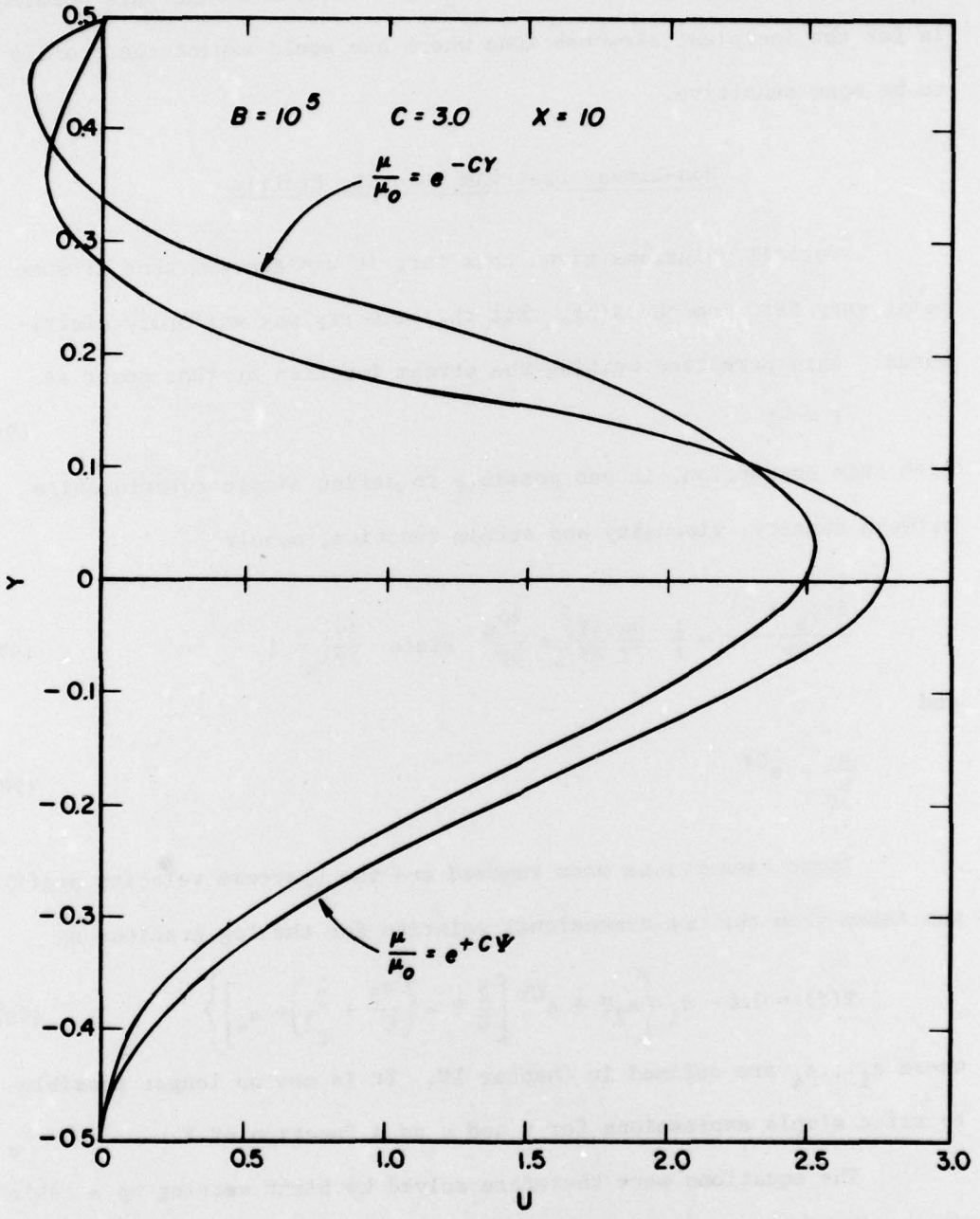

Fig. 37. Effect of substituting Y = -Ψ

Note that the solutions do not differ by much even though this solution is for the incipient skewness zone where one would expect the profile to be most sensitive.

Non-Linear Upstream Velocity Profile

For all solutions given thus far, it was assumed that at some point very far from the sink, that the velocity was uniformly distributed. This permitted writing the stream function at that point as

$$\Psi = -Y \tag{96}$$

With this assumption, it was possible to define simple relationships between density, viscosity and stream function, namely

$$\frac{\partial(\rho_s + \rho)}{\partial y} = \frac{1}{\ell} \frac{\partial \rho}{\partial \Psi} \frac{\partial \Psi}{\partial Y}\bigg|_\infty = \frac{\partial \rho_s}{\partial y} \quad \text{since} \quad \frac{\partial \Psi}{\partial Y}\bigg|_\infty = 1 \tag{97}$$

and

$$\frac{\mu}{\mu_o} = e^{C\Psi} \tag{98}$$

These assumptions were removed and the upstream velocity profile was taken from the one-dimensional solution for the log gradient as

$$\Psi(Y) = 0.5 - a_1 \left\{ a_2 Y + e^{CY} \left[\frac{2}{C} Y - \left(\frac{a_3}{C} + \frac{2}{C^2} \right) + a_4 \right] \right\} \tag{99}$$

where $a_1 \ldots a_4$ are defined in Chapter IV. It is now no longer possible to write simple expressions for μ and ρ as a function of Ψ.

The equations were therefore solved by first setting up a table of μ and ρ vs. Ψ upstream. Then after each iteration a value of viscosity and density could be assigned to each grid cell by interpolating from the internal table.

Equation 95 was solved and the results were found to be identical in virtually all cases. This could have been anticipated by noting that the corrections on both viscosity and density were in the B term in the equations. From earlier solutions it was clear that B had to be changed a great deal to significantly affect the solutions. The corrections introduced in this section only changed B slightly from the values obtained from the assumption of a linear profile far upstream.

The principal difference between solutions developed from this method and those from methods presented earlier is the cost of the computation, which increased greatly because of the table lookups. This solution method was not investigated any further.

Effect of Back Wall on Density Field

In a tank with a fixed back wall, it is not possible to maintain a constant density field since layers of the fluid near the sink elevation are being withdrawn much as one would withdraw a single card from a deck of playing cards. To correctly model a tank, an unsteady-state model is necessary to account for the changing density field. The question is one of how different are the flows in an infinite duct with a steady-state model from those in a tank.

Since in this experiment the flow is such that the surface of the tank drops extremely slowly, the velocity field similarly changes very slowly. The principal effect is that in the tank the density is not constant along a streamline as it is in the duct model.

The species (or density) continuity equation for unsteady,

non-diffuse flow is

$$\frac{\partial \rho}{\partial t} + U \frac{\partial \rho}{\partial x} + V \frac{\partial (\rho + \rho_s)}{\partial y} = 0 \tag{100}$$

While $\partial\rho/\partial t$ can be known everywhere only by solving the complete unsteady momentum and continuity equations, it can be stated that at the top boundary

$$\frac{\partial \rho}{\partial t} = V^* \frac{\partial \rho_s}{\partial y} \tag{101}$$

where V* is the velocity at which the surface is dropping. At the bottom boundary

$$\frac{\partial \rho}{\partial t} = 0 \tag{102}$$

The effect of this term on the solution can be seen by remembering that the species continuity equation entered the mathematical model by replacing $\partial\rho/\partial x$ by $V\varepsilon\rho_o/U_\infty$. The substitution now becomes

$$\frac{\partial \rho}{\partial x} = \frac{V\varepsilon\rho_o}{U} - \frac{\partial \rho}{\partial t} \frac{1}{U} \tag{103}$$

At the surface

$$\frac{\partial \rho}{\partial x} = \frac{\varepsilon \rho_o}{U} \quad (V - V^*) \tag{104}$$

Since $\partial\rho/\partial x$ is substituted into the buoyancy force term, it can be concluded that the existence of the back wall of the tank reduces the effect of the buoyancy forces. The magnitude of this effect depends on the length to depth aspect ratio of the tank. If it is small, the effect of the falling surface can be significant. The experimental data in this study indicate that buoyancy forces were somewhat smaller than

predicted. This may be explained by the moderate length to depth aspect ratio used.

Effect of Inertial Forces

In most of the solutions presented thus far, inertial forces have been neglected. The experimental results presented in Chapter XI indicate that this did not seriously affect the correlation of results from the mathematical and experimental model, since the Reynolds numbers were small in the experimental model.

The question remains as to what the mathematical model would look like if inertial forces were included. Such a model using similar assumptions to those presented in Chapter III can be written

$$\frac{\partial^4\Psi}{\partial Y^4} - 2C\frac{\partial^3\Psi}{\partial Y^3} + C^2\frac{\partial^2\Psi}{\partial Y^2} + R\left(\frac{\mu_o}{\mu}\right)\left[\left(\frac{1}{F^2} + \frac{\partial^3\Psi}{\partial Y^3}\right)\frac{\partial\Psi}{\partial X} - \frac{\partial^3\Psi}{\partial X\partial^2 Y}\frac{\partial\Psi}{\partial Y}\right] = 0 \qquad (105)$$

(viscous) (viscosity stratification) (buoyancy) (inertia)

where $F^2 = R/B = q^2/\ell^4\varepsilon g$

Near the sink the inertia and buoyancy terms tend to mask viscous forces but as $X \to \infty$, the velocity profiles will approach those presented for one-dimensional flow. This viscous zone most likely occurs even farther upstream when R becomes larger. When buoyancy forces are large (small F), they not only can mask the viscous forces but the inertial forces as well. The buoyancy forces may also inhibit turbulence which will make the above model applicable at much higher Reynolds numbers than if F were large.

CHAPTER X

LABORATORY PROCEDURES

The velocity profiles were measured in experimental flumes by photographing the locations of dye streaks at various times. The desired gradients of viscosity and density were developed by placing layers with decreasing sugar or CMC (carboxymethylcellulose) concentration in the flume. This chapter of the report describes the equipment and procedures used in conducting the experiments.

Experimental Flumes

The physical model runs were conducted in three different flumes. The three flumes are referred to in the report as the big, narrow, and wide flumes. They are pictured in Figures 38, 39, and 40, and their dimensions are given in Table 1. The length is the distance from the sink to the back wall of the flume; the height is the distance from the bottom to the greatest depth used; and the width is the distance between the sides. The camera location is the distance from the sink to the point at which the camera recording the position of the dye streaks was usually located. This procedure is described later.

The big flume was used first. When the density gradients used were large, the results of the experimental runs were satisfactory. When the density gradients became small, convective mixing currents in the tank became significant since temperature was not controlled in

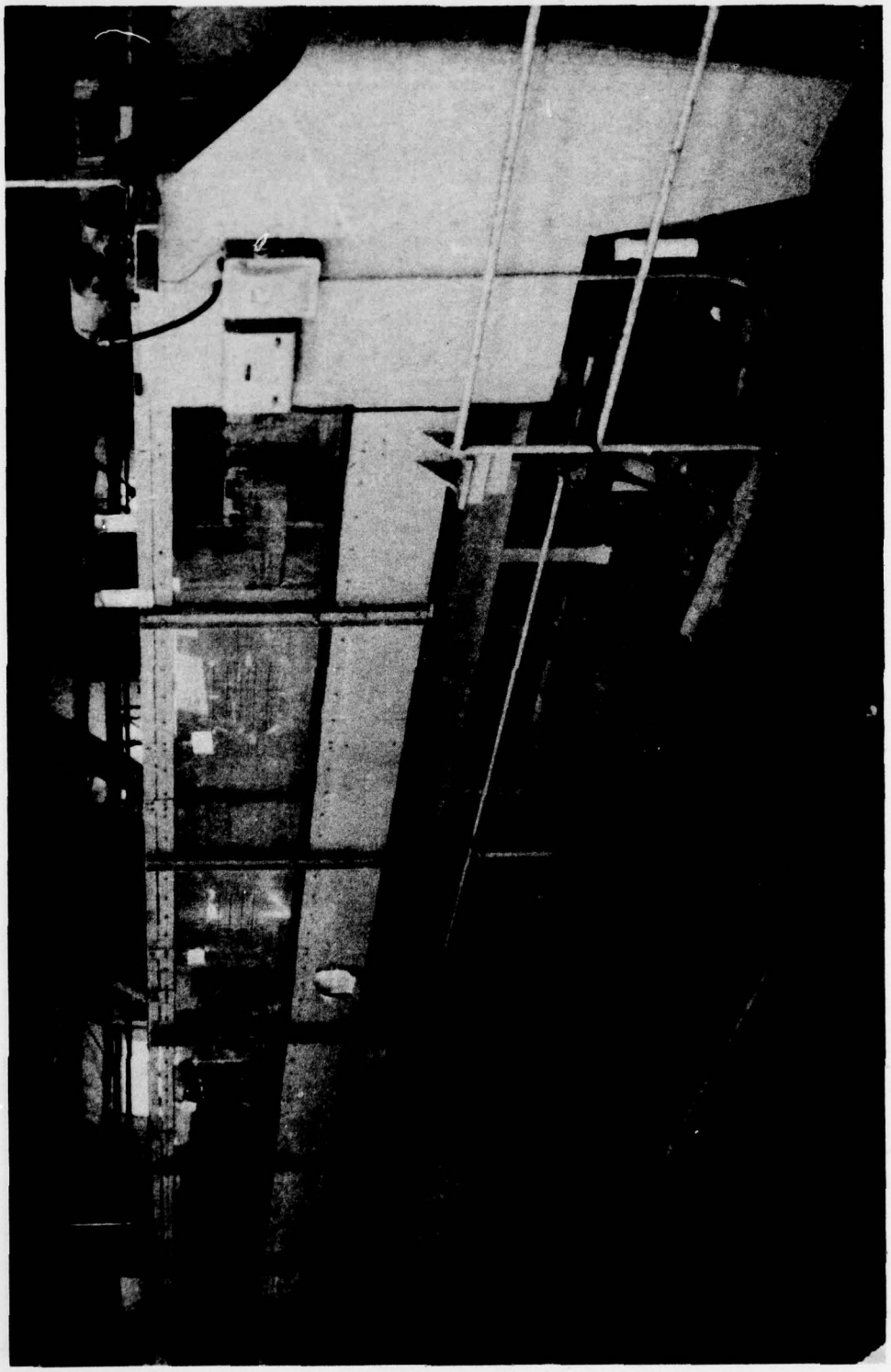

Fig. 38. Big flume

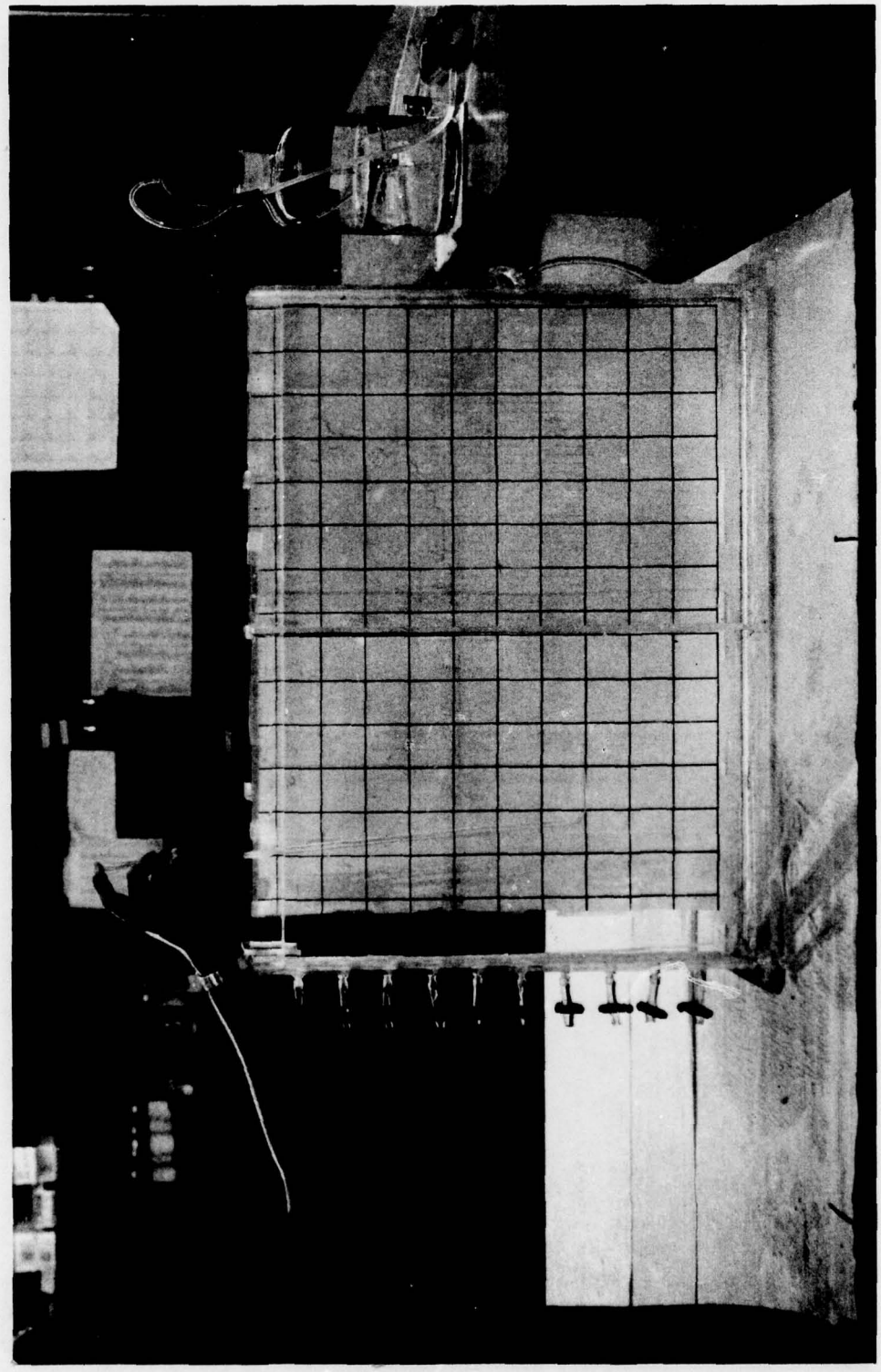

Fig. 39. Narrow flume

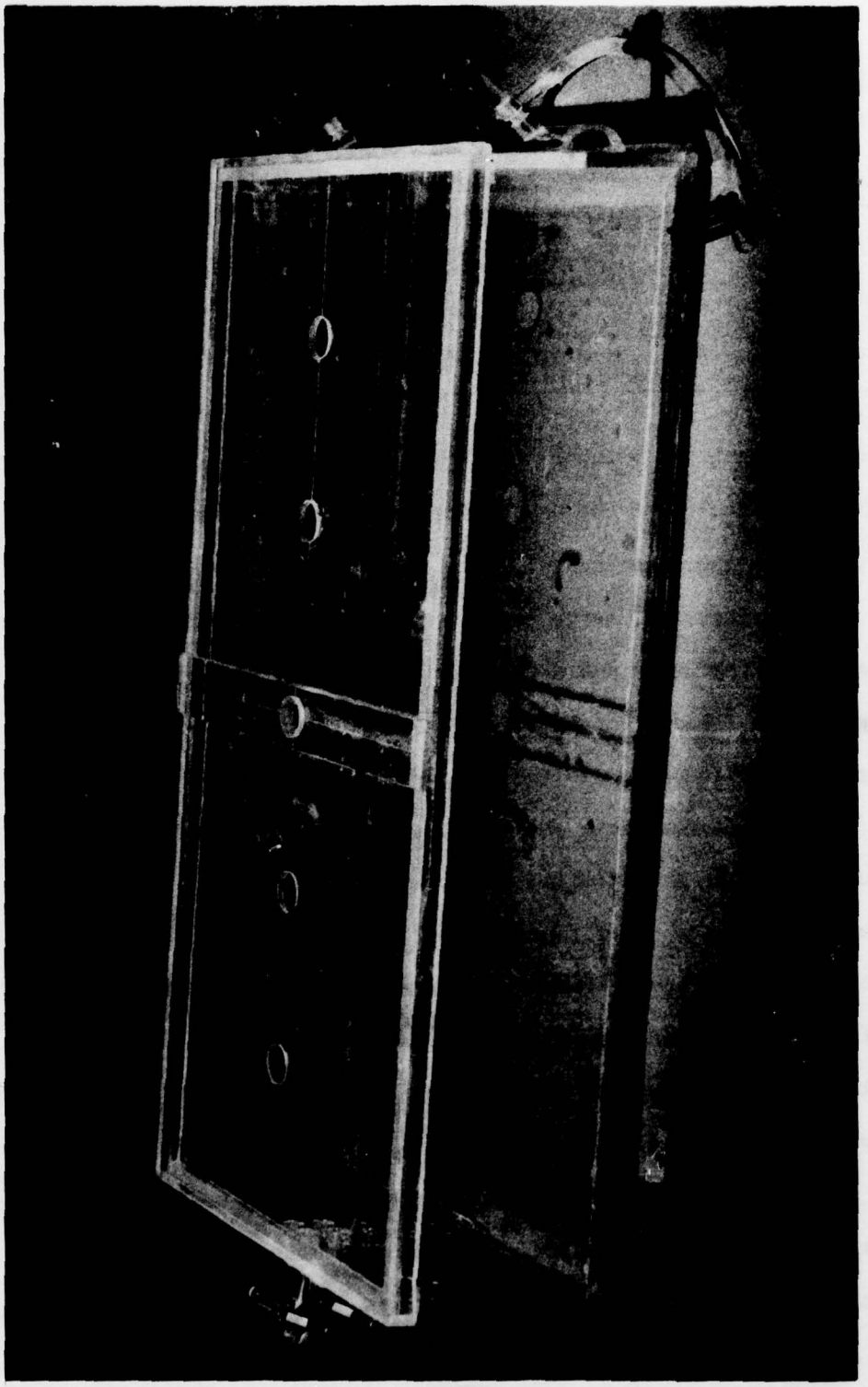

Fig. 40. Wide flume

TABLE 1

CHARACTERISTICS OF FLUMES

Flume	Length (cm)	Height (cm)	Width (cm)	Camera Location (cm)
Big	732	60	30	73, 222, 317
Narrow	78	58	3	32
Wide	67	12	30	31

the building housing the flume. (It would change by as much as 15°C during the course of the day.) These secondary currents often interferred with the experiments.

Furthermore, large concentration gradients could not be used because of the costs and difficulty of handling large quantities of the stratifying fluid. For example, it would require one-half tonne of sugar to achieve some of the desired gradients.

The narrow flume was then constructed so that the experiments could be run in a controlled environment and would not require large quantities of the model fluids. Most of the successful runs were conducted in this flume. Some question arose as to possible sidewall effects in such a narrow flume. To avoid the effects of the sidewall, the wide flume was constructed. This flume had a depth to width aspect ratio of 1:3.

In this study the depth to width ratio was varied from 1:3 to 20:1. This was a much wider range than previous investigators, as Koh (1964) used 3:1, Imberger (1970) used 4:1, and Kao et al. (1972)

used 2:1.

The flow was regulated in the large flume by a gate in the downstream wall in the big flume. The opening in the gate was controlled by a set of screws at the top of the gate (see Figure 38). In the narrow and wide flumes, the flow was regulated by a clamp on the tubing flowing out of the sink (see Figures 39 and 40).

Measuring Velocity Profiles

The velocity profiles were measured by determining the displacement of dye streaks during known time intervals. Once the flow had reached steady-state, small pellets of erio-glaucine dye were dropped into the flume. These were photographed at several intervals. A clock was placed in the photograph to record the time at which each was taken.

The pictures, which were taken as 35-mm slides, were read using a microfiche reader. The location of the dye streak and time of the slide were recorded and input into a computer program, VELPRO. VELPRO corrected the profiles for parallax error, calculated the velocity profile and integrated the profile to obtain the flow rate. The formulas for parallax correction and a description of the VELPRO program are given in Appendix B.

Figure 41 is a schematic diagram of a typical dye streak during a run. Figures 42, 43, and 44 show actual dye streaks in the big, narrow, and wide flumes, respectively. Only one camera was used for the narrow and wide flumes. Three cameras were used in the big flume since the entire flume could not fit into one shot. The horizontal distance from the sink to the point at which the cameras were perpendicular is listed for

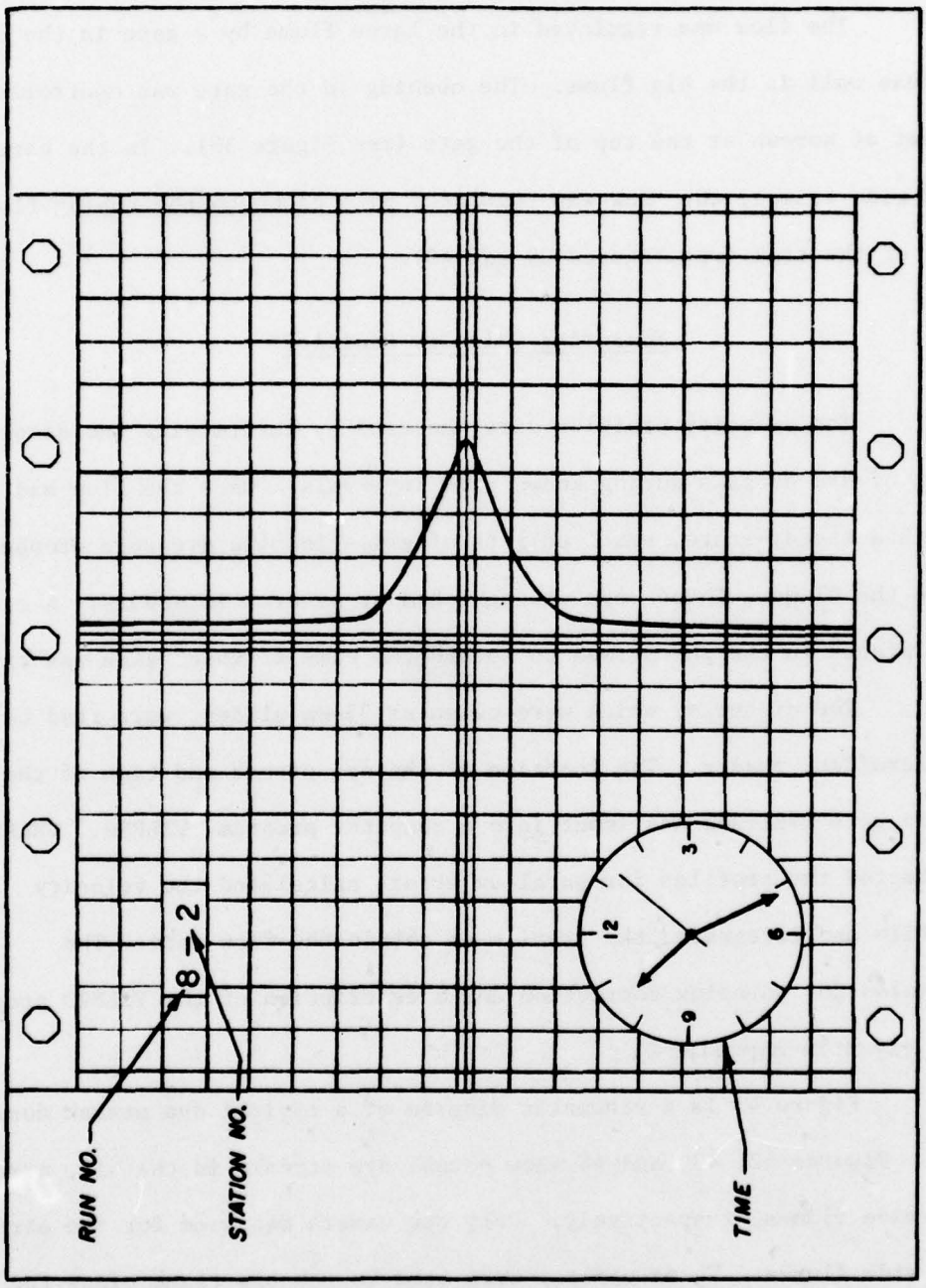

Fig. 41. Typical dye streak

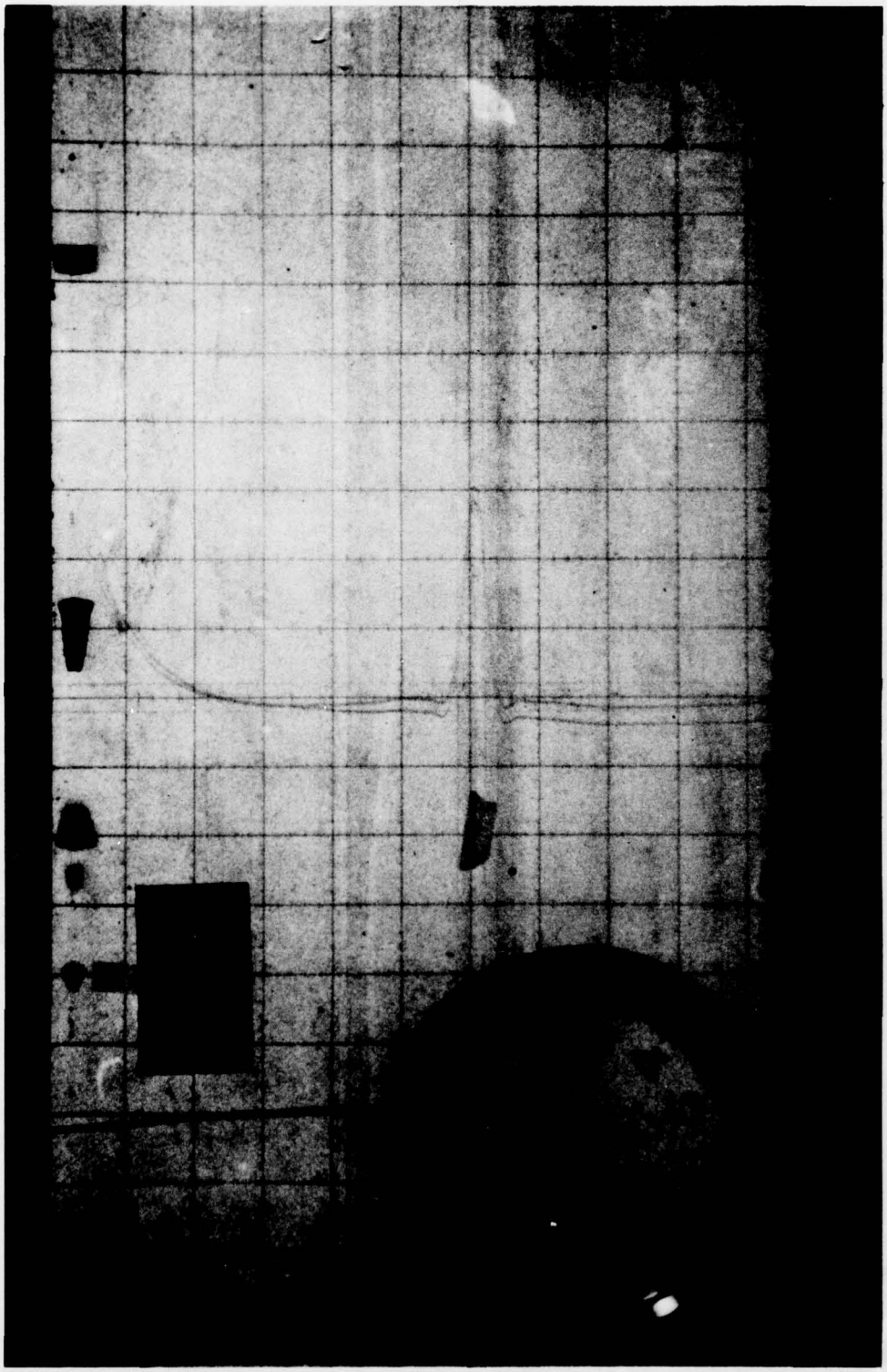

Fig. 42. Typical photo, big flume

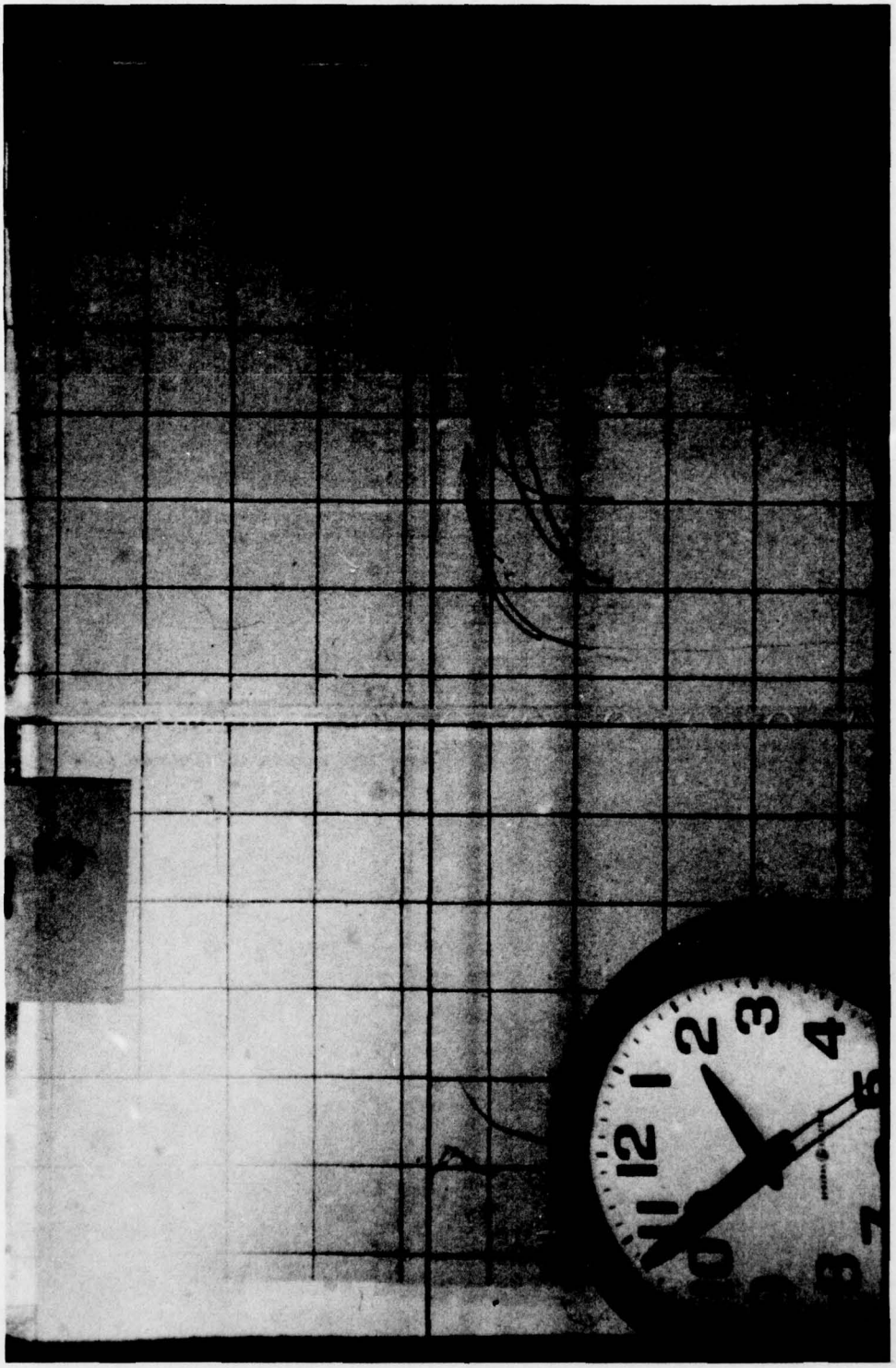

Fig. 43. Typical photo, narrow flume

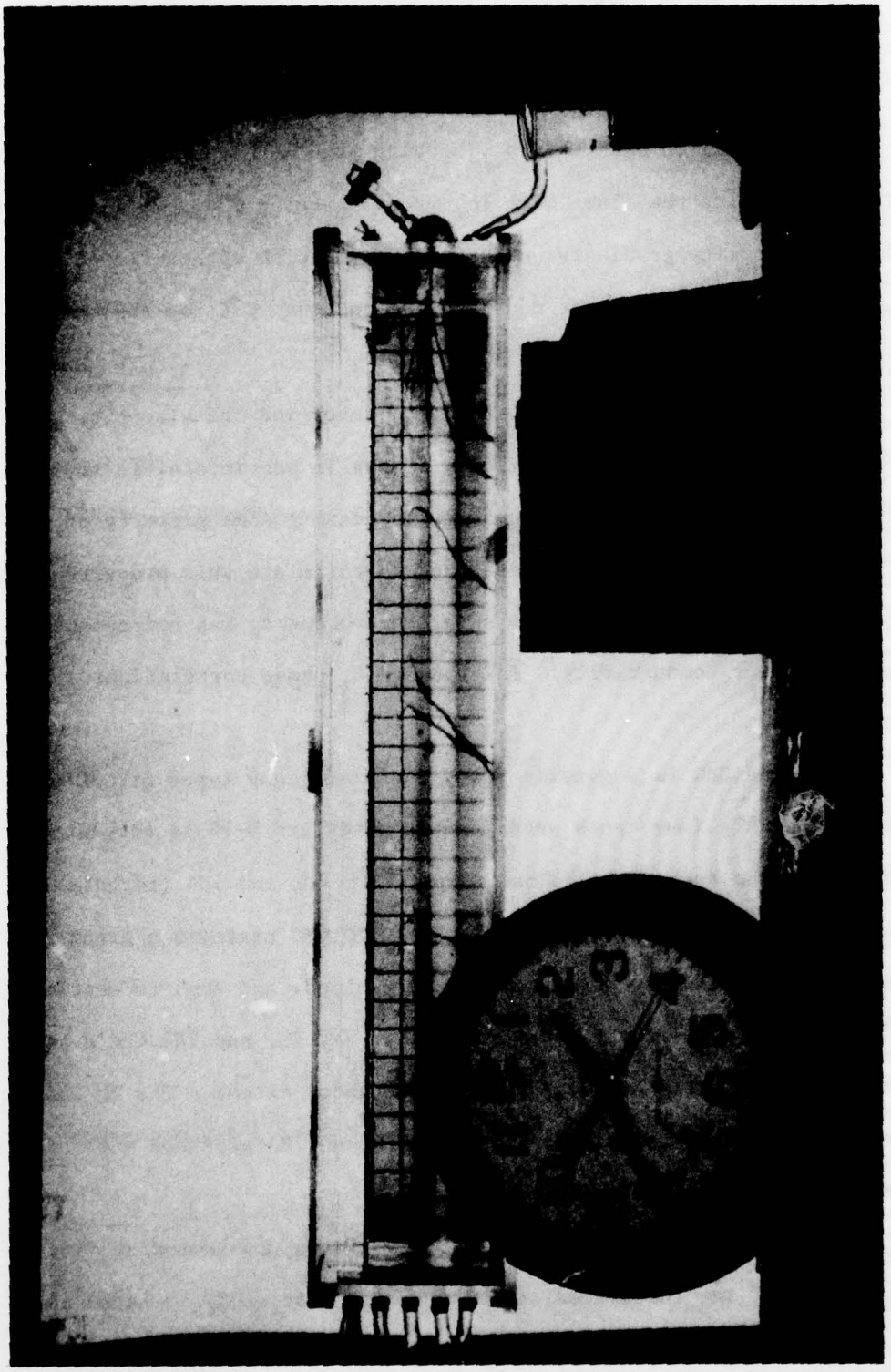

Fig. 44. Typical photo, wide flume

each flume in Table 1 and is shown for the large flume in Figure 45.

Model Fluids

The desired density and viscosity gradients were achieved in the flume by filling the flume with layers of sugar or CMC solutions. While similar viscosity gradients could be achieved with either fluid, the sugar created a much larger density gradient than CMC for the same viscosity gradient.

For each run it was necessary to determine the viscosity and density at every point in the fluid. Since it was impossible to make direct measurements, it was necessary to measure some property of the fluid which could be easily tested and to correlate this property with the viscosity and density. For sugar this property was refractance; for CMC it was conductivity. In Appendix C, these correlations are developed.

Since CMC is a generic name, there are many types of CMC's available. The four types used in this study are D-70 (detergent grade from the Buckeye Cellulose Corp.), 7M, 7H, and 7H4 (technical grade from Hercules Incorporated). The D-70 CMC contains a great deal of suspended cellulose which made it very cloudy and tend to settle. D-70 CMC was used only in a few runs. The 7M, 7H, and 7H4 CMC's dissolved completely and were used to a greater extent. The 7M CMC produced moderate viscosities while the 7H and 7H4 produced much higher viscosities at the same concentration.

In high concentrations, CMC behaves as a non-Newtonian fluid. Since most of the theoretical development in this study is based on

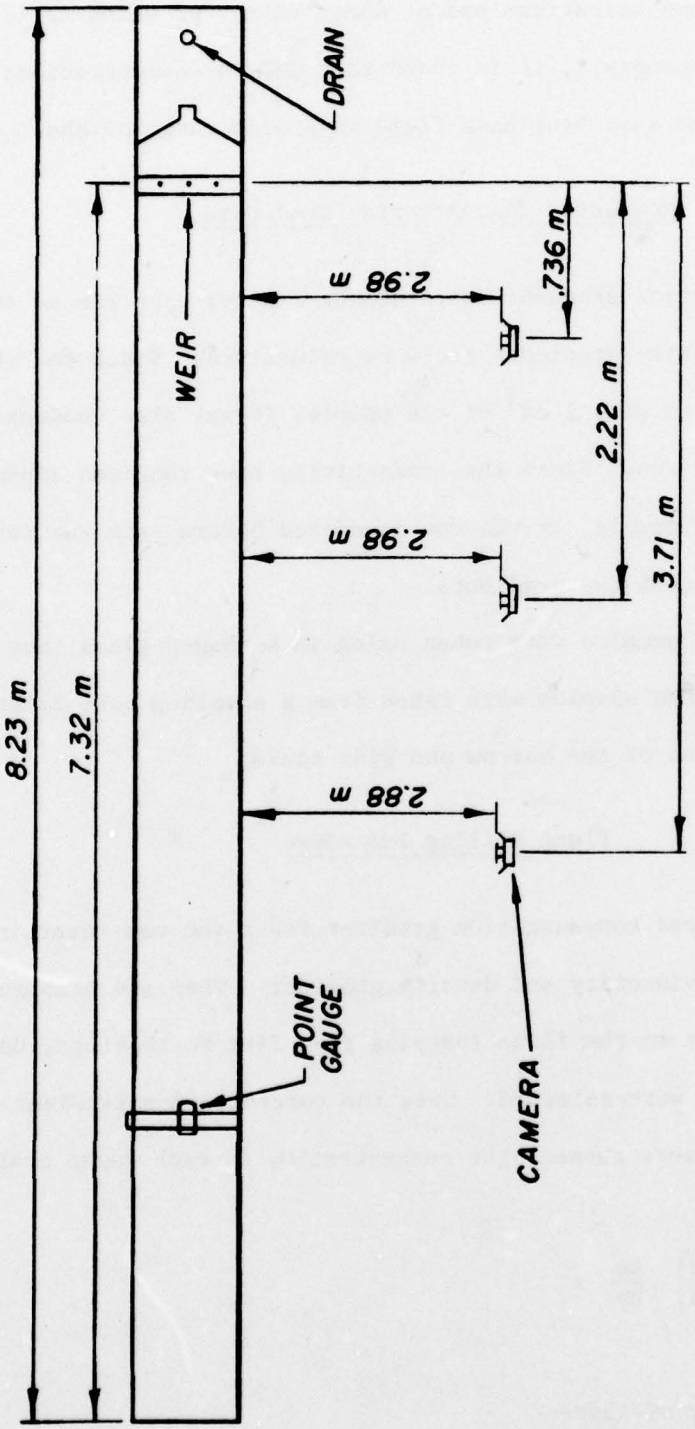

Fig. 45. Plan view of big flume

the assumption of non-Newtonian behavior, it was important that the CMC be used only in concentrations and at shear rates for which it is Newtonian. In Appendix C, it is shown that CMC in concentrations less than 5 g/ℓ behaves as a Newtonian fluid in a wide range of shear rates.

Measuring Concentration Gradients

Concentration gradients were measured after each run so that the viscosity and density gradients could be determined. Since the refractance test requires only 1 cm^3 of the sample, it was also conducted before each sugar run. Since the conductivity test requires approximately 100 cm^3 of sample, it was not conducted before each run for fear that it might disturb the gradients.

The sugar samples were taken using an L-shaped glass tube (see Figure 39). The CMC samples were taken from a sampling port located at the upstream end of the narrow and wide tanks.

Flume Filling Procedure

The required concentration gradient for a run was determined from the desired viscosity and density gradient. Then the numbers of layers to be input to the flume (varying from five to thirteen, depending on the flume) were selected. Once the concentration gradient and number of layers were chosen, the concentration in each layer could be calculated from

$$j = \left(\frac{n - j}{n - i}\right) \frac{\partial s}{\partial y} \ell \tag{106}$$

where

n = number of layers

$\partial s/\partial y$ = concentration gradient

ℓ = depth of flume

j = concentration in jth layer

The flume was filled starting with the bottom layer using the apparatus shown in Figure 46 for the wide and narrow flumes. The fluid was poured into the top container. The flow was then regulated by the elevation of the top container and a stopcock. The fluid flowed through the tubing to the plate located at the desired elevation of the layer. A sponge was located on the plate to dissipate any momentum the fluid may have had to prevent mixing of the layers.

In the case of the big flume, the fluid was pumped in through a hose onto a much larger plate. Very little mixing occurred when the narrow and wide flumes were filled. Some mixing did occur in the big flume so the actual concentration gradients were somewhat smaller than the desired.

In later runs the layers were alternately colored orange and clear. This was done to better track motion of the layers and to observe when the layers began diffusing into one another.

Once the flume was filled (which took approximately one day), from one to three days were allowed to elapse to let the interfaces between the layers diffuse into a linear gradient.

Run Procedure

Before the run the concentration gradient was checked and a dye particle was dropped and observed to determine if there was significant background motion. The clock and run number were set up in front of the

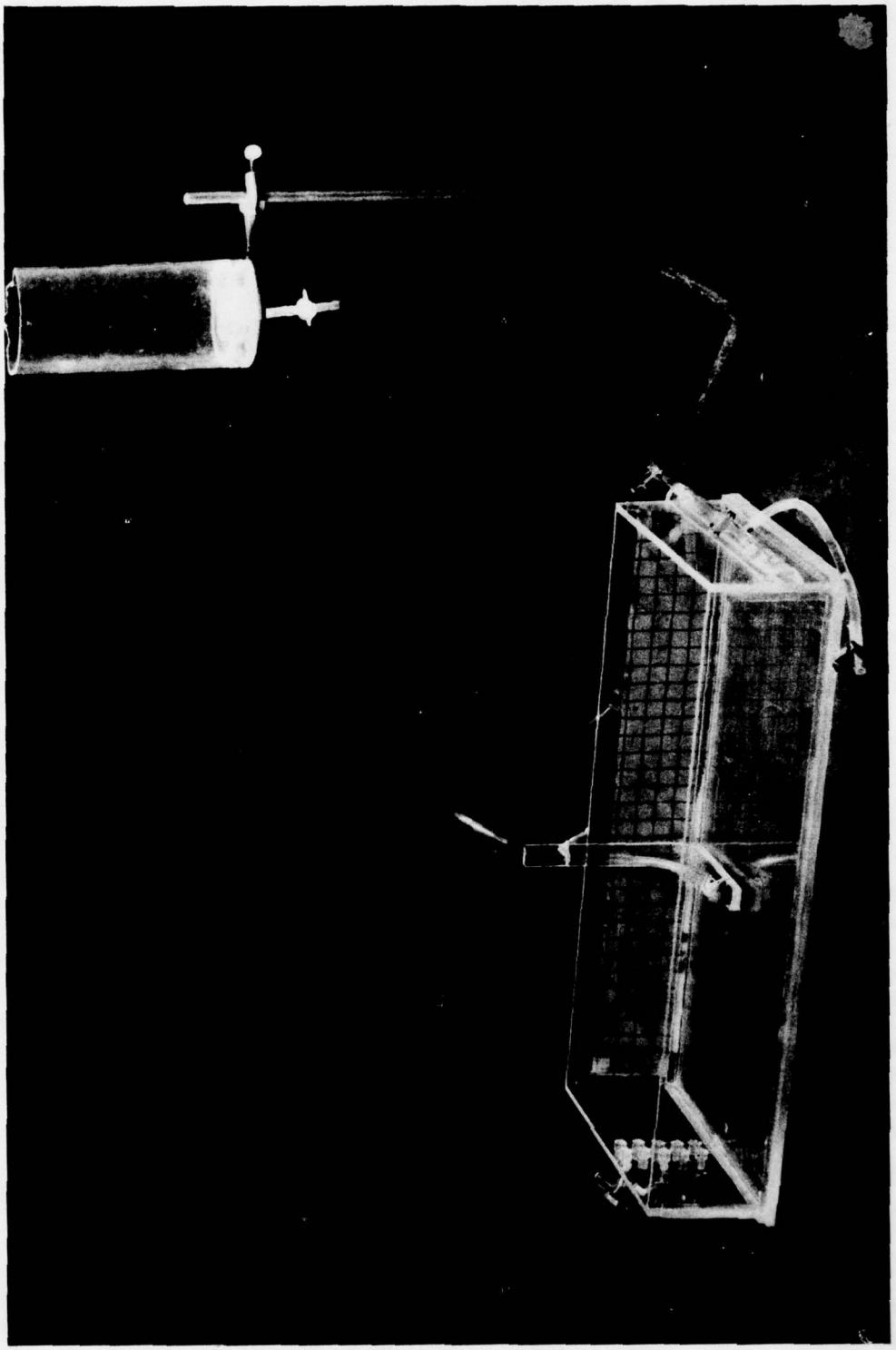

Fig. 46. Flume filling technique

flume and the camera and lighting were checked.

The flow was initiated by opening the clamp or gate, and the rate was checked using a cup and stopwatch. Once the rate was set, it was usually not adjusted as transient currents might have interfered with results.

The flow was allowed to come to steady-state. This time was given by Koh (1966b) as

$$t = \frac{1}{\sqrt{\varepsilon g}} \frac{x}{\delta_s} \tag{107}$$

where

δ_s = thickness of withdrawal zone, cm

x = distance from sink, cm

For the big flume, this time was on the order of 5 minutes. For the narrow and wide flumes it was on the order of 1 minute. Usually, approximately twice this time was allowed before velocities were measured.

Once steady-state was achieved, the dye pellets were dropped. While several may have been dropped to illustrate withdrawal layer growth, one was always dropped at the location labeled "camera location" in Table 1. The dye was dropped as close to the flume center line as possible to minimize any side-wall effects. The dye streak was photographed at least four times as it deformed.

Once the run was completed, the flow rate might have been adjusted and the run repeated. In the narrow flume, only three runs could be attempted until the surface elevation dropped significantly. In the other flumes, this effect did not occur, but usually only three runs were made with any flume.

CHAPTER XI

EXPERIMENTAL RESULTS

The results of experimental runs are presented in this chapter. First the parameters for the runs are presented. The mathematical model results are compared with the experimental results on a run-by-run basis. The overall results of the experimental runs are summarized in terms of the dimensionless numbers B and C.

Data Summary

Table 2 summarizes the values for the most important parameters for each run. Each column is explained below. Instruments used to measure the parameters are discussed in more detail in Appendix C.

The run number is the ordinal number of the run. Runs in the big flume have only one number since every time a parameter was changed, the run number was changed. Runs in the other two flumes take the form M.N where M is the run number assigned when the flume is filled, while N is the number of the flow rate used. For example, run 50.1 is run 50 with flow rate 1 while 50.3 is run 50 with flow rate 3.

Note that many run numbers do not appear in the table. Runs 20-29 were made using CMC in the small flume. There were problems with turbulence in most of these runs which rendered them useless. Some of the runs with numbers in the 30's were attempted while additional model fluid was injected in the sampling ports at the upstream end of

TABLE 2

SUMMARY OF PARAMETERS FOR EXPERIMENTS

Run No.	Flume	Model Fluid	q (cm^2/sec)	ρ_o (gr/cm^3)	μ_o (cp)	ε (1/cm)	ℓ (cm)	C	B	R	F
8	B	S	.029	1.002	1.03	.00017	50.	.058	4.2E+8	2.8	2.3E-4
9	B	S	.090	1.001	1.03	.00017	50.	.058	1.1E+9	8.7	8.9E-5
11	B	S	.055	1.037	1.38	.0012	50.	.33	1.0E+10	4.1	2.0E-5
12	B	S	.023	1.037	1.38	.0012	50.	.33	2.4E+10	1.9	8.9E-6
13	B	S	.23	1.037	1.38	.0012	50.	.33	2.4E+9	19.	8.9E-5
14	B	S	.44	1.037	1.38	.0012	50.	.33	1.2E+9	33.	1.9E-4
15	B	S	.078	1.037	1.38	.0013	50.	.33	7.6E+9	5.6	2.7E-5
16	B	S	.13	1.037	1.38	.0013	50.	.33	4.5E+9	9.2	4.5E-5
19	B	D-70	.56	1.005	66.3	.0002	50.	6.6	3.3E+6	.84	4.4E-4
24	B	D-70	.069	.997	12.	.000002	50.	.38	1.7E+6	.57	4.8E-4
32.1	N	S	.072	1.100	2.6	.0082	25.	2.3	1.7E+9	3.0	4.1E-5
36.3	N	S	.019	1.140	3.8	.010	20.	5.7	2.4E+11	.58	1.5E-6
41.1	N	7M	.12	1.100	6.64	.00006	45.	3.5	3.0E+7	1.8	2.6E-4
42.3	N	7H	.325	1.000	71.	.00005	16.	2.2	1.4E+4	.45	2.5E-3
43.2	N	7H	.10	1.000	65.	.00004	20.	1.3	9.6E+4	.17	1.2E-4
44.1	N	S	.030	1.096	2.17	.0080	20.	2.0	1.9E+9	1.4	2.7E-5
47.2	N	S	.325	1.036	1.21	.0010	16.	.32	1.3E+7	2.8	1.5E-3
48.2	N	7H	.79	.998	85.	.0002	8.	3.0	1.1E+3	.86	2.7E-2
49.1	N	7M	.10	1.003	4.8	.0017	8.	2.4	1.4E+5	2.1	1.7E-3
50.3	N	7H4	.58	.998	134.	.0002	8.	2.6	1.0E+3	.43	4.1E-3
51.1	W	S	.075	1.080	2.2	.021	10.	2.4	1.3E+8	3.7	1.6E-4
51.3	W	S	.106	1.080	2.2	.021	10.	2.4	9.5E+7	5.2	2.3E-4
52.1	N	S	.124	1.035	1.2	.0013	30.	.48	6.7E+8	10.	1.2E-4
52.3	N	S	.041	1.035	1.2	.0013	30.	.48	2.0E+7	3.5	4.2E-5
53.2	W	S	.054	1.028	1.2	.0083	10.	.57	1.1E+8	4.8	2.1E-4
54.2	N	S	.85	1.021	1.2	.0010	50.	.57	5.8E+8	85.	3.8E-4
55.3	W	7H	.058	.974	103.	.0001	8.	2.2	5.7E+3	.054	2.8E-3
56.2	N	S	1.52	1.000	.97	.003	50.	.002	1.2E+9	156.	3.5E-4
57.1	W	7H	.11	.999	58.	.00023	8.	2.1	1.4E+4	.19	3.6E-3

the narrow flume to maintain steady-state conditions. It was found that inertia from these inflows caused turbulence so this method was abandoned.

The "flume" column contains the abbreviated flume name: B-big N-narrow, and W-wide, as defined earlier. The "model fluid" column designates whether the model fluid was sugar (S) or one of the CMC's (D-70, 7H, 7M or 7H4).

The flow at the sink is given in the "q" column in cm^2/sec. This value was determined from the output from the VELPRO program and the fact that q increased linearly from zero at the back wall. This is given by the formula

$$q = q_x \left(\frac{x_{max} - x}{x_{max}} \right) \tag{108}$$

where

q_x is flow at position x

x_{max} is length of flume

The relationship is plotted in Figure 47 for three runs which had velocity profiles measured at several locations.

ρ_o and μ_o are the density and viscosity at the sink elevation. ε was determined by plotting density vs. depth and fitting a straight line. The slope of the line was $\partial\rho_s/\partial y$ and $\varepsilon = -1/\rho_o \; \partial\rho_s/\partial y$.

ℓ is the distance from the bottom of the fluid to the surface of the model fluid. The sink was always at approximately $\ell/2$ from each boundary. Note that in some runs a false bottom was developed by filling the bottom of the flume with a very dense sugar solution. The CMC or lighter sugar solutions were laid on top as shown in Figure 48.

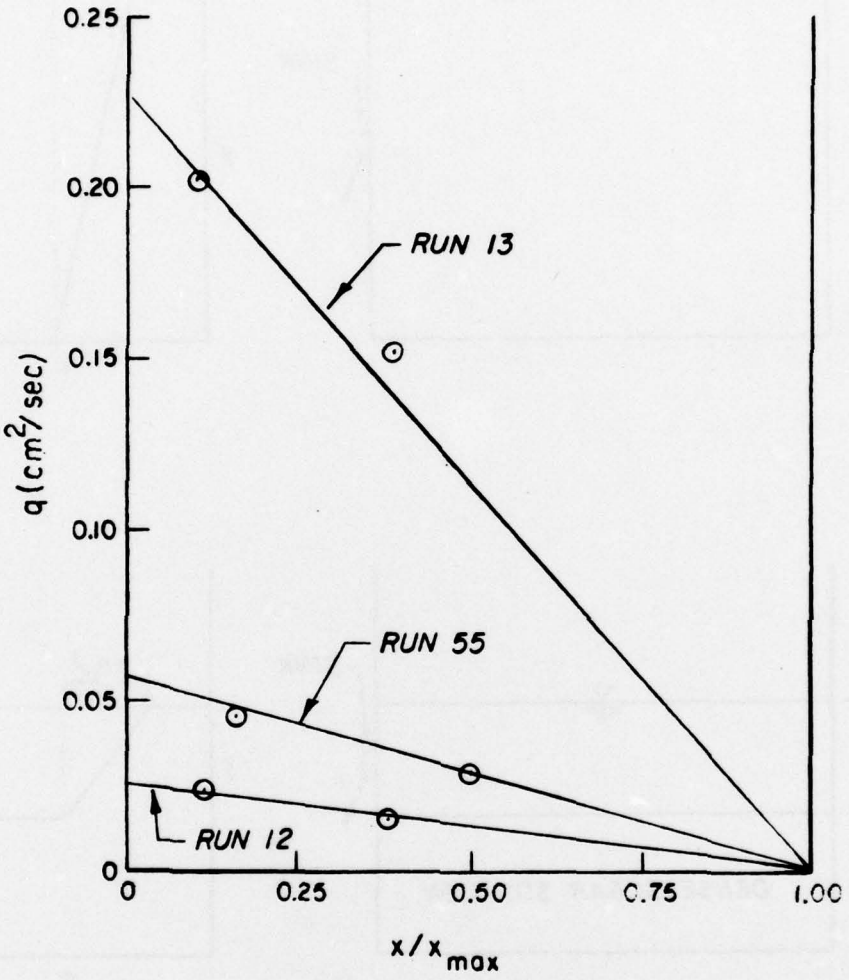

Fig. 47. Flow rate as function of distance from sink

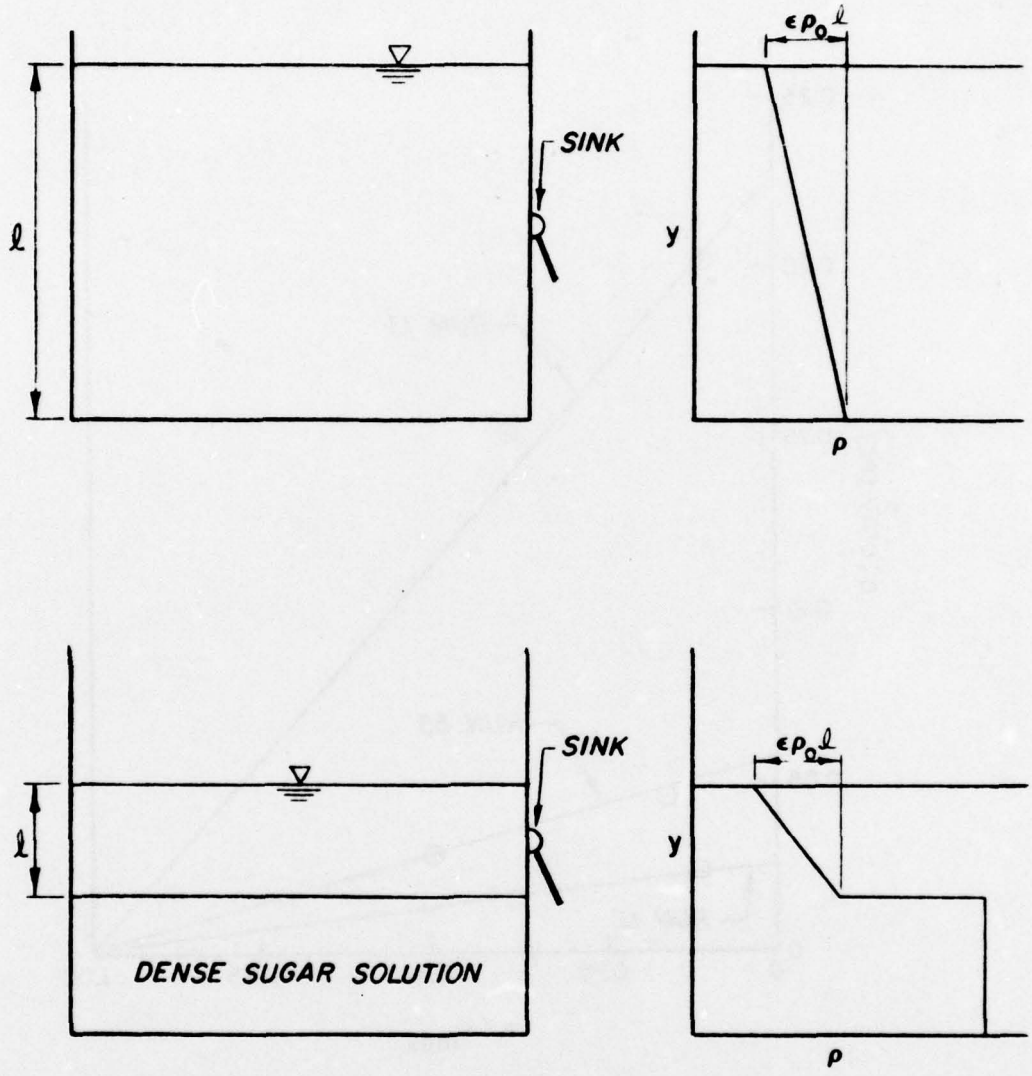

Fig. 48. Control of ℓ with false bottom

This allowed ℓ to be set at a much smaller value than the total tank depth.

The parameter C was defined earlier as $c\ell_1$ where c_1 is the slope of a semi-log plot of viscosity vs. elevation. The parameter B is the ratio of the Reynolds number ($R = q\rho_o/\mu_o$) and the densimetric Froude number ($F = q/\ell^2\sqrt{\varepsilon g}$) squared. That is

$$B = \frac{g\,\ell^4\varepsilon\rho_o}{q\,\mu_o} \tag{109}$$

Note that the B and F are written in scientific notation where 4.2E+8 is $4.2\text{x}10^8$ and 2.3E-4 is $2.3\text{x}10^{-4}$.

The experimental runs covered a fairly wide range of the important parameters

$1.1 \times 10^3 \leq B \leq 2.4 \times 10^{11}$

$0.002 \leq C \leq 6.6$

$0.054 \leq R \leq 156$

$1.5 \times 10^{-6} \leq F \leq 2.7 \times 10^{-2}$

All the runs are summarized in Figure 49 with respect to the values of B and C. As was predicted by the mathematical model, runs with large values of B do not show skew because of the masking effect of the large buoyancy forces. As B decreases skewness becomes evident and finally predominates for sufficiently low B.

Velocity Profile Results

Figures 50-54 contain graphs of the observed (experimental model) velocity profiles plotted with the corresponding predicted (mathematical model) profiles from the numerical solution of equation

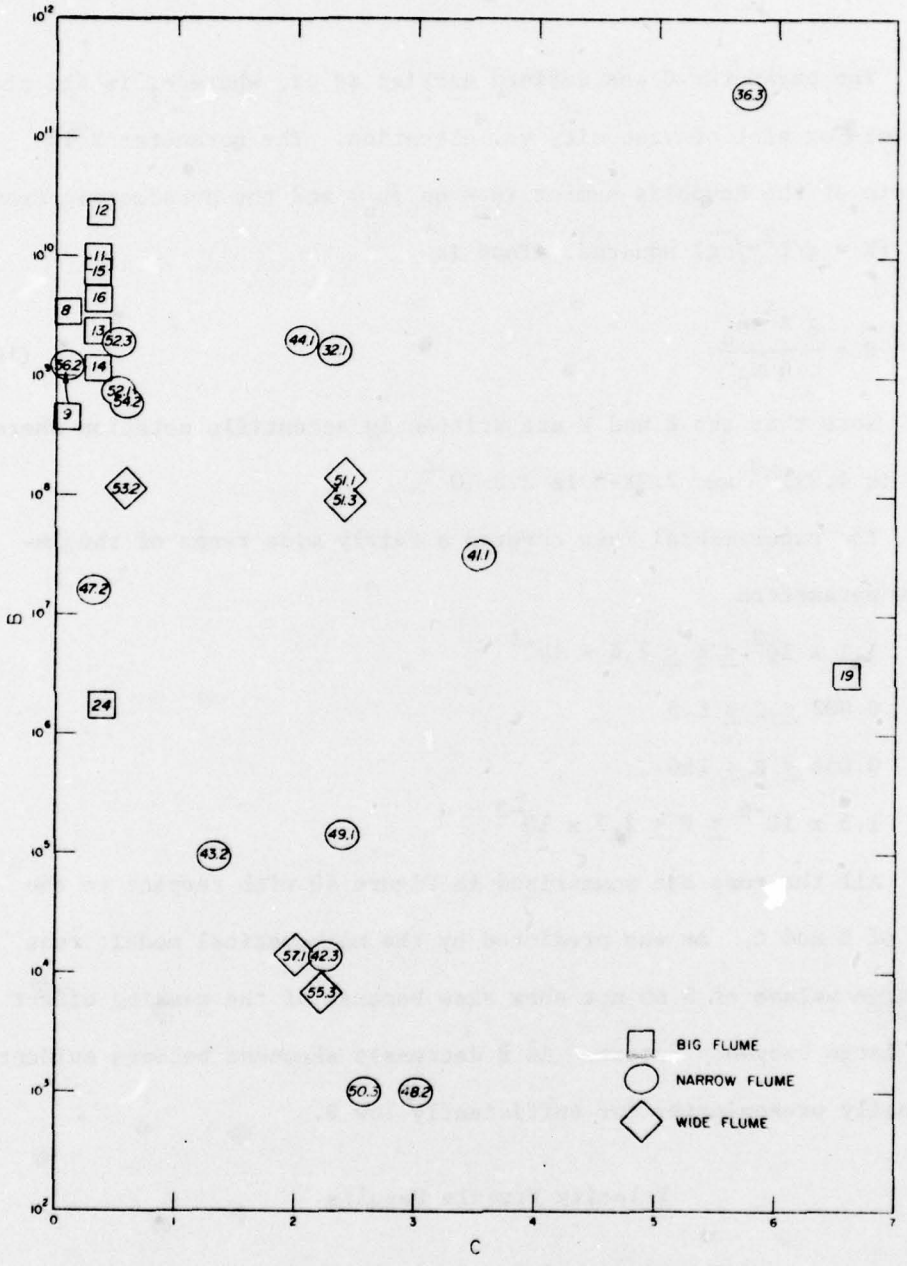

Fig. 49. Summary of experimental runs

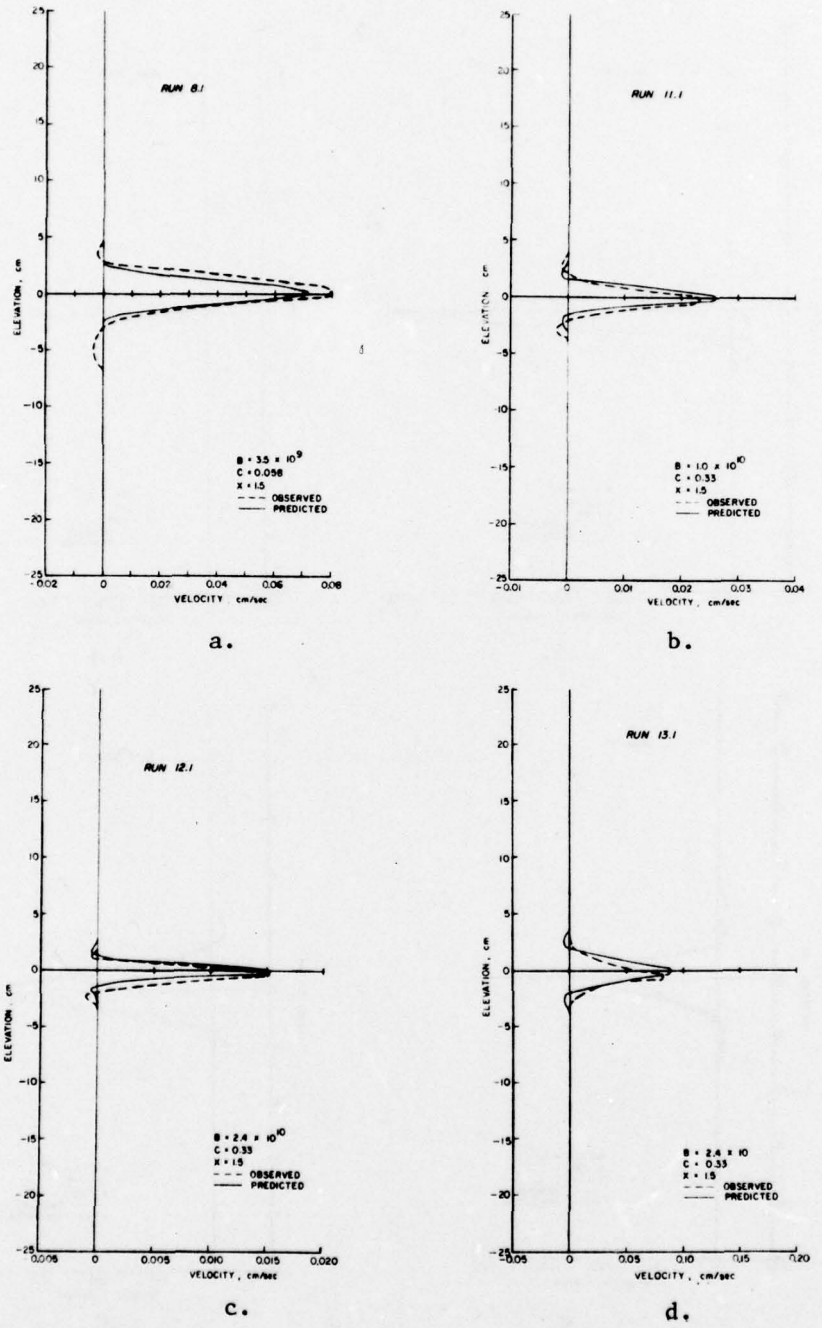

Fig. 50. Results of runs 8, 11, 12, and 13

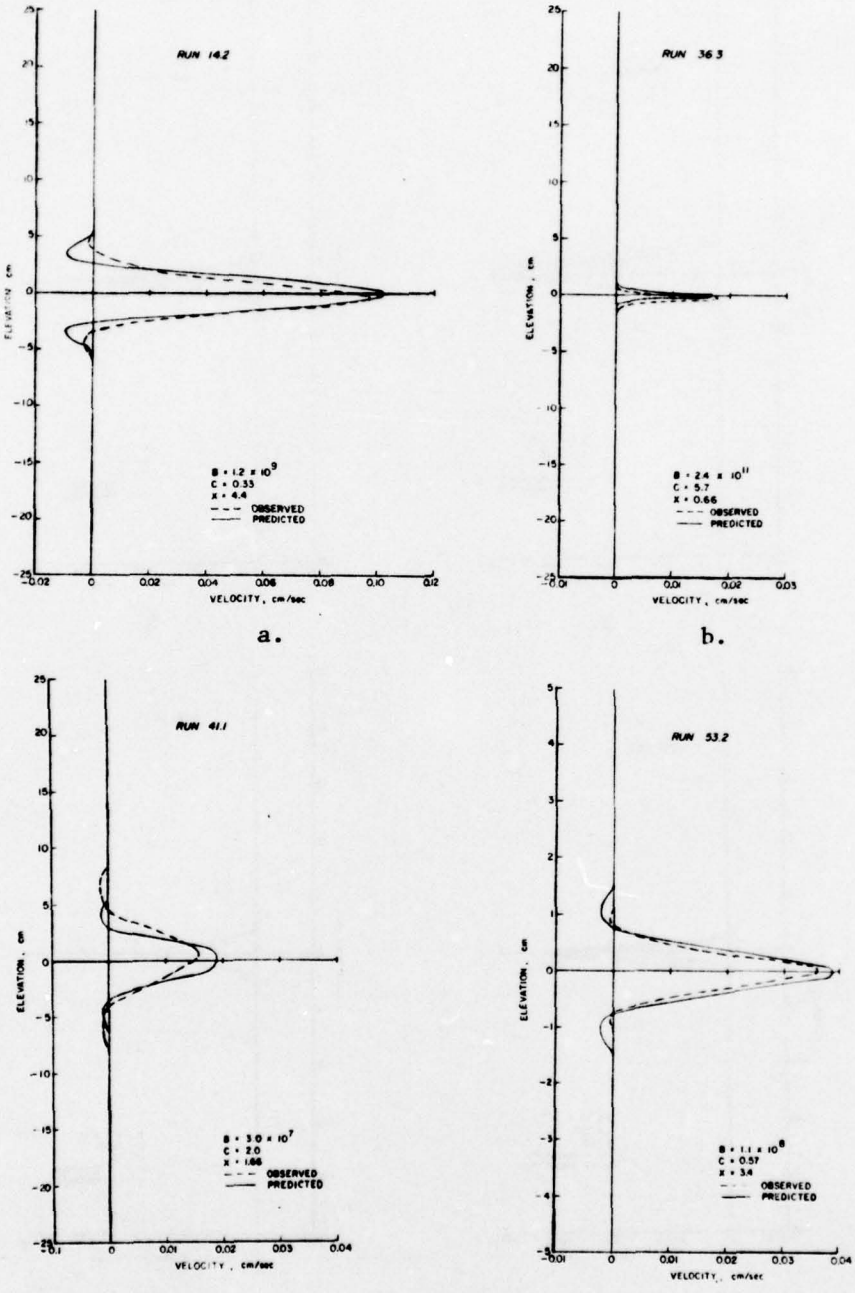

Fig. 51. Results of runs 14, 36, 41, and 53

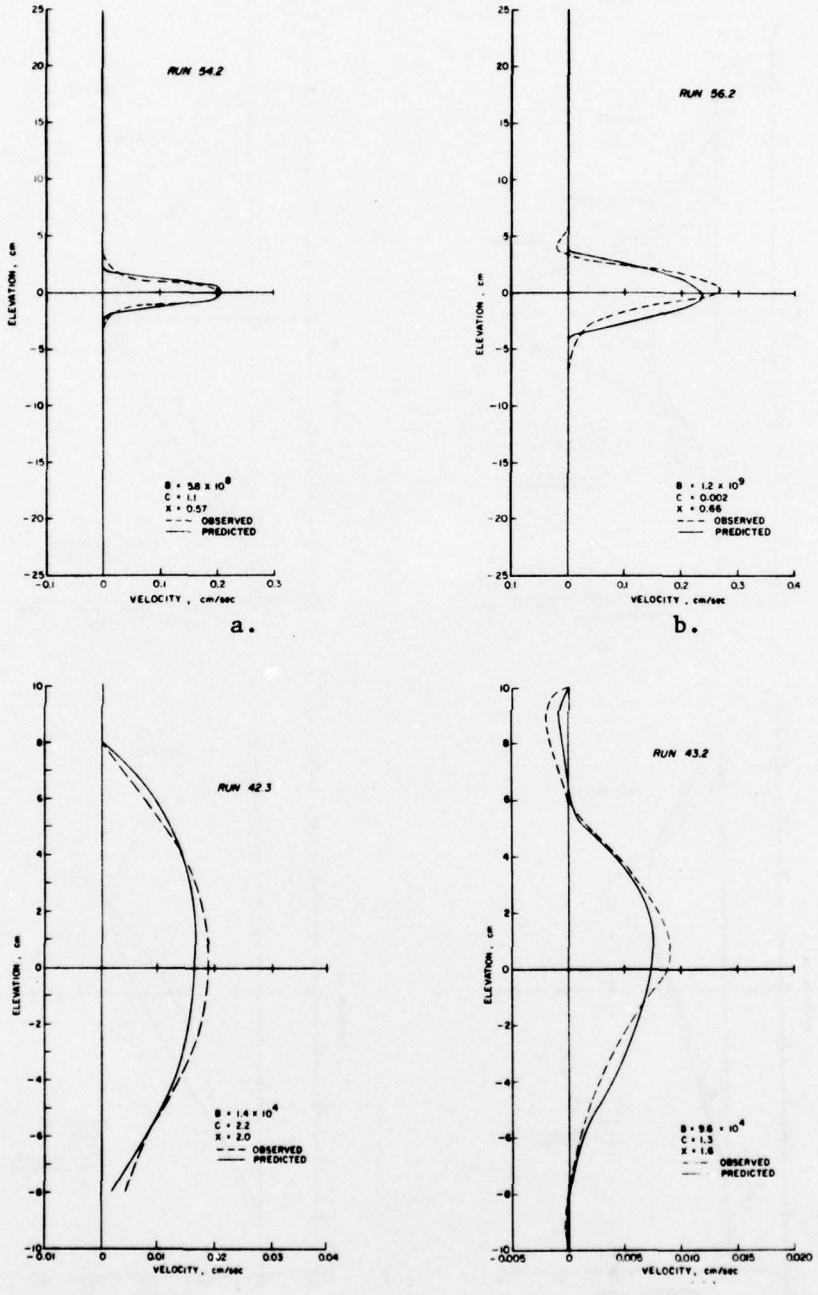

Fig. 52. Results of runs 54, 56, 42, and 43

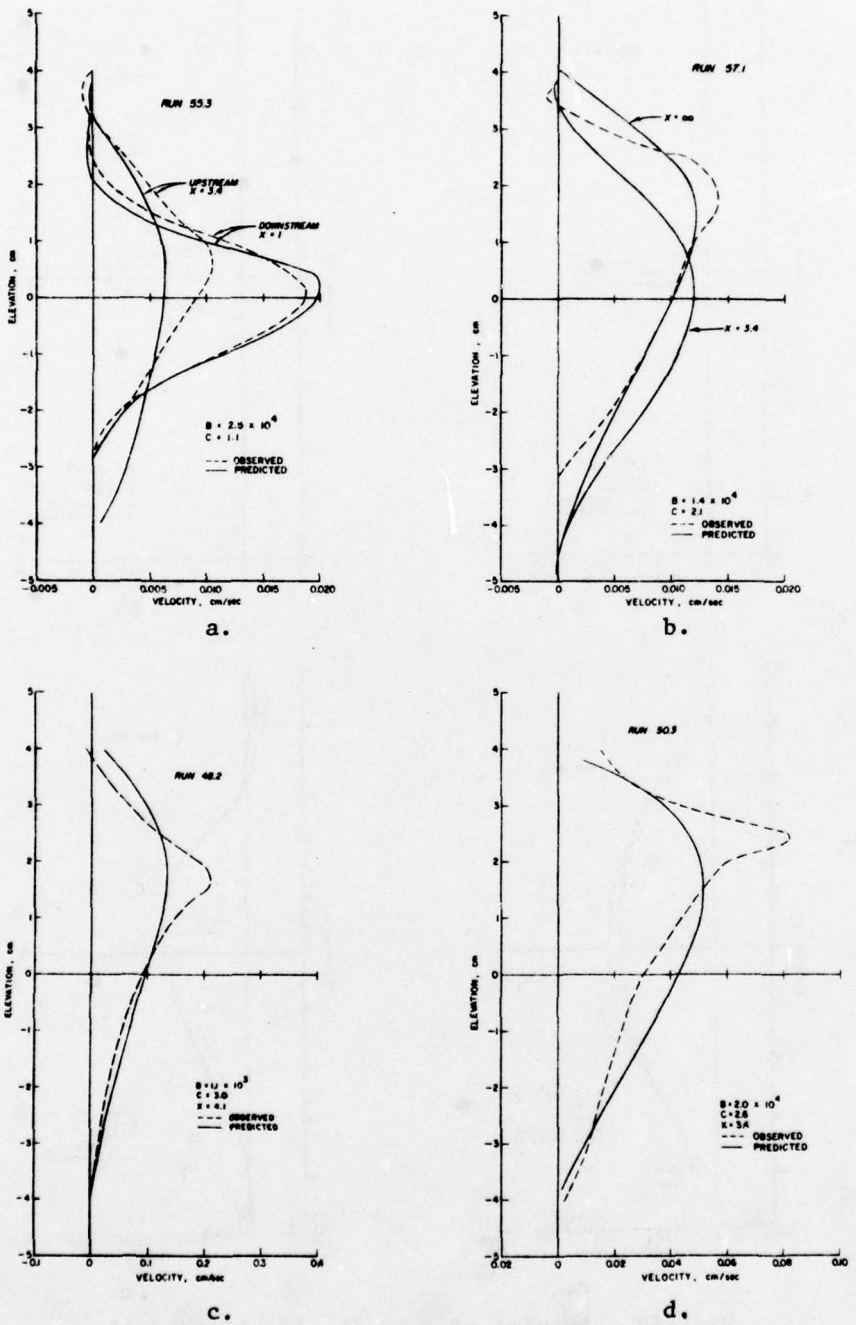

Fig. 53. Results of runs 55, 57, 48, and 50

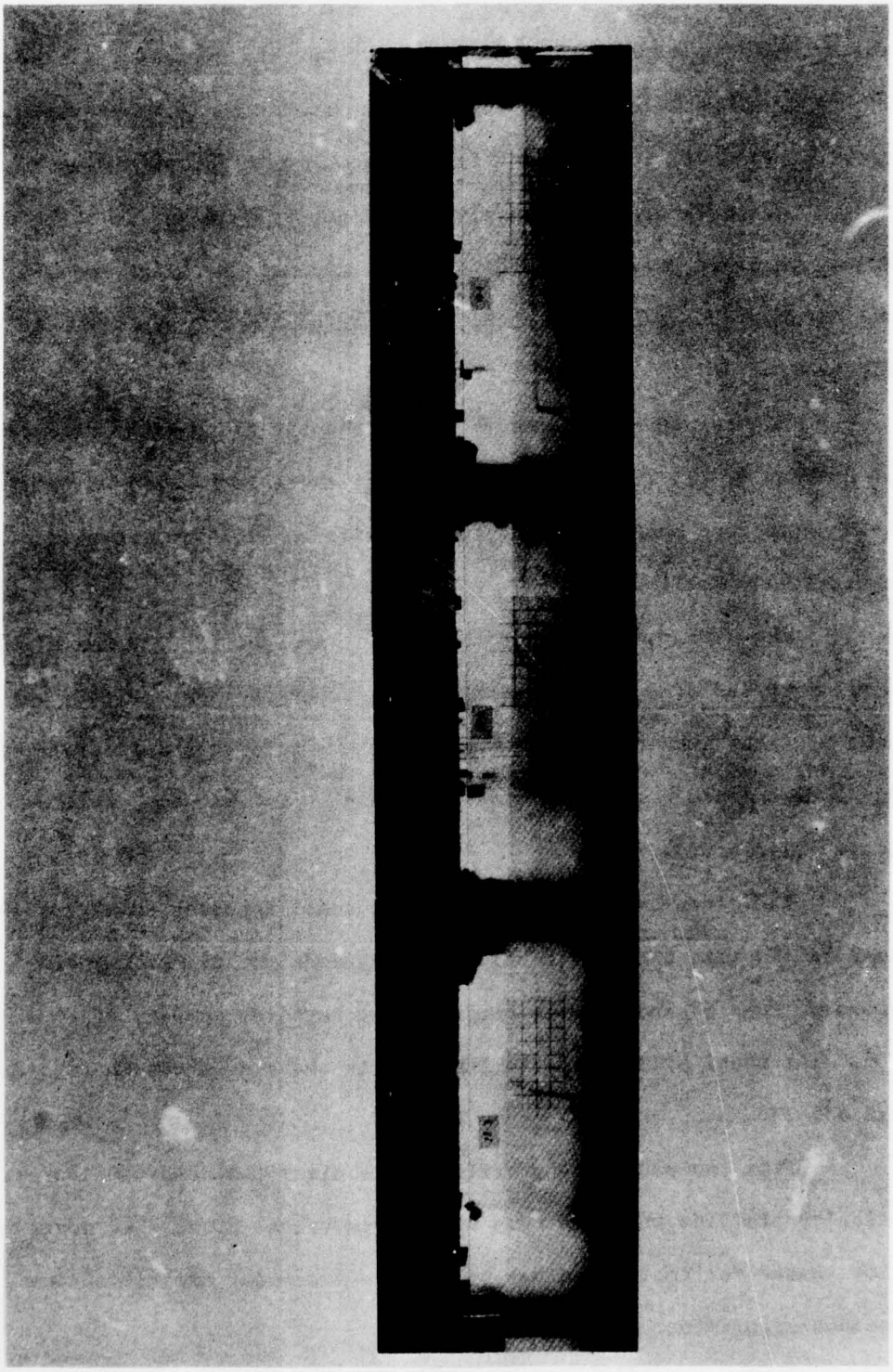

Fig. 54. Run with two-layer stratification

95. The actual velocity profiles have been smoothed in some cases where there was turbulence or a secondary surface current. For example, Figure 42 shows a forward flowing current at the surface (probably due to wind stress). This current is not shown in the graph of run 11.

Velocity profiles are given in Figures 50-54 for 16 different runs. They are grouped according to the size of the flume and the magnitude of B. The values of B, C, and X for the run are given on each figure.

Figures 50 and 51a show runs in the big flume with large values of B (runs 8, 11, 12, 13, 14). Note that there is a small withdrawal layer with some backflow. Outside the withdrawal layer there is no horizontal velocity.

The next two figures (51b and 51c) are for runs 36 and 41 with similar values of B in the narrow flume. They show essentially the same profiles even though the scales of the experiments were smaller. Run 53 was conducted in the wide flume and shows the same profile shape (Figure 51d).

The preceding runs were all for small Reynolds numbers (0.58 to 23). To test the applicability of the model at higher Reynolds numbers, runs 54 and 56 were conducted at Reynolds numbers of 85 and 156. The model still predicts the profile shape as shown in Figures 52a and 52b.

From the preceding profiles it is clear that the model predicts velocity profiles well for runs with large values of B. The model was also tested for smaller values of B where viscosity stratification becomes significant.

Runs 42 and 43, in Figures 52c and 52d, illustrate the occurrence of incipient skewness in the narrow flume. The bottom of the profile looks like the one-dimensional velocity profiles while the top resembles the buoyancy dominated profiles. The same type of profiles exist in the wide flume for runs 55 and 57 (Figures 53a and 53b).

There were some problems with run 57 since in the mathematical model prediction the profile has not yet begun to skew while in the physical model significant skewing has occurred. While this is more dramatic in this run than some others, it occurred in some runs with small values of B. That is, the forward flowing layer reaches the boundaries for lower values of X in the physical model. This can be explained by: (1) the non-linear inertial terms have been neglected near the sink. Imberger has shown that the predicted withdrawal layer is larger when these terms are included and would therefore match the experimental data better, and (2) in applying a duct model to experimental data from a tank with a fixed back wall, the horizontal accelerations are not accounted for in the mathematical model. This is explained in greater detail in Chapter IX.

Nevertheless, the mathematical model does account for the transition from buoyancy dominated to viscosity dominated flow very well. This is illustrated for run 55 (Figure 53a) in that the experimental profiles are matched with predicted profiles both near the sink and away from the sink for the same run.

Fully developed skewness was observed only in two experimental runs (48 and 50). In these cases the experimental profile can actually be matched with the one-dimensional profile. Runs 48 and 50 (Figures

53c and 53d) show no backflow at the surface while the peaks in the observed and predicted profiles occur at the same elevation.

The peaks of the profiles were considerably higher in the experimental profile. It was postulated that this was due to the fact that the CMC did not have time to form a linear concentration and density gradient and a smooth viscosity gradient. That is, the profiles contained some steps.

To test this, the results of runs 18 and 19 were used. In these runs a sharp interface existed above the sink elevation. The bottom layer had a viscosity of 120 cp while the top layer had a viscosity of 4 cp. If buoyancy forces predominated, flow would only occur below the interface (see cloudy layer in Figure 54). Because of the viscosity difference, most of the flow occurred above the interface.

The profile resembles those obtained from the one-dimensional, two-layer case in Chapter IV. The profiles are compared in Figure 55 and are shown to be very close. Note that the profile in the two-layer case shows a much higher peak than in cases with a smooth viscosity gradient. It was concluded that the peaks in the observed profiles were due to steps in the density and viscosity profiles.

So while the correlations between the observed and predicted velocity profiles are reasonably good, the results would be even better if the back wall were farther upstream (or removed completely) and if steps did not exist in some gradients. The mathematical model proposed for viscosity-stratified flow in this report does account for the important trends observed in the experiments.

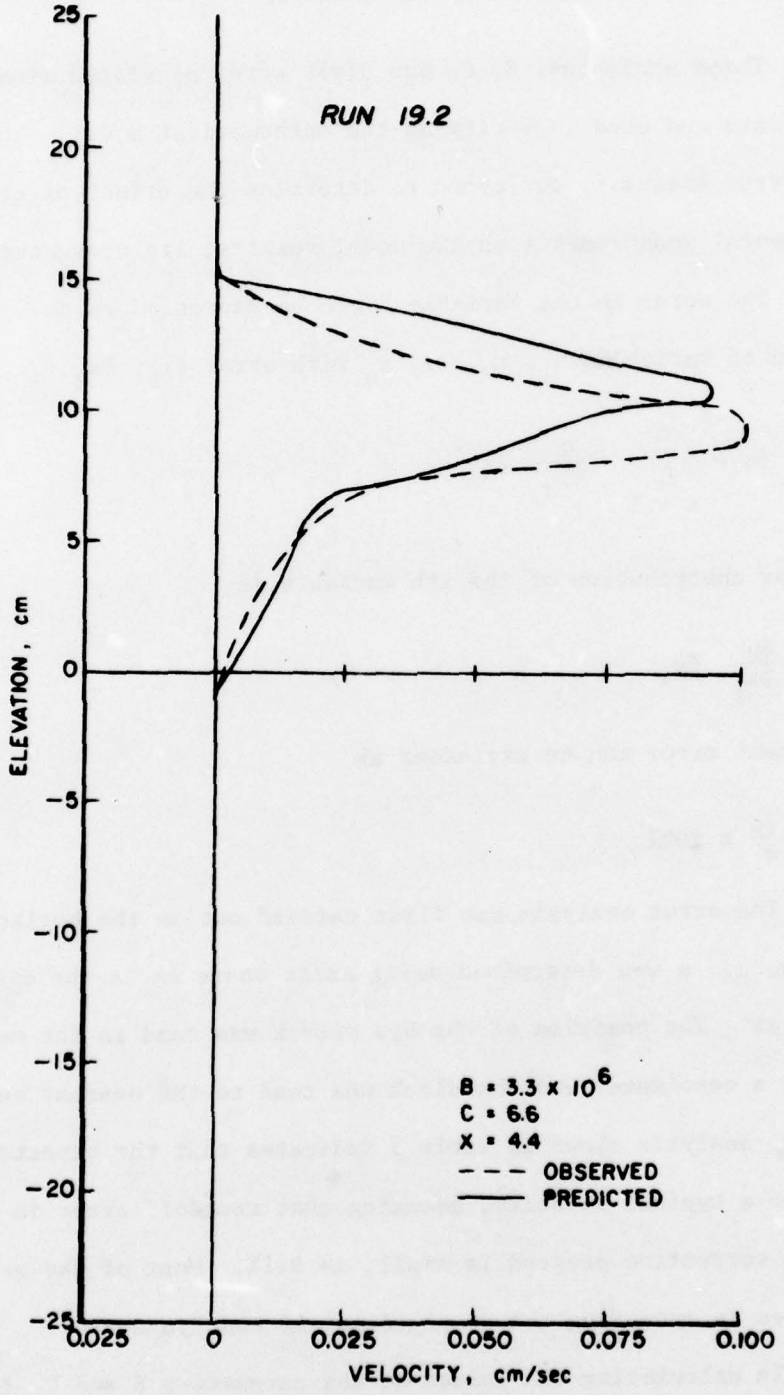

Fig. 55. Results of run 19

Error Analysis

Three variables, B, C, and u(y), were calculated from the experimental data and used in verifying the mathematical model. The results of an error analysis, performed to determine the effect of error in experimental measurements on the model results, are presented below.

The error in the variable u can be expressed as δu. If u is a function of variables $x_1, x_2, .., x_n$ with error $\delta x_1, \delta x_2, .., \delta x_n$, then

$$\delta u = \sum_{i=1}^{n} \frac{\partial u}{\partial x_i} \delta x_i \tag{110}$$

The error contribution of the ith variable is

$$\frac{\partial u}{\partial x_i} \delta x_i$$

The percent error can be expressed as

$$\frac{\delta u}{u} \times 100\%$$

The error analysis was first carried out on the horizontal velocity, u. u was determined using $\Delta x/\Delta t$ where Δx is the displacement in time Δt. The position of the dye streak was read to the nearest tenth of a centimeter and the clock was read to the nearest second. The error analysis shown in Table 3 indicates that the expected maximum error for a typical velocity, assuming that roundoff error in the parallax correction program is small, is 9.1%. Most of the error originates in measuring the displacement of the dye streak.

In calculating the values of the parameters B and C, it is necessary to measure the concentration gradient of the substance

TABLE 3

ERROR ANALYSIS FOR VELOCITY (u)

Parameter	Typical Value	Error	% Error	Error Contribution	% Error Contribution
Δx	1.2	0.1	8.3	0.00167	8.3
Δt	60.	0.5	0.83	0.00017	0.8
u	0.02			0.00184	9.1

causing the density and viscosity gradient. This measurement was subject to error in the instrument used to determine the concentration and in exactly measuring the elevation at which the sample was taken. Another problem is that the gradient was treated as a constant; yet the fluid was placed in the flume in discrete layers. These layers may not have faded into a smooth gradient by the time of the run.

The confidence limits of a slope of a regression line, where b is the regression coefficient for the slope, are

$$b \pm t_{\alpha/2} \frac{S_e}{S_x} \sqrt{\frac{1}{n-1}}$$

where

$t_{\alpha/2}$ = student's t for significance $\alpha/2$

S_e = standard error of estimate

S_x = standard deviation of x

n = number of observations

For this study $\alpha = 0.025$.

Using the above formula for $b = d\mu/dy$ and $d\rho/dy$, the error in

the viscosity and density gradients was estimated. The error in determining $d\mu/dy$ was virtually always less than 30% and in determining $d\rho/dy$ was less than 20%.

The accuracy of the density (specific gravity) measurement using the Pycnometer method according to ASTM Standard D 1429 (1971b) is $\pm$0.005 specific gravity. The viscometer is accurate to 1% while the conductivity meter is accurate to 1% according to the manufacturer. The less accurate of the refractometers is accurate to 0.5% but it was difficult to obtain readings with better than 1% repeatability.

Length measurements were accurate to the nearest 0.5 cm while the accuracy of the flow measure was taken as 10% since it was determined by integrating the velocity profile. Length could be read to the nearest 0.1 cm but it varied during the run and was recorded to the nearest centimeter.

The results of the error analysis for the parameter C shown in Table 4 indicate that most of the error is contributed by the measurement of the viscosity gradient. As mentioned earlier, this was due to the fact that the viscosity gradient did not always fall on a straight line on a semi-log graph.

The error analysis for B is given in Table 5. The principal source of error was the inability to obtain a perfectly linear density gradient. The characteristic length also contributed some error since it varied during the run and was only recorded to the nearest centimeter.

While the percent error on both B and C is large, it must be remembered that these values represented the maximum error, and almost all

TABLE 4

ERROR ANALYSIS FOR C

Parameter	Typical Value	Error	% Error	Error Contribution	% Error Contribution
ℓ	20.	0.5	2.5	0.05	2.5
μ	2.00	0.02	1.	0.02	1.
$d\mu/dy$	0.20	0.06	30.	0.60	30.
C	2.00			0.67	33.

TABLE 5

ERROR ANALYSIS FOR B

Parameter	Typical Value	Error	% Error	Error Contribution	% Error Contribution
ℓ	20.	0.5	2.5	0.18E08	10
ε	0.0012	0.00024	20.	0.38E08	20
ρ_o	1.00	0.01	1.	0.18E07	1
μ_o	2.00	0.02	1.	0.18E07	1
q	0.05	0.005	10.	0.18E08	10
B	1.88E08			0.78E08	42

of the error is contributed by error in fitting a slope to the density and viscosity gradients. In general the error was much less than the values used in the error analysis.

The velocity profiles are in general not extremely sensitive to changes in B. The only zone in which B affects the profile significantly is the transition zone from buoyancy to viscosity dominated flow. An error in B would affect the x-coordinate at which this transition occurs. The velocity profile for run 57 (Figure 53b) appears to be the only profile seriously affected by this type of error. A 42% maximum error is not extremely significant when one realizes that in the experiment, B varied over eight orders of magnitude. The effect of B on skewness can be found in Figures 29 through 31 in Chapter VIII.

Since the flume was filled to produce a linear concentration and density gradient, a linear or log-linear viscosity gradient could not be achieved since viscosity does not vary linearly or log-linearly with concentration. Therefore, it was necessary to settle for whatever viscosity gradient resulted from the linear concentration gradient. This type of error shows up most dramatically in run 50.3 (Figure 53d). The viscosity gradients in most runs contained much less error than the 33% shown in Table 4. The effect of C on skewness can be found in Figures 13 and 14.

CHAPTER XII

EXTENSION TO WEIR FLOW

In most practical problems the type of line sink that is of most interest is a weir. If a stratified fluid is flowing over a weir with a substance whose concentration gradient is known upstream, the problem is then to predict the concentration of that parameter as it flows over the weir.

Problem Formulation

This problem is solved using the log viscosity gradient model

$$\frac{\partial^4\Psi}{\partial Y^4} - 2C\frac{\partial^3\Psi}{\partial Y^3} + C^2\frac{\partial^2\Psi}{\partial Y^2} + Be^{-C\Psi}\frac{\partial\Psi}{\partial Y} = 0 \qquad (111)$$

The principal differences between flow to a line sink at mid-depth and a weir are the boundary conditions. The weir is merely a line sink located at the surface rather than at mid-depth. The flow is also allowed to slip along the top boundary, since this represents an air-water interface. The boundary conditions, shown in Figure 56, can be written as

$$\Psi(0,0) = 0 \qquad (112)$$

$$\Psi(X,0) = -0.5\ , \quad X>0 \qquad (113)$$

$$\Psi(0,Y) = +0.5\ , \quad Y<0 \qquad (114)$$

$$\Psi(X,1) = +0.5\ , \quad X>0 \qquad (115)$$

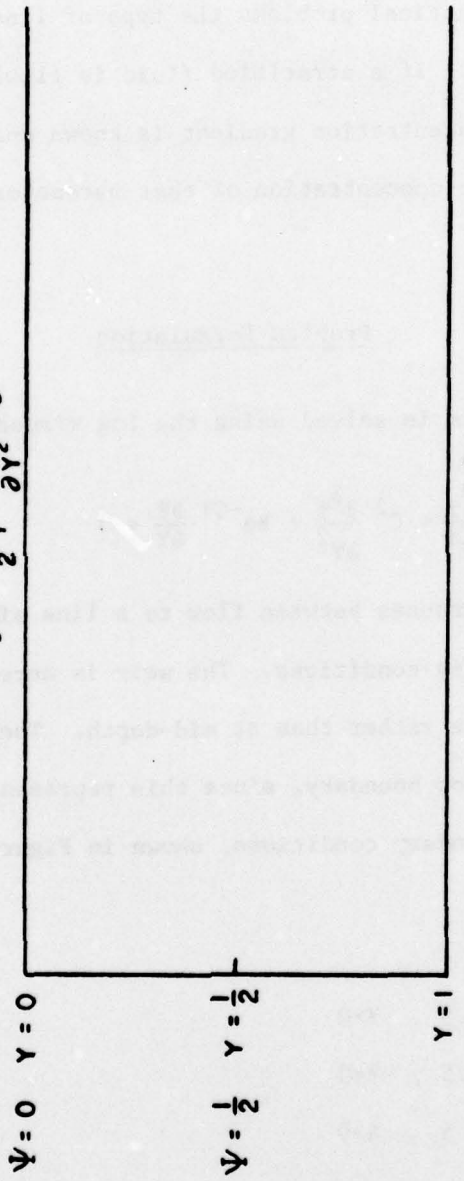

Fig. 56. Boundary conditions for weir problem

$$\frac{\partial \Psi}{\partial Y}(X,1) = 0 \tag{116}$$

$$\frac{\partial^2 \Psi}{\partial Y^2}(X,0) = 0 \tag{117}$$

The first condition (equation 112) represents the weir; the next three (equations 113, 114, and 115) represent no flow through the top, bottom, or downstream boundary; the fifth (equation 116) represents drag on the bottom; and the sixth (equation 117) represents slip along the surface.

Note that the solution presented is valid only for the case in which the depth of flow over the weir is small in comparison to the total height over the weir, since the sink in the model is treated as being only one grid cell wide. A weir with large head can be modeled by using a sink several cells wide, provided the inertial forces are small.

Velocity Profiles

The equations were solved numerically using the same techniques as with the line sink. First the parameter B was varied to determine how it would affect the flow. The streamlines of the solution for $B = 10^3, 10^5, 10^7$ are shown in Figure 57. As was demonstrated earlier, for large values of B, the withdrawal layer is very narrow, since buoyancy forces predominate. As B decreases, the viscous effects become greater and the profile reaches the bottom of the duct.

Figure 58 gives the velocity profiles at X = 10 for the streamlines shown in Figure 57. For large B the velocity tends to be restricted to the surface layers.

Next the parameter C was varied (0.1, 2.0, 5.0) for a constant

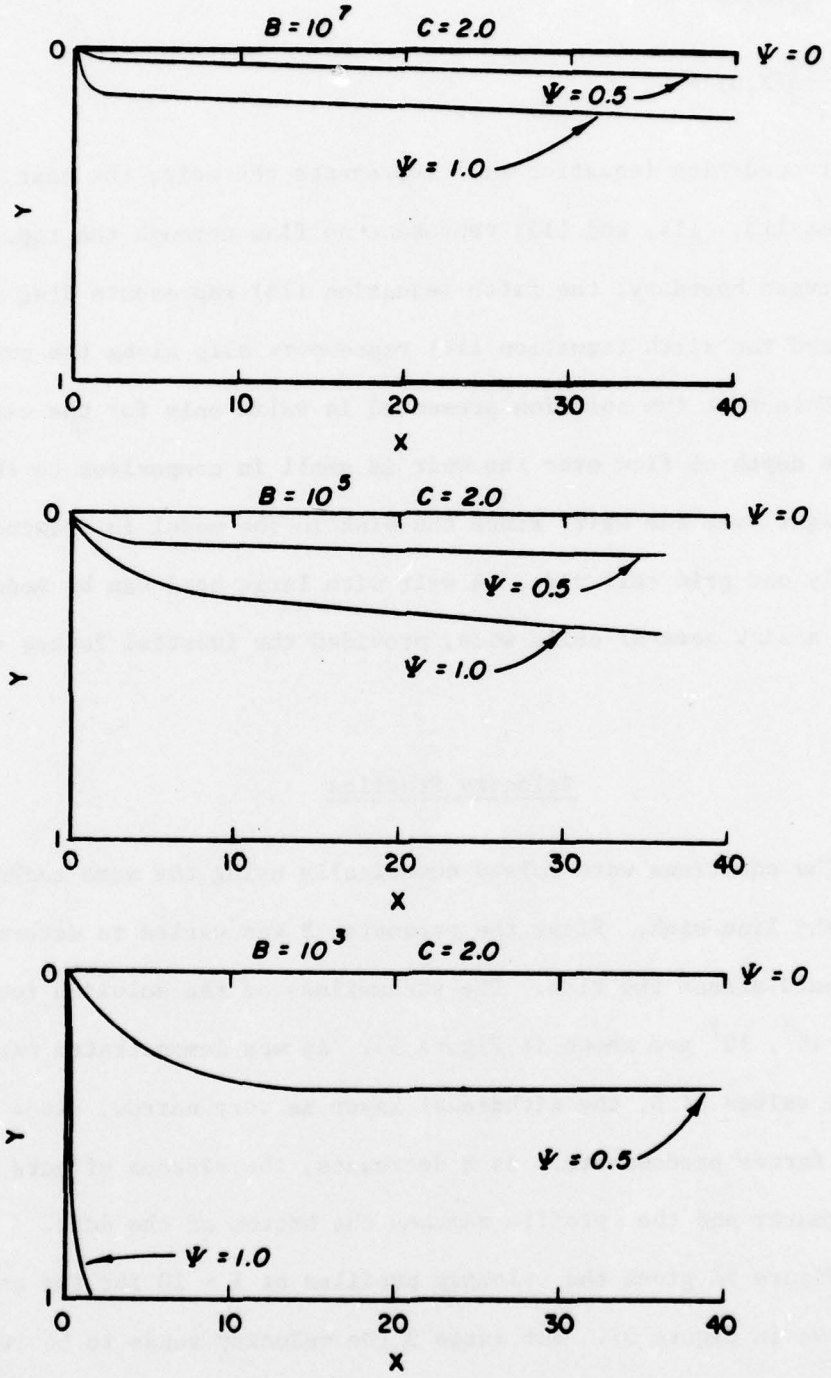

Fig. 57. Effect of B on streamlines

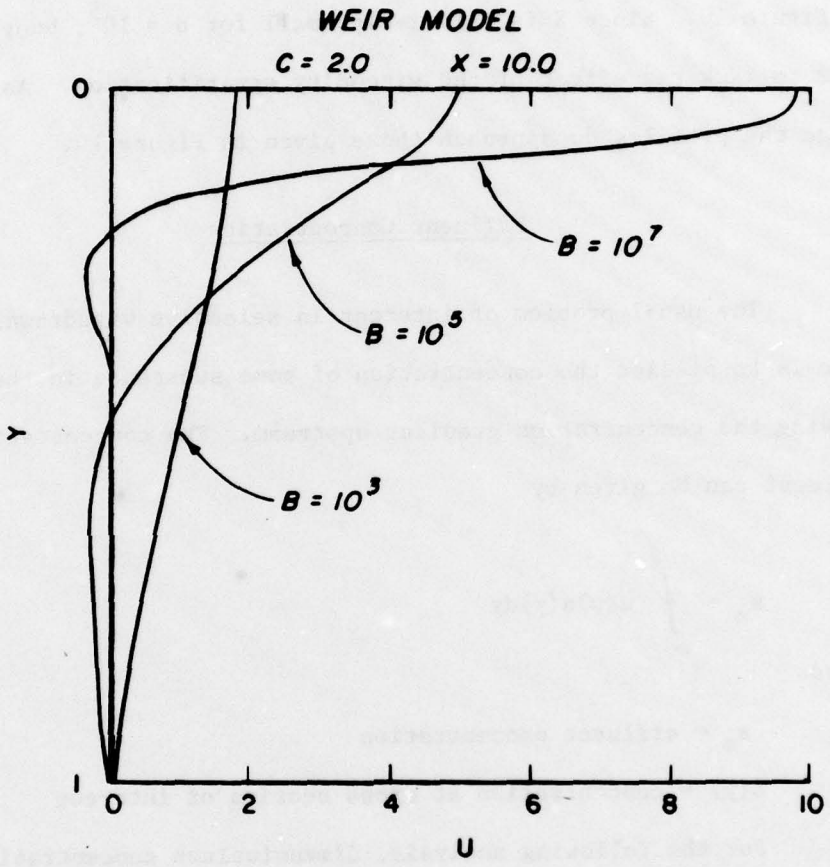

Fig. 58. Effect of B on velocity profiles

value of $B = 10^5$. The resulting velocity profiles at X = 10 are given in Figure 59. The effect of C on these profiles is not significant until C becomes fairly large as was shown in the one-dimensional results in Figure 10. Since X is relatively small for $B = 10^5$, buoyancy forces tend to mask the effect of the viscosity stratification. As X becomes large the profiles do approach those given in Figure 10.

Effluent Concentration

The usual problem of interest in selective withdrawal over a weir is to predict the concentration of some substance in the effluent knowing the concentration gradient upstream. The concentration in the effluent can be given by

$$s_e = \int_0^{\ell} u(y)s(y)dy \tag{118}$$

where

s_e = effluent concentration

$s(y)$ = concentration at cross section of interest

For the following analysis, dimensionless concentration $S = s/s(1/2)$ will vary linearly with dimensionless depth as given by

$$S = 2Y \tag{119}$$

If a uniform velocity profile exists, then $S_e = 1$. If the velocity is greater near the surface, then the effluent concentration will be less than one. Dimensionless effluent concentration is therefore

$$S_e = \int_1^0 U(Y)2YdY \tag{120}$$

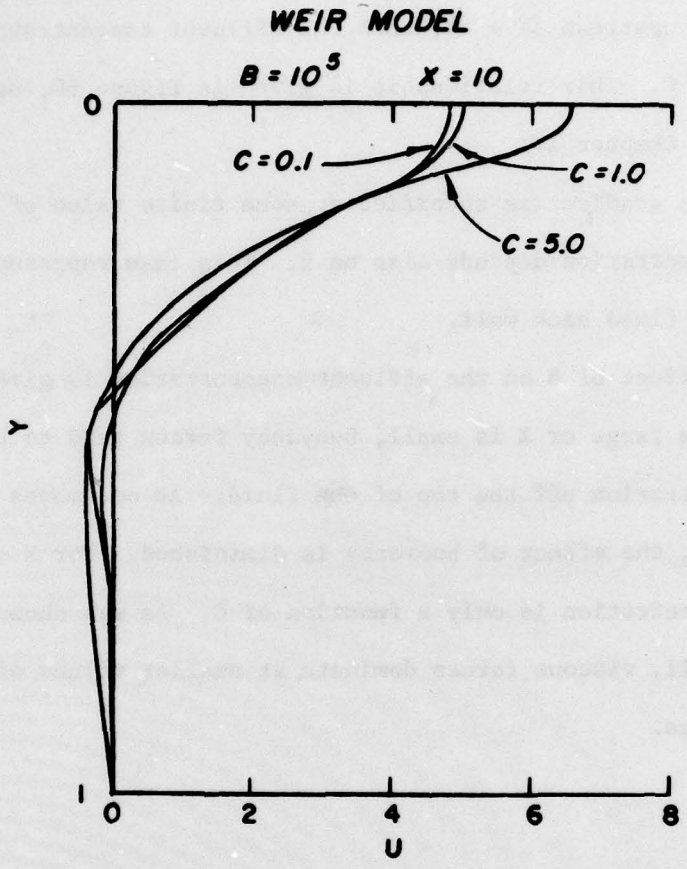

Fig. 59. Effect of C on velocity profiles

The effluent concentration depends on the distance from the weir at which the concentration gradient is specified. If the gradient is specified far upstream ($X \to \infty$), then the effluent concentration is purely a function of C. This relationship is given in Figure 60, using the solution from Chapter IV.

If the gradient is specified at some finite value of X, the effluent concentration depends also on B. This case represents that of a tank with a fixed back wall.

The effect of B on the effluent concentration is given in Figure 61. When B is large or X is small, buoyancy forces tend to skim layers of low concentration off the top of the fluid. As one moves farther from the weir, the effect of buoyancy is diminished. For $X \to \infty$, the effluent concentration is only a function of C. As was shown earlier, when B is small, viscous forces dominate at smaller values of X than when B is large.

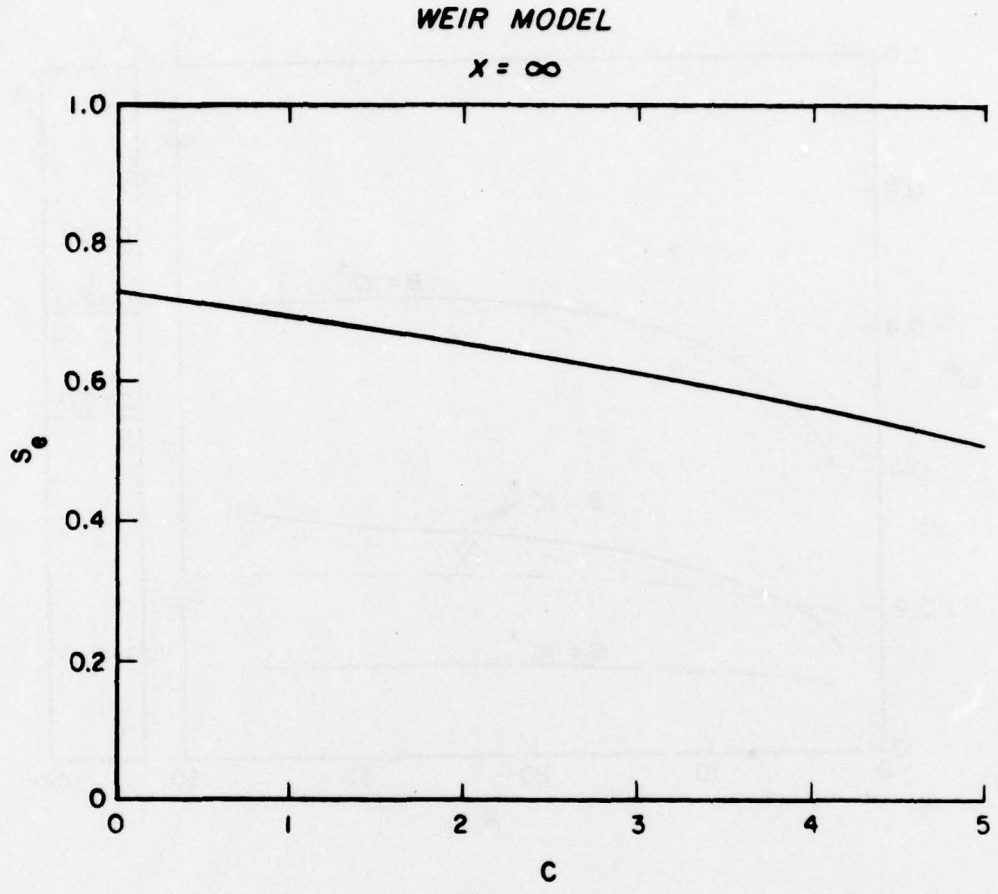

Fig. 60. Effect of C on effluent concentration for large X or small B

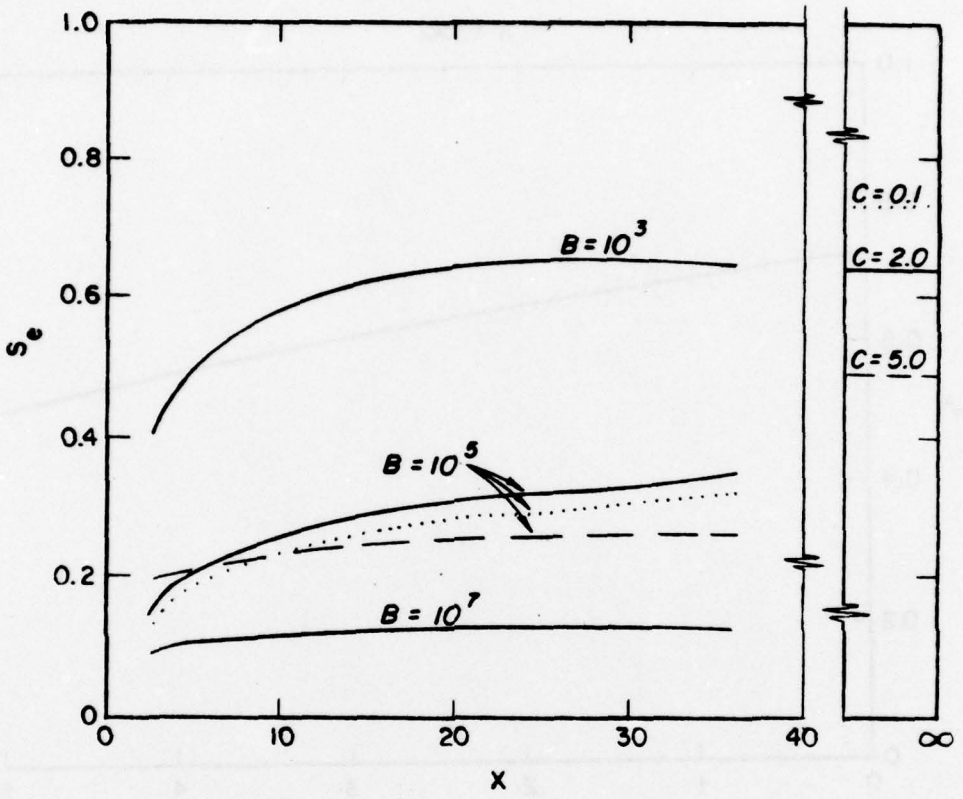

Fig. 61. Dimensionless effluent concentration for weir model

CHAPTER XIII

EXTENSION TO NON-NEWTONIAN FLUIDS

The problem of stratified flow in a non-Newtonian fluid is more complicated than the Newtonian case since more than one parameter is required to describe the relationship between shear stress and shear rate. When the flow is stratified, all of these parameters may vary with depth. In this chapter, only the parameter that changes dramatically with depth will be treated as a variable in modeling the flow. A stratified Bingham plastic fluid is studied for two cases: yield stress varying as a function of the logarithm of depth and yield stress varying as a linear function of depth.

For a Bingham plastic fluid, represented by the model

$$\tau_{yx} = \mu \frac{du}{dy} + \tau_{oyx}, \quad |\tau| > \tau_{oyx} \tag{121}$$

both μ and τ_o can vary with depth. The Bingham plastic model is important since suspensions of fine-grained sediments behave as Bingham plastics.

Concentration of fine-grained suspended solids in a dredged material containment area have been reported to increase with depth by Montgomery (1978) and Walski and Schroeder (1978). This would imply that both μ and τ_{oyx} increase with depth.

In Appendix D, it is shown that the increased suspended solids with depth affect the yield stress more than the viscosity so that the μ term can be treated as a constant in the model developed in this

chapter. This means that once the yield stress is exceeded, the fluid behaves as an unstratified fluid.

In this part of the report, a one-dimensional model is developed for a Bingham plastic fluid in which yield stress varies with depth. The model predicts depth of flowing zone and velocity profile for this type of flow.

Logarithmic Yield Stress Gradient

The definition sketch of the system to be investigated in this chapter is given in Figure 62. Note that the boundary conditions have more in common with the weir model than the one-dimensional line sink models. The yield stress varies with depth as given by

$$\tau_{oyx} = \tau_{ayx} y^b \tag{122}$$

The model to be investigated can be given by

$$-\frac{\partial \tau_{yx}}{\partial y} = \frac{\partial p}{\partial x} \tag{123}$$

$$\tau_{yx} = -\mu \frac{du}{dy} + \tau_{oyx} \quad , \quad |\tau_{yx}| \geq \tau_{oyx} \tag{124}$$

$$\frac{du}{dy} = 0 \quad , \quad |\tau_{yx}| < \tau_{oyx} \tag{125}$$

with boundary conditions

$$u(\ell) = 0 \tag{126}$$

$$\tau_{yx}(0) = 0 \tag{127}$$

$$\int_0^{\ell} u\,dy = q \tag{128}$$

These equations can be non-dimensionalized using q, ℓ, μ as

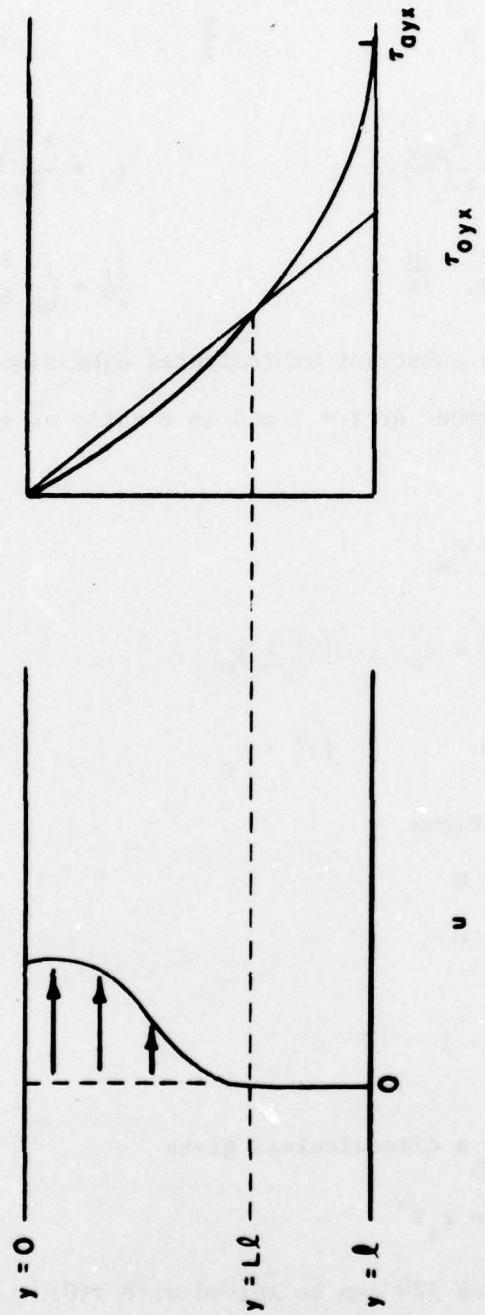

Fig. 62. Definition sketch, Bingham plastic, log gradient

characteristic flow, length and viscosity. The non-dimensionalization gives the following substitutions

$$U = \frac{\ell}{q} u \qquad Y = \frac{y}{\ell} \qquad \tau = \frac{\ell^2 \tau_{yx}}{q\mu}$$

$$\tau_a = \frac{\ell^2 \tau_{ayx}}{q\mu} \qquad \tau_o = \frac{\ell^2 \tau_{oyx}}{q\mu}$$

$$P_x = \frac{\ell^3}{q\mu} \frac{\partial p}{\partial x} \qquad \frac{\partial \tau}{\partial Y} = \frac{\ell^3}{q\mu} \frac{\partial \tau_{yx}}{\partial y}$$

Note τ without subscript yx indicates dimensionless τ_{yx}. τ_a is known as the Bingham number at Y = 1 and is a ratio of viscous to yield force.

Substituting

$$-\frac{\partial \tau}{\partial Y} = P_x \tag{129}$$

$$\tau = \frac{dU}{dY} + \tau_o \quad , \quad |\tau| \geq \tau_o \tag{130}$$

$$\frac{dU}{dY} = 0 \quad , \quad |\tau| < \tau_o \tag{131}$$

Boundary conditions

$$\tau(0) = 0 \tag{132}$$

$$U(1) = 0 \tag{133}$$

$$\int_0^1 U dY = 1 \tag{134}$$

Treating y^b as a dimensionless gives

$$\tau_o(Y) = \tau_a Y^b \tag{135}$$

Equation 129 can be solved with $\tau(0) = 0$ to give

$$\tau = -P_x Y \tag{136}$$

There are two cases, the first is where

$$|\tau(Y)| \geq \tau_o \tag{137}$$

where the fluid behaves as a Newtonian fluid and

$$|\tau(Y)| < \tau_o \tag{138}$$

where the velocity gradient is zero. These cases give rise to three types of flow

1. $|\tau(Y)| \geq \tau_o$ for all Y, the fluid behaves as a Newtonian fluid and the solution given in Chapter IV is valid.

2. $|\tau(Y)| < \tau_o$ for all Y, the fluid behaves as a solid plug. The boundary condition U(1) = 0 forces the plug to be stationary.

3. There exists Y = L such that

$|\tau(Y)| > \tau_o$ for $Y \leq L$

$|\tau(Y)| < \tau_o$ for $Y > L$

which combined with the boundary condition (U(1) = 0), means that there is a stationary zone on the bottom with flow above. This type of flow is examined below in greater detail. L is referred to as the depth of the flowing zone.

L can be determined by noting that at L

$$|\tau(Y)| = \tau_o \tag{139}$$

which, upon substituting from equations 135 and 136, implies

$$-\frac{P_x}{\tau_a} = L^{b-1} \quad , \quad 0 < L \leq 1 \tag{140}$$

For Y>L

$$\frac{dU}{dY} = 0 \tag{131}$$

which implies

$$U(Y) = 0 \quad , \quad Y > L \tag{141}$$

For $Y \leq L$ the Bingham plastic model gives

$$- \frac{dU}{dY} + \tau_a Y^b = P_x Y \tag{142}$$

which can be solved to yield

$$U = \begin{cases} \frac{\tau_a L^{b+1}}{b+1} \left[\left(\frac{Y}{L} \right)^{b+1} - 1 \right] + \frac{P_x L^2}{2} \left[\left(\frac{Y}{L} \right)^2 - 1 \right] , & 0 \leq Y \leq L \\ 0 , & L \leq Y \leq 1 \end{cases} \tag{143}$$

The continuity boundary condition (equation 134) can be used to solve for P_x

$$- P_x = \frac{3}{L^3} \left(1 + \tau_a \frac{L^{b+2}}{b+2} \right) \tag{144}$$

Recalling $- P_x / \tau_a = L^{b-1}$, the above relation can be substituted for P_x and solved for L

$$L = \left[\frac{3}{\tau_a} \left(\frac{b+2}{b-1} \right) \right]^{1/(b+2)} \tag{145}$$

The above equation gives the depth of the forward flowing layer as a function of τ_a and b only. The results are plotted in Figure 63.

The depth of the flowing zone (L) is dependent on both the yield stress of the fluid on the bottom (τ_a) and the curvature of the relationship between yield stress and depth (b). As b approaches one, it becomes less likely that the case in which part of the fluid moves and part remains stationary will occur. This type of zone will occur when the τ_{yx} and τ_{oyx} lines intersect as shown in Figure 62. This is much more likely to occur when the τ_{oyx} is highly curved (large b) since the τ_{yx} line is straight.

Velocity profiles for the case in which $\tau_o = \tau_a Y^b$ are shown in

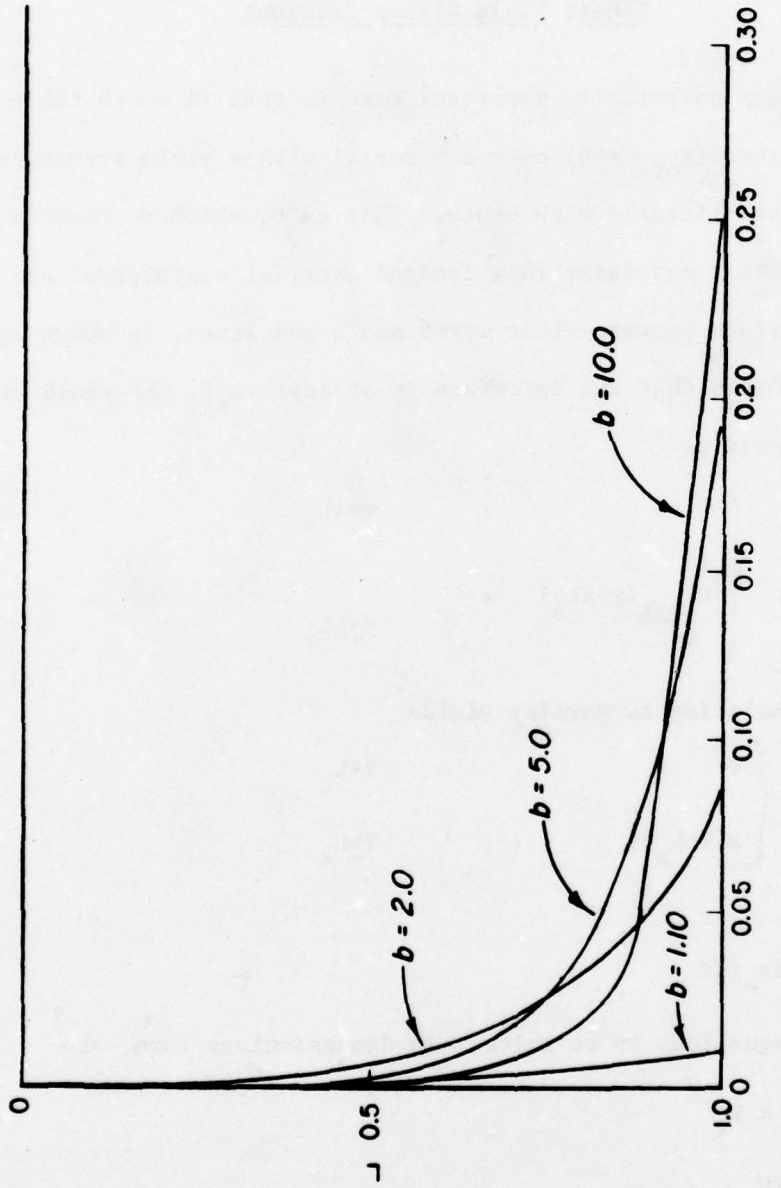

Fig. 63. Depth of flowing zone vs. Bingham number

Figure 64 for a series of values of b and τ_a.

Linear Yield Stress Gradient

Another potentially important case is that in which there exists a layer of water ($\tau_{oyx} = 0$) over a material with a yield stress gradient which increases linearly with depth. This case, which represents the type of flow that may exist in a dredged material containment area with a sharp interface between clear water and a mud layer, is shown in Figure 65. Given that the interface is at depth $L_a \ell$, the yield stress can be expressed as

$$\tau_{oyx} = \begin{cases} 0 & , \quad y > \ell L_a \\ \dfrac{d\tau_{oyx}}{dy}(y - \ell L_a) & , \quad y \leq \ell L_a \end{cases} \tag{146}$$

Non-dimensionalizing as earlier yields

$$\tau_o = \begin{cases} 0 & , \quad Y < L_a \\ a(Y - L_a) & , \quad Y \geq L_a \end{cases} \tag{147}$$

where

$$a = d\tau_o/dY$$

The equations to be solved, in dimensionless form, are

$$-\frac{\partial \tau}{\partial Y} = P_x \tag{129}$$

$$\tau = \frac{dU}{dY} + \tau_o \quad , \quad (L_a \leq Y \leq L) \tag{148}$$

$$\frac{dU}{dY} = 0 \quad , \quad (Y > L) \tag{149}$$

$$\tau = -\frac{dU}{dY} \quad , \quad Y \leq L_a \tag{150}$$

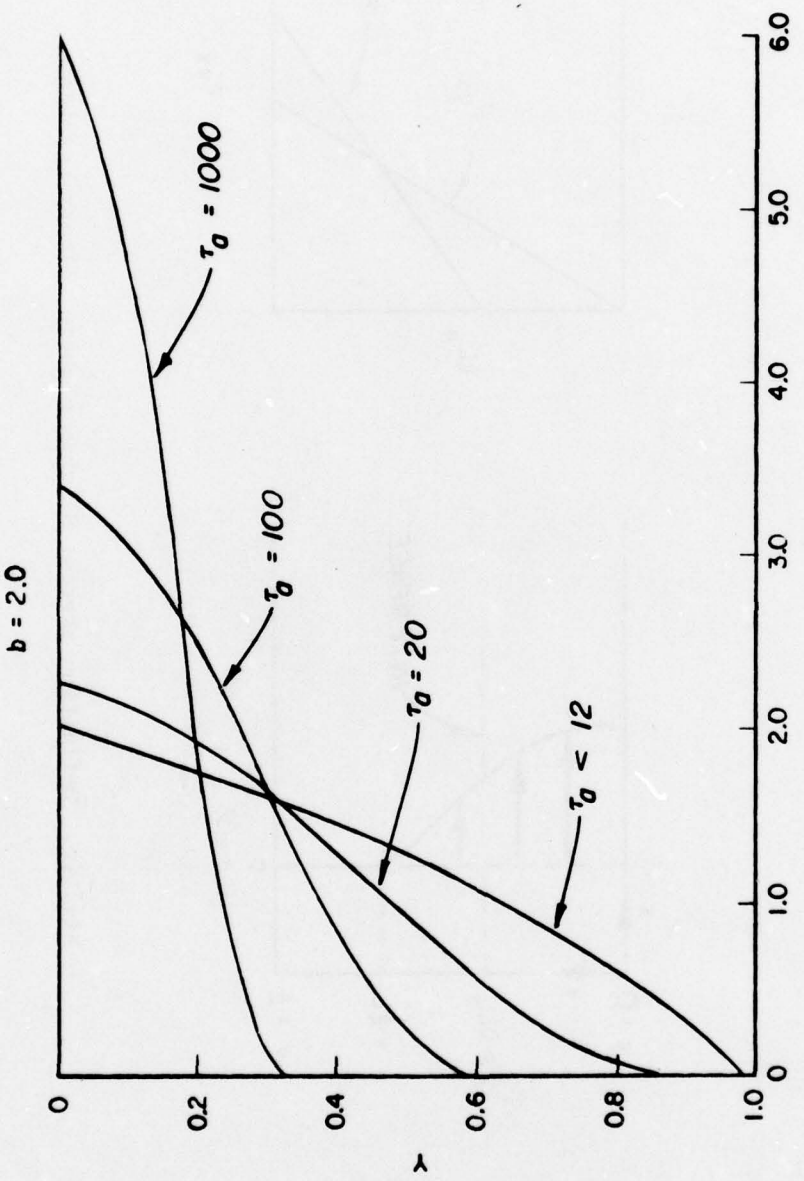

Fig. 64. Effect of Bingham number on velocity profiles

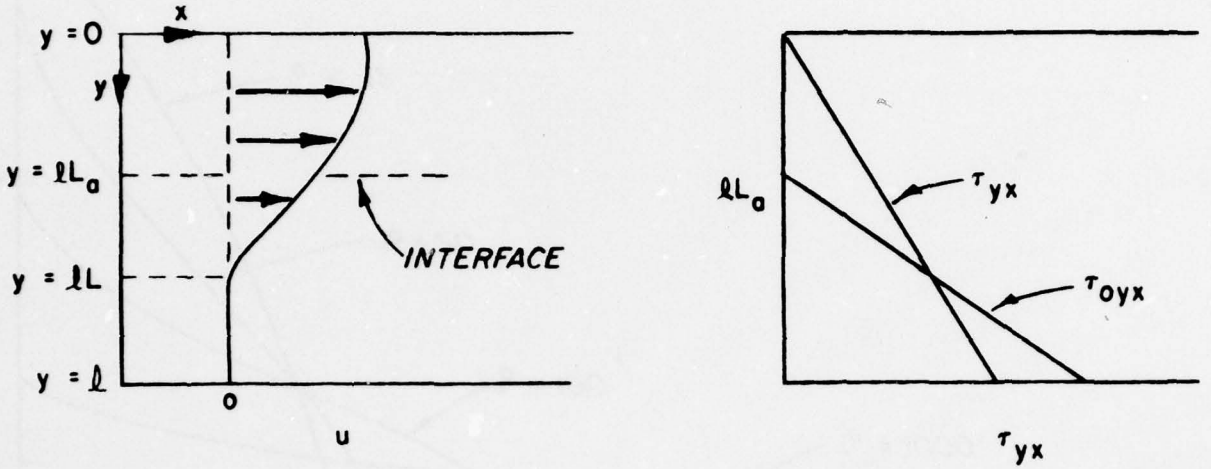

Fig. 65. Definition sketch, Bingham plastic, linear gradient

$$\tau_o = a(Y-L_a) \quad , \quad 1 \geq Y \geq L_a \tag{151}$$

with boundary conditions given by equations 132, 133, and 134. τ and U are continuous at L_a.

As in the log type yield stress gradient, three types of flow may exist

1. ($L_a = L$) Newtonian flow above Y = L; no flow below.
2. (L = 1) Newtonian flow throughout fluid.
3. ($L_a > L > 1$) forward flowing layer penetrates into the portion of the fluid that is a Bingham plastic.

The x-momentum equation can be solved to yield (with $\tau(0) = 0$)

$$\tau = -P_x Y \tag{136}$$

L can be found by substituting for τ in the above equation and noting that the case that is of interest is $L_a \leq L$

$$a(Y-L_a) = -P_x Y \text{ for } Y = L \tag{152}$$

substituting L for Y yields

$$L = \frac{aL_a}{a + P_x} = \frac{L_a}{1 + (P_x/a)} \tag{153}$$

For Y>L

$$\frac{dU}{dY} = 0 \tag{149}$$

which implies U(Y) = 0

For $Y \leq L$, there are two possible velocity profiles $Y \geq L_a$, $Y < L_a$. For $Y \leq L_a$, $\tau_o = 0$ and $\tau(L_a) = -P_x L_a$

The last condition serves as a top boundary condition for the case $Y \geq L_a$. Substituting for τ using the Bingham model and $\tau_o = a(Y-L_a)$

$$-\frac{dU}{dY} + \tau_o = -\frac{dU}{dY} + a(Y-L_a) = -P_x Y \tag{154}$$

which can be solved using U(L) = 0 to give

$$U = (P_x + a)\frac{L^2}{2}\left[\left(\frac{Y}{L}\right)^2 - 1\right] - a\,L_a L\left[\left(\frac{Y}{L}\right) - 1\right] \quad , \quad L_a \leq Y \leq L \tag{155}$$

Substituting L_a into equation 155 gives

$$U = (P_x + a)\frac{L^2}{2}\left[\left(\frac{L_a}{L}\right)^2 - 1\right] - a\,L_a L\left(\frac{L_a}{L} - 1\right) \tag{156}$$

which is the boundary condition needed to solve for the velocity in the Newtonian depths ($Y<L_a$). That solution is

$$U = \frac{P_x L_a^2}{2}\left[\left(\frac{Y}{L_a}\right)^2 - 1\right] + (P_x + a)\frac{L^2}{2}\left[\left(\frac{L_a}{L}\right)^2 - 1\right] - a\,L_a L\left(\frac{L_a}{L} - 1\right) \quad , \quad 0 \leq Y < L_a \tag{157}$$

In summary, the velocity profile can be written

$$U = \begin{cases} U_1 = 0 & , \; Y>L \\ U_2 = (P_x + a)\frac{L^2}{2}\left[\left(\frac{Y}{L}\right)^2 - 1\right] - a\,L_a L\left(\frac{Y}{L} - 1\right) & , \; L_a \leq Y \leq L \\ U_3 = \frac{P_x L_a^2}{2}\left[\left(\frac{Y}{L_a}\right)^2 - 1\right] + U_2(L_a) & , \; 0 \leq Y < L_a \end{cases} \tag{158}$$

To eliminate P_x from the equation, the continuity boundary condition is used

$$1 = \int_{L_a}^{L} U_2 dY + \int_{o}^{L_a} U_3 dY \tag{159}$$

The integrals can be evaluated to give

$$P_x = \frac{-\left[6 + a\left(L_a^3 - 3L_aL^2 + 2L^3\right)\right]}{2L^3} \tag{160}$$

The expression for P_x can now be substituted into equation 153 and solved for L

$$L = \sqrt{L_a^2 + \frac{6}{aL_a}} \tag{161}$$

The above relationship can be plotted as shown in Figure 66 which can be used to determine the depth of the flowing zone, knowing only a and L_a.

Velocity profiles generated using the above model for $L_a = 0.2$ are shown in Figure 67. As a becomes larger the velocity profiles are cut off much sharper below the interface. Figure 68 shows that the velocity profiles may not be identical even though the withdrawal depth and flow are the same.

Implications

The above solutions can be used to describe flow in a dredged material containment area at locations far from the weir and at times when wind-generated currents are negligible. Once suspended solids in the area have settled to depths greater than L, they are removed from the water column. Unless they are resuspended by wind-generated turbulence, they will not flow over the weir.

The velocity profile can be predicted knowing only the flow, dimensions of the basin, concentration gradient, and relationship of concentration to yield stress. The log gradient case should be

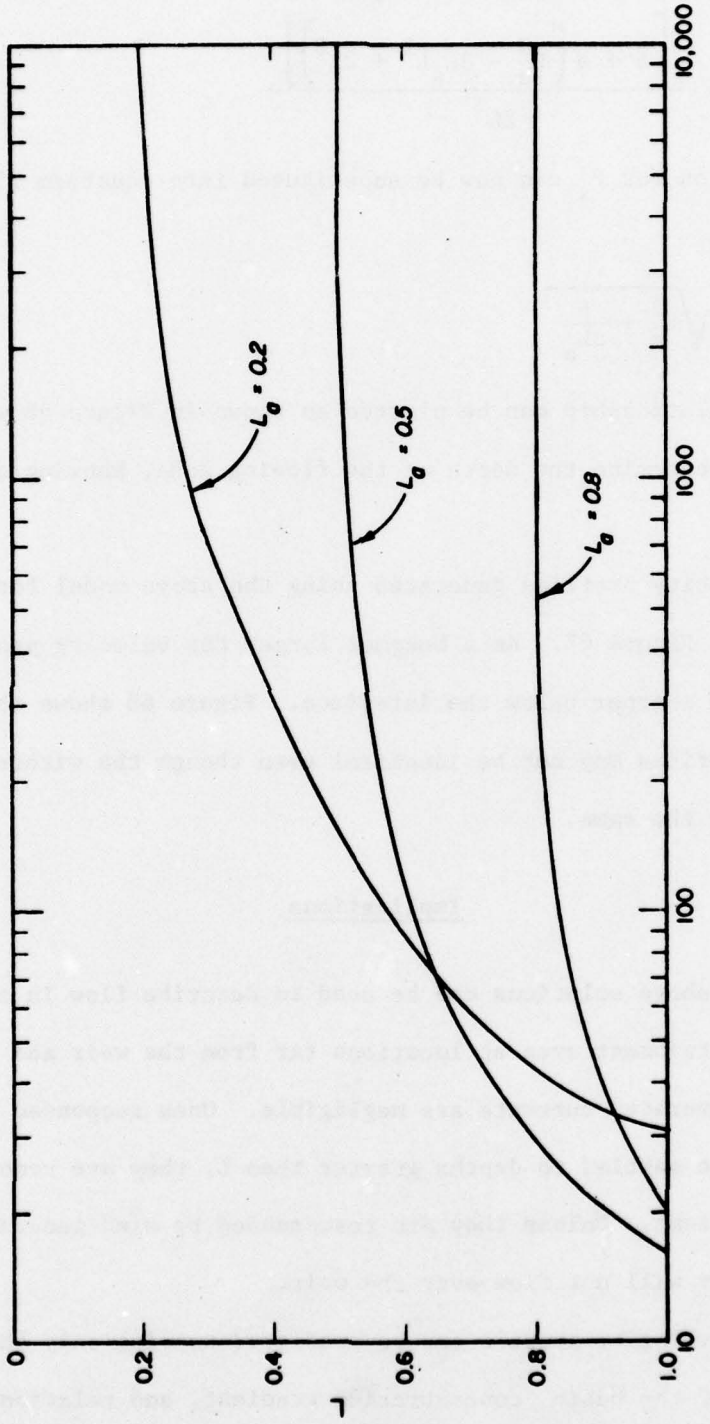

Fig. 66. Depth of flowing layer vs. gradient

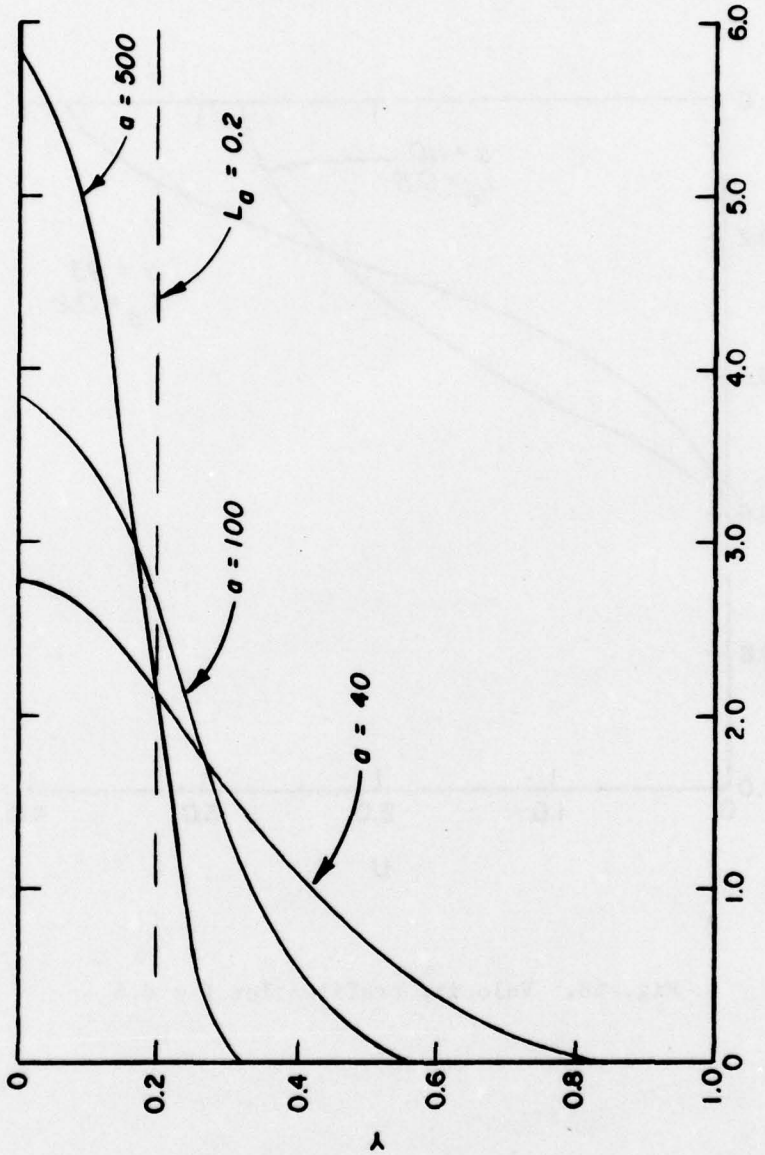

Fig. 67. Velocity profiles for $L_a = 0.2$

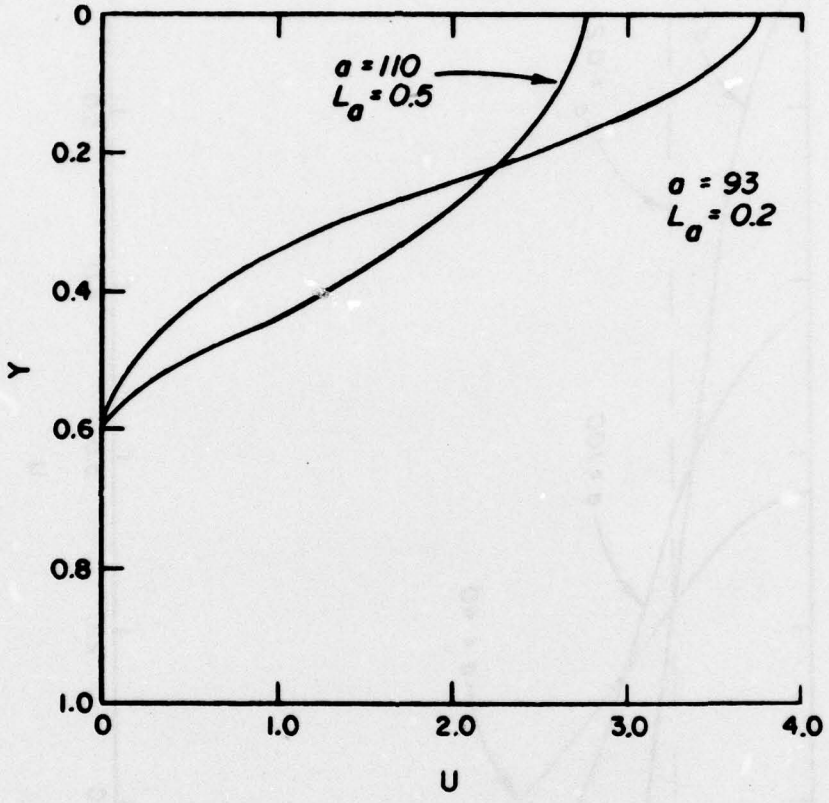

Fig. 68. Velocity profiles for L = 0.6

applicable to areas without a sharp interface while the linear gradient should be appropriate when a sharp interface between a clear water layer and a layer with high solids concentrations exists. If the yield stress gradient does not fit one of the cases solved in this chapter of the report, the equations of motion can be solved with the appropriate yield stress gradient.

In the area near the weir, buoyancy forces predominate and the model presented in the previous chapter should be appropriate. The model presented in this chapter is appropriate when buoyancy and inertial forces are no longer important. This will occur when the streamlines are horizontal. The location at which this occurs is given in Chapter XII.

CHAPTER XIV

CONCLUSIONS AND OBSERVATIONS

Velocity profiles in a fluid in which the viscosity varies vertically will be different than those for a fluid with constant viscosity. This vertical variation in viscosity is referred to as viscosity stratification.

In regions of a fluid where buoyancy and inertial forces are of a smaller magnitude than viscous forces, viscosity stratification will cause the velocity profile to skew positively in the direction of low viscosity.

When flow is to a line sink located at mid-depth in a duct, the skewness can be represented by the third moment of the dimensionless velocity distribution about the sink elevation. This unarbitrary indicator of skewness can be defined as

$$\text{skew} = \frac{\int_{-1/2}^{1/2} U(Y)Y^3 dY}{\int_{-1/2}^{1/2} U(Y)dY} \tag{57}$$

For viscosity-stratified flows with Reynolds number less than 100, the flow can be modeled by the dimensionless equation

$$\frac{\mu}{\mu_o}\frac{\partial^4\Psi}{\partial Y^4} + \left(\frac{\ell}{\mu_o}\frac{\partial\mu}{\partial y}\right)\frac{\partial^3\Psi}{\partial Y^3} + \left(\frac{\ell^2}{\mu_o}\frac{\partial^2\mu}{\partial y^2}\right)\frac{\partial^2\Psi}{\partial Y^2} + \frac{g\ell^4\epsilon\rho_o}{q\mu_o}\frac{\partial\Psi}{\partial X} = 0 \tag{26}$$

where the first term represents viscous forces, the next two represent viscosity stratification and the final term represents buoyancy forces.

For significantly large values of the $\ell/\mu_o \ \partial\mu/\partial y$ parameter, viscosity stratification will occur at some distance from the sink. The distance at which viscosity stratification becomes significant is dependent on the parameter $B = g\ell^4\varepsilon\rho_o/q\mu_o$. That is, buoyancy forces may mask the viscosity stratification near the sink.

In viscosity-stratified flow there exists a region in which viscous forces dominate at lower elevations in the fluid while buoyancy forces dominate in the top layers. This type of flow is referred to as having "incipient skewness."

The velocity profiles in a two-dimensional duct approach the profiles for one-dimensional flow as the distance from the sink increases. Skewness can develop in a flow even with a fixed back wall.

The above conclusions were made using results from both the mathematical model and the experimental model.

With the appropriate boundary conditions, the model for viscosity-stratified flow can be used to predict velocity profiles for flow over weirs, when the conditions assumed in developing the model exist.

Velocity profiles in a Bingham plastic with varying yield stress can be dramatically affected by this variation in yield stress. A mathematical model for this type of flow may be used to predict motion of cohesive sediments. Algebraic equations were developed relating yield stress gradient to the depth of the flowing zone.

REFERENCES

American Society for Testing and Materials, 1971a, "ASTM Hydrometers," Designation: E 100-66, Annual Book of ASTM Standards, Part 30, ASTM, Philadelphia, Pa.

_____, 1971b, "Specific Gravity of Industrial Water and Industrial Wastewater," Designation: 1429-60, Annual Book of ASTM Standards, Part 23, ASTM, Philadelphia, Pa.

Armi, L., 1975, The internal hydraulics of two flowing layers of different densities, 1975, IAHR 16th Congress, Sao Paulo, 8-C-1.

Bird, R. B., Stewart, W. E., and Lightfoot, E. N., 1960, Transport Phenomena, John Wiley & Sons, Inc., New York.

Bohan, J. P., and Grace, J. L., 1973, Selective Withdrawal from Man-Made Lakes, Technical Report H-73-4, U. S. Army Engineer Waterways Experiment Station, CE, Vicksburg, Miss.

Brooks, N. H., and Koh, R. C. Y., 1968, Selective withdrawal from density-stratified reservoirs, Current Research into the Effects of Reservoirs on Water Quality, Vanderbilt University, Nashville, Tenn.

Carnahan, B., Luther, H. A., and Wilkes, J. O., 1969, Applied Numerical Methods, John Wiley & Sons, Inc., New York.

Clark, G. R., 1974, Selective Withdrawal from an Intermediate Depth from a Density Stratified Impoundment, Master's Thesis, University of Wisconsin, Madison, Wisc.

Clements, M. S., 1966, Velocity variations in rectangular settling tanks, Proc. ASCE 6923, 171-200.

Craya, A., 1949, Theoretical research on the flow of superposed layers of fluids of different densities, La Houille Blanche, 4-1, 44-55.

Debler, W. R., 1959, Stratified Flow into a Line Sink, J. ASCE Eng. Mech, 85, EM3, 51-65.

Fandry, C. B., 1974, Unsteady, two-dimensional sink flow in a stratified fluid, Fifth Australian Conference on Hydraulics and Fluid Mechanics, Christchurch, New Zealand, 436-443.

Fontane, D. G., Bohan, J. P., and Grace, J. L., 1973, Mathematical Simulation of the Turbidity Structure Within an Impoundment, Research Report H-73-2, U. S. Army Engineer Waterways Experiment Station, CE, Vicksburg, Miss.

Frisch, H. L., and Simha, R., 1956, The viscosity of colloidal suspensions and macromolecular solutions, Rheology, 1, 525-613.

Gariel, P., 1949, Experimental research on the flow of superposed layers of fluids with different densities, La Houille Blanche, 4, 56-64.

Gelhar, L. W., and Mascolo, D. M., 1966, Non-Diffusive Characteristics of Slow Viscous Stratified Flow Towards a Line Sink, MIT Hydrodynamics Laboratory Report No. 88, Cambridge, Mass.

Grace, J. L., 1971, Selective Withdrawal Characteristics of Weirs, Technical Report H-71-4, U. S. Army Engineer Waterways Experiment Station, CE, Vicksburg, Miss.

Harleman, D. R. F., 1961, Stratified Flow, Handbook of Fluid Dynamics, 26-1, Addison-Wesley, Reading, Mass.

Harleman, D. R. F., Gooch, R. G., and Ippen, A. T., 1958, Submerged sluice control of stratified flow, J. ASCE Hyd. Div., 84, HY2, 1584-1.

Harleman, D. R. F., Morgan, R. L., and Purple, R. A., 1959, Selective withdrawal from a vertically stratified fluid, IAHR 8th Congress, Montreal, 10-C-1.

Ho, J. C., 1973, Planar and Axisymmetric Bottom Withdrawal from a Density Stratified Reservoir, Ph.D. Thesis, University of Wisconsin, Madison, Wisc.

Huber, D. G., 1960, Irrotational motion of two fluid strata towards a line sink, J. ASCE Eng. Mech, 86, EM4, 71-86.

Imberger, J., 1970, Selective Withdrawal from a Stratified Reservoir, Ph.D. Dissertation, University of California-Berkeley, Berkeley, Calif.

Imberger, J., and Fandry, C., 1975, Withdrawal of stratified fluid from a vertical duct, J. Fluid Mech, 70, 321-332.

Imberger, J., and Fischer, H. B., 1970, Selective Withdrawal from a Stratified Reservoir, EPA 15040 EJZ, Washington, D. C.

Imberger, J., Thompson, R., and Fandry, C., 1976, Selective withdrawal from a finite rectangular tank, J. Fluid Mech, 78, 489-512.

Ingersoll, A. C., McKee, J. E., and Brooks, N. H., 1956, Fundamental concepts of rectangular settling tanks, ASCE Transactions, Paper 2837, 121, 1189.

Janowitz, G. S., 1973, Unbounded stratified flow over a vertical barrier, J. Fluid Mech, 58, 375-388.

Jeffrey, D. J., and Acrivos, A., 1976, The rheological properties of suspensions of rigid particles, AIChE Journal, 22, 417-432.

Johnson, P. C., 1974, Selective Withdrawal from Reservoirs, ERC-74-1, Bureau of Reclamation, Denver, Colo.

Kao, T. W., 1965, A free streamline solution for stratified flow into a line sink, J. Fluid Mech, 21, 535-543.

Kao, T. W., 1976, Selective withdrawal criteria of stratified fluids, J. ASCE Hyd. Div., 102, HY6, 717-729.

Kao, T. W., Pao, H. P., and Wei, S. N., 1972, Time-dependent behavior of stratified flow in a channel towards a line sink, Int. Sym. on Stratified Flow, IAHR, Novosibirsk, USSR.

Kao, T. W., Pao, H. P., and Wei, S. N., 1974, Dynamics of establishment of selective withdrawal from a line sink--experiment, J. Fluid Mech, 65, 659-710.

Keulegan, G. H., 1949, Interfacial instability and mixing in stratified flows, Journal of Research of National Bureau of Standards, RP2040, 43, 487-500.

King, I. P., Norton, W. R., and Orlob, G. T., 1973, A Finite Element Solution for Two-Dimensional Density Stratified Flow, Water Resources Engineers, Walnut Creek, Calif.

Koh, R. C. Y., 1964, Viscous Stratified Flow Towards a Line Sink, Ph.D. Dissertation, California Institute of Technology, Pasadena, Calif.

_____, 1966a, Viscous stratified flow towards a sink, J. Fluid Mech, 24, 555-575.

_____, 1966b, Unsteady stratified flow into a sink, Journal of Hydraulic Research, 4, 21-35.

Krone, R. B., 1963a., Flume Studies of the Transport of Sediment in Estuarial Shoaling Process, U. of California-Berkeley, Berkeley, Calif.

_____, 1963b, A Study of Rheological Properties of Estuarial Sediments, Technical Bulletin 7, U. S. Army Engineer Waterways Experiment Station, CE, Vicksburg, Miss.

Long, R. R., 1962, Velocity concentrations in stratified fluids, J. ASCE Hyd. Div., 88, HY1, 9-26.

Lust, E., and Wood, I. R., 1974, An Extension to the Theory of Selective Withdrawal, Fifth Australian Conference in Hydraulics.

Martin, H. M., and Schuster, J. C., 1956, Hydraulic Model Study of Stratified Flow over Weir, Bureau of Reclamation, Lab Report, Hyd 425, Denver, Colo.

Metzner, A. B., 1956, Non-Newtonian technology: fluid mechanics, mixing and heat transfer, Advances in Chemical Engineering, 1, 77-153.

Migniot, C., 1968, A study of the physical properties of various very fine sediments on their behavior under hydrodynamics action, La Houille Blanche, 23, 591-620.

Montgomery, R. L., 1978, Methodology for Design of Fine-Grained Dredged Material Containment Areas, Technical Report D-78-56, U. S. Army Engineer Waterways Experiment Station, CE, Vicksburg, Miss.

Orszag, S. A., and Israeli, M., 1974, Numerical simulation of viscous incompressible flows, Annual Review of Fluid Mechanics, 6, 281-318.

Pao, H. P. and Kao, T. W., 1974, Dynamics of establishment of selective withdrawal from a line sink--theory, J. Fluid Mech, 65, 657-688.

Reiner, M., 1960, Deformation, Strain and Flow, Interscience Publ., New York.

Roscoe, R., 1953, Suspensions, pp 1-38 in J. J. Hermans, ed., Flow Properties of Disperse Systems, Amsterdam North-Holland Publishing Co.

Sardon, C., 1953, Dilute suspensions of impenetrable rigid particles, Flow Properties of Disperse Systems, 131-198.

Schlag, A., 1965, Withdrawal of stratified fluid, La Houille Blanche, 20, 21-23.

Taylor, G. I., 1931, Effect of variation of density on the stability of superposed streams of fluids, Proceedings of Royal Society, 132, 499-523.

Tiederman, W. C., and Reischman, J. C., 1973, Feasibility Study of Hydrocyclone Systems for Dredge Operations, Contract Report D-73-1, U. S. Army Engineer Waterways Experiment Station, CE, Vicksburg, Miss.

Trustrum, K., 1964, Rotating and stratified fluid flow, J. Fluid Mech, 19, 415-432.

Turner, J. S., 1973, Buoyancy Effects in Fluids, Cambridge Univ. Press, Cambridge, Eng.

Van Wazer, J. R., Lyons, J. W., Kim, K. Y., and Colwell, R. E., 1963, Viscosity and Flow Measurement, Interscience Publ., New York.

Walesh, S. G., and Monkmeyer, P. L., 1973, Bottom withdrawal of viscous stratified fluid, J. ASCE Hyd. Div., 99, HY9, 1401-1419.

Walski, T. M., and Schroeder, P. R., 1978, Design of Weirs to Maintain Effluent Quality from Dredged Material Containment Areas, Technical Report D-78-18, U. S. Army Engineer Waterways Experiment Station, CE, Vicksburg, Miss.

Weast, R. C. (Ed.), 1968, Handbook of Chemistry and Physics, The Chemical Rubber Co., Cleveland, Ohio.

Wood, I. R., 1968, Selective withdrawal of stability stratified fluid, J. Fluid Mech, 32, 209-223.

Wood, I. R., and Lai, K. K., 1972a, Flow of layered fluid over broad-crested weir, J. ASCE, Hyd. Div., 98, HY1, 87-104.

_____, 1972b, Selective withdrawal from a two-layered fluid, Journal of Hydraulic Research, 10, 475-496.

Yih, C. S., 1958, On the flow of a stratified fluid, Third U. S. National Congress of Applied Mechanics, 857-861.

_____, 1961, Flow of a non-homogeneous fluid in a porous media, J. Fluid Mech, 10, 133-140.

_____, 1965, Dynamics of Nonhomogeneous Fluids, Macmillan, New York.

_____, 1967, Stratified flow, Annual Review of Fluid Mechanics, 1, 73-110.

_____, 1970, Studies of Stratified Flows, Rotating Fluids and Fluid-Mechanics Problems Related to Geophysical Phenomena, Army Research Office, Durham, N. C.

APPENDIX A

PROGRAMS FOR NUMERICAL SOLUTIONS

PROGRAMS FOR NUMERICAL SOLUTIONS

The equations presented earlier in the text were solved using a series of computer programs each with a different combination of boundary conditions, viscosity gradients and simplifying assumptions. The programs all had the same overall layout shown in the flowchart in Figures 69 and 70.

The program first reads the data for the run, echoes the data, and calculates initial and boundary conditions and other constants for the solution. It then prompts the user with a question mark. The user then selects whether to advance the solution through N iterations; output stream function, dimensionless velocity profile, scaled velocity profile, or skewness at any combination of cross section; output the coordinates of the stream function; or stop the program.

A list of the programs developed and their features is given below.

DUCT - constant density; linear upstream velocity profile and viscosity gradient; inertia terms included.

TANKU - constant density; fixed back wall; linear viscosity gradient.

BUOY - variable density included; linear viscosity gradient; slip at boundary.

DRAG - same as BUOY with no slip at boundary.

TRY - same as DRAG with log viscosity gradient.

VISC - same as TRY except $\mu = f(\Psi)$ instead of $f(Y)$.

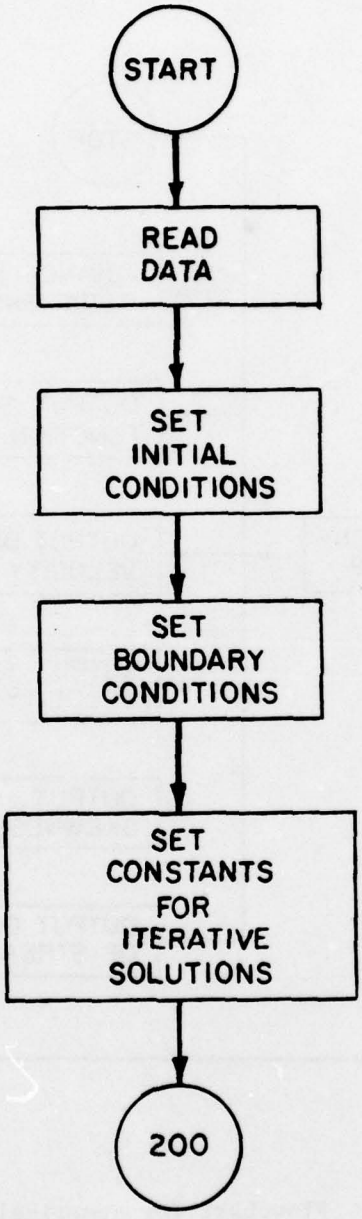

Fig. 69. Flowchart for numerical solutions - 1

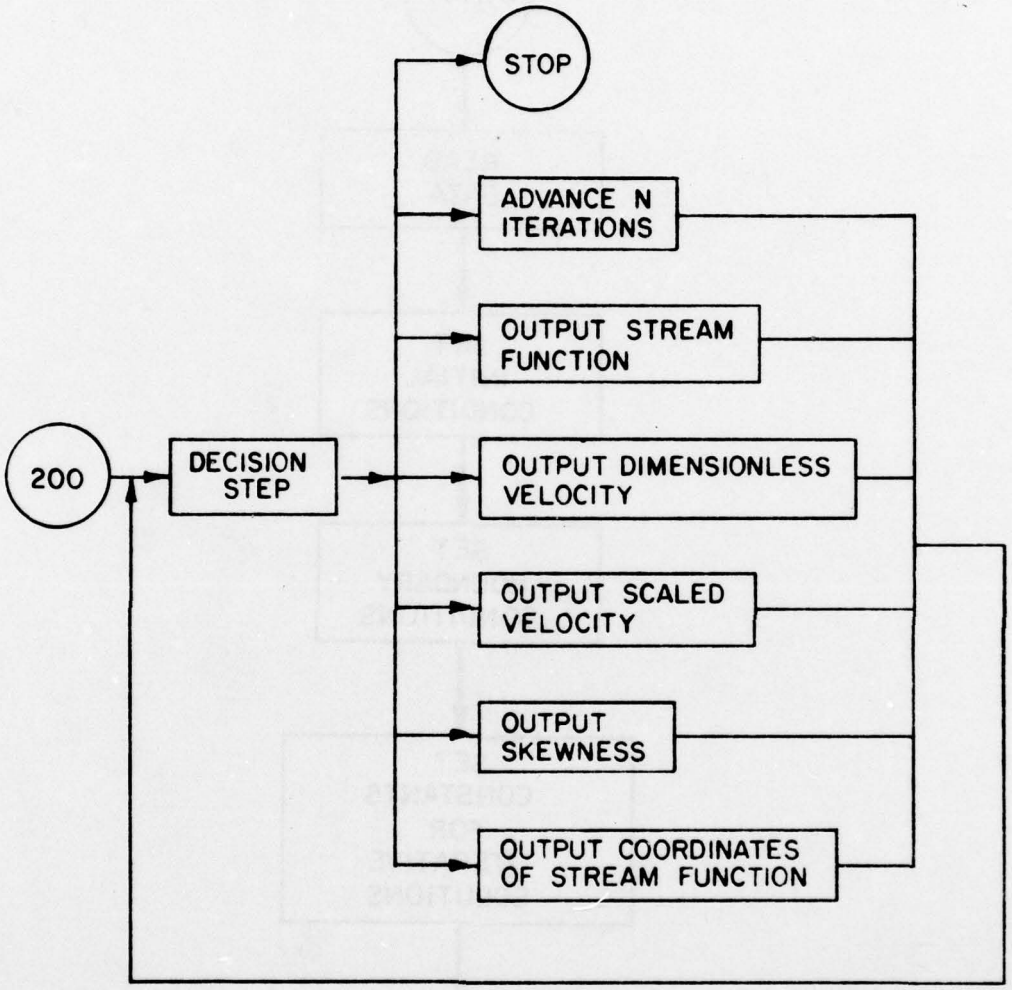

Fig. 70. Flowchart for numerical solutions - 2

There were a number of smaller programs written to solve one-dimensional problems simplifying the evaluation of long expressions. These are too trivial to merit listing in the report.

APPENDIX B: VELOCITY DATA REDUCTION

In determining the location of the dye streak from the photograph, a correction must be made due to the fact that light bends in passing from one medium to another and that there is a finite distance between the dye streak and the back wall of the flume on which the grid is located. In this appendix, a formula for correcting the apparent position of the dye streak is developed.

The apparent location of the dye streak as given on the slide is designated (x_A, y_A) where x and y are horizontal and vertical distances, respectively, from the point perpendicular to the camera (the camera location is fixed for each flume (Figure 71)). The distance from this center point d_A is given by

$$d_A = \sqrt{x_A^2 + y_A^2} \tag{162}$$

Since the thickness of the glass or plexiglass is very small in relation to the thickness of water and air through which the light must pass and the index of refraction of glass and plexiglass is not greatly different from water, the refractance due to the tank walls will be neglected. Furthermore, the sugar and CMC have a negligible effect on the refractance of water compared to the differences between the refractance of air and water.

Consider Figure 72 in which $x_A = 0$ so that $d_A = y_A$. It is desired to find y, the actual location of the dye streak in the center of the tank (w/2 from back wall).

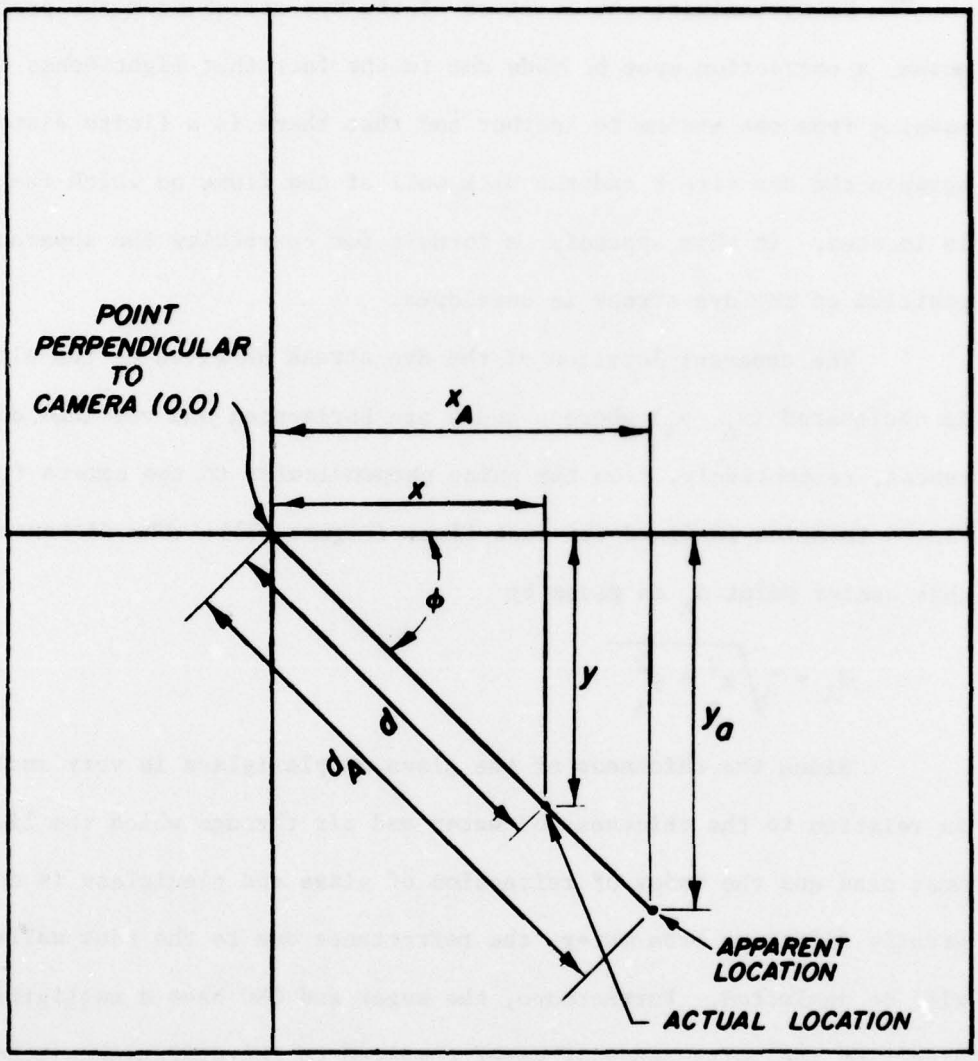

Fig. 71. Definition sketch (x-y plane)

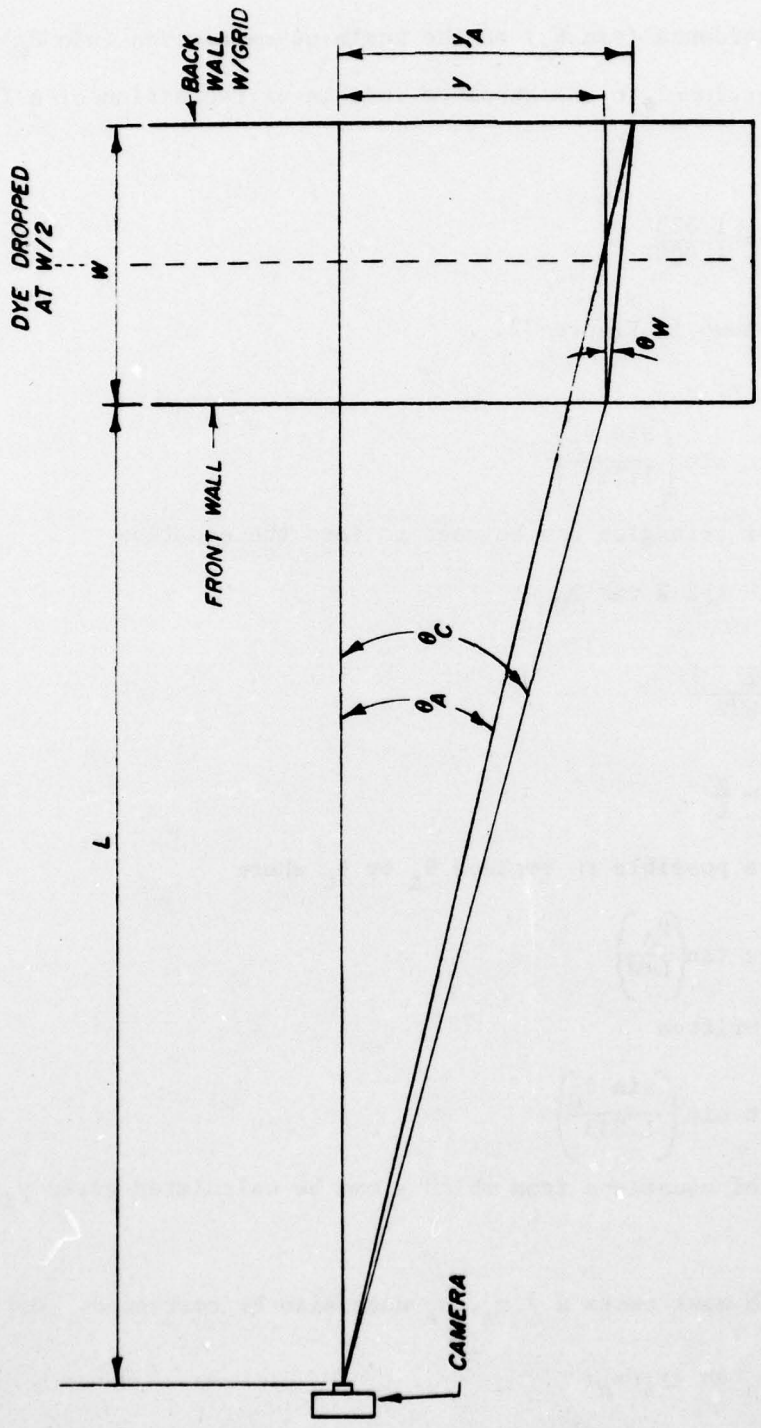

Fig. 72. Definition sketch (y-z plane)

Snell's Law of Refraction states that the ratio of the sine of the angle of incidence ($\sin \theta_A$) to the angle of refraction ($\sin \theta_W$) is inversely proportional to the absolute indices of refraction of A (air) and W (water).

$$\frac{\sin \theta_A}{\sin \theta_W} = \frac{1.333}{1.000} \tag{163}$$

θ_A and θ_W are shown in Figure 72.

θ_W is therefore

$$\theta_W = \text{arc sin}\left(\frac{\sin \theta_A}{1.333}\right) \tag{164}$$

Rules of similar triangles can be used to form the equation

$$y = y_A - 1/2\ W \tan \theta_W \tag{164}$$

$$\text{from } \tan \theta_W = \frac{y_A - y}{W/2} \tag{165}$$

$$\tan \theta_A = \frac{y}{L} \tag{166}$$

When W<<L, it is possible to replace θ_A by θ_C where

$$\theta_C = \text{arc tan}\left(\frac{y_A}{L+W}\right) \tag{167}$$

θ_W can then be written

$$\theta_W = \text{arc sin}\left(\frac{\sin \theta_C}{1.333}\right) \tag{168}$$

given a series of equations from which y can be calculated given y_A, L, and W.

Since in most cases $x \neq x_A$, x_A must also be corrected. Defining

$$\phi = \text{arc tan}\ (y_A/x_A) \tag{169}$$

it is possible to solve the above equations for d knowing d_A instead of

x knowing x_A and to convert the results using

$$x = d \cos \phi \tag{170}$$

$$y = d \sin \phi \tag{171}$$

The working set of equations to obtain (x, y) given (x_A, y_A), L, and W is

$$d = \sqrt{x_A^2 + y_A^2} \tag{162}$$

$$\phi = \text{arc tan } (y_A/x_A) \tag{169}$$

$$\theta_C = \text{arc tan } (d_A/L+W) \tag{167}$$

$$\theta_W = \text{arc sin } (\sin \theta_C/1.333) \tag{168}$$

$$d = d_A - 1/2W \tan \theta_W \tag{165}$$

$$x = d \cos \phi \tag{170}$$

$$y = d \sin \phi \tag{171}$$

Given the location of the velocity profile at any two times, it is a complicated and tedious process to correct from parallax error and then using the correction locations to calculate velocity profiles. It is even more difficult when the profile is made by averaging several profiles each of which must be done separately.

To circumvent these problems, the program VELPRO was prepared. VELPRO consists of a calling program, VELPRO, which reads the data and four subroutines:

1. PARA which performs parallax error corrections for each point input;

2. INTER which interpolates between the points to form corrected dye streaks;

3. PRO which calculates the velocity between each combination of two streaks, and averages these values to obtain an average maximum and minimum velocity at each point;

4. STAT which calculates the skew of the average profile and integrates the profile to obtain the flow rate.

APPENDIX C

PROPERTIES OF MODEL FLUIDS

PROPERTIES OF MODEL FLUIDS

This Appendix contains data on the concentrative properties of the sugar and CMC used in the experimental model. The procedure for determining viscosity, density, refractance, and conductivity are presented, followed by a check on the Newtonian behavior of 7H CMC.

Viscosity Procedure

The viscosity was measured using Brookfield Synchro-Lectric viscometer models LVF and LVT, as pictured in Figure 73. Tests were run using spindle Nos. 1 and 4, and the UL Adaptor.

Spindle 4 was used for high viscosities; spindle 1 was used for intermediate viscosities; and the UL adaptor was used for viscosities less than 10 cp. Spindles 1 and 4 are shown in the rack in the front right in Figure 73, whereas the sleeve for the UL is shown on the viscometer in the figure.

The readings were taken by lowering the viscometer into the sample of known concentration to the designated level. Readings were taken at as many rotational speeds as produced readings away from the ends of the scale, as repeatability could not be achieved at the low end of the scale.

The temperature was measured and the relative viscosity was obtained by dividing the viscosity by the viscosity of water at that temperature. The relative viscosity was plotted vs. concentration.

During the viscosity tests, a sample of National Bureau of

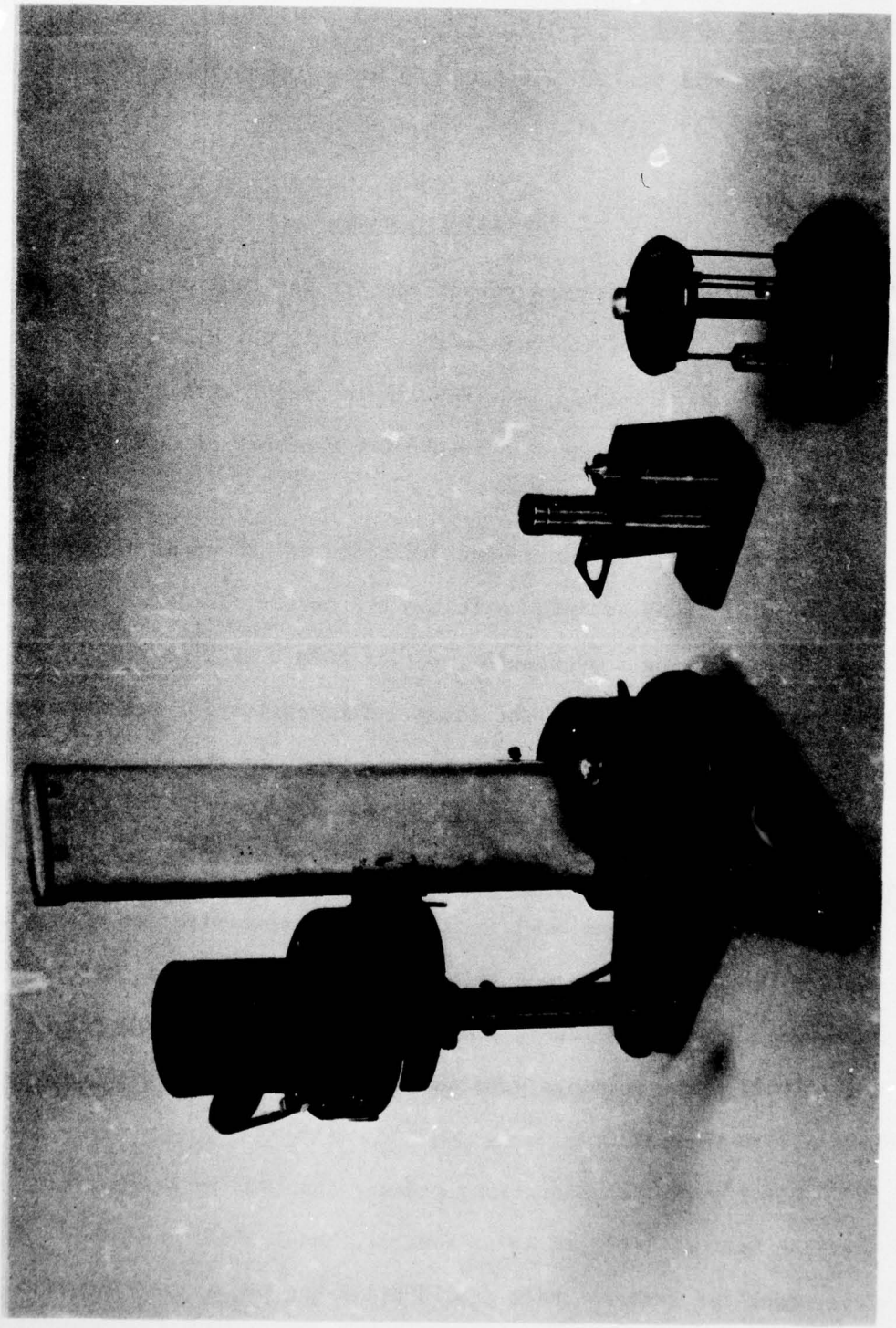

Fig. 73. Brookfield Syncro-Lectric viscometer

AD-A073 371 ARMY ENGINEER WATERWAYS EXPERIMENT STATION VICKSBURG MS F/G 13/2
PROPERTIES OF STEADY, VISCOSITY-STRATIFIED FLOW TO A LINE SINK.(U)
JUL 79 T M WALSKI

UNCLASSIFIED WES-TR-EL-79-6 NL

3 OF 3
AD
A073371

END
DATE
FILMED
9-79
DDC

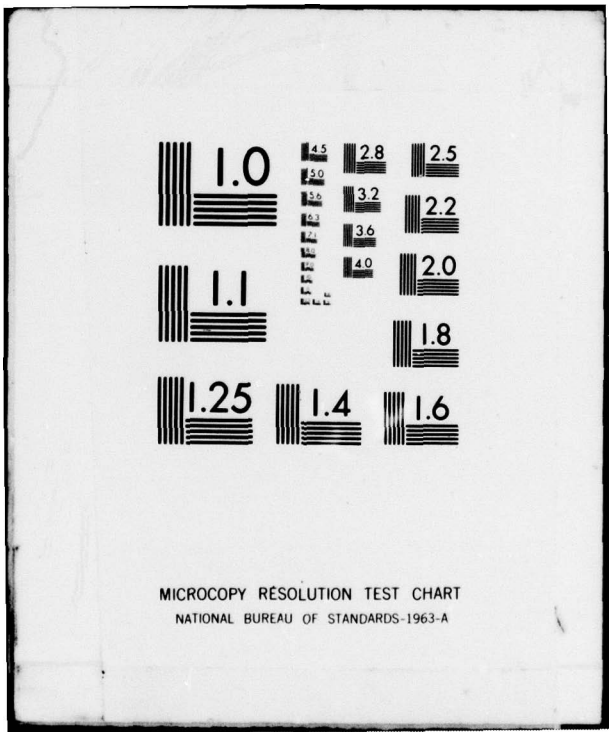
1.0
1.1
1.25
1.4
1.6
1.8
2.0
2.2
2.5
2.8
3.2
3.6
4.0
4.5
5.0
5.6
6.3
7.1
MICROCOPY RESOLUTION TEST CHART
NATIONAL BUREAU OF STANDARDS-1963-A

Standards oil, standard number S20, was tested. Since the volume of the sample (1 pint) was small, it could only be tested using the UL Adaptor. The oil at 26°C was found to have a viscosity of 28.9 cp, which agreed well with the given value of 29.2 cp.

Density Procedure

The specific gravity of all samples was read using an ASTM Hydrometer No. 151H-62 (ASTM E 100-66, 1971a), which corresponds to ANSI standard Z102.1-1967. The results for sugar agreed well with values for sucrose as reported in the CRC Handbook of Chemistry and Physics (Weast 1968).

Because of the small concentrations of CMC used, very poor reproducibility was achieved with the hydrometer for CMC. The tests were repeated using a pycnometer meeting ASTM D 1429-60 (1971b). These results were used in the study. The results for specific gravity were converted to density when the temperature of the samples was known.

Refractance Procedure

Refractance was used to indicate the concentration of sugar in the samples. In low concentrations, the refractance was measured using an American Optical Goldberg Temperature Compensated (T/C) Refractometer, Model 10423. The readings were an index of refraction with full scale from 1.3330 to 1.3730.

For sugar concentrations greater than 30% by weight, an American Optical T/C Hand Refractometer, Model 10431 was used. This instrument was less accurate (±0.25° Brix) but had a range of 0-50

Brix. The refractance readings agreed well with values reported in the CRC Handbook (Weast 1968).

Conductivity

The concentration of CMC solutions could be determined by measuring the conductivity of the solutions using a Yellow Springs Instrument Co. Model 31 Conductivity Bridge. The probe was lowered into the sample, the instrument dial was adjusted to maximize the "shadow" and was then read in μmho/cm.

No temperature correction was done for the conductivity since the meter and flume were used in the same room which was kept at 25°C continuously.

Results

Figures 74, 75, 76, 77, and 78 give relationships between concentration, specific gravity, relative viscosity, and conductivity (at 25°C) or refractance for sugar, 7M, 7H, 7H4, and D-70 CMC. In general, the refractance, specific gravity, and conductivity were linear functions of concentration while the viscosity increased at an increasing rate with concentration.

Non-Newtonian Behavior

An investigation was made of the 7H CMC to check if it exhibited Newtonian behavior in the concentrations used in this study. It was felt that if the CMC was non-Newtonian, it would obey a power law model.

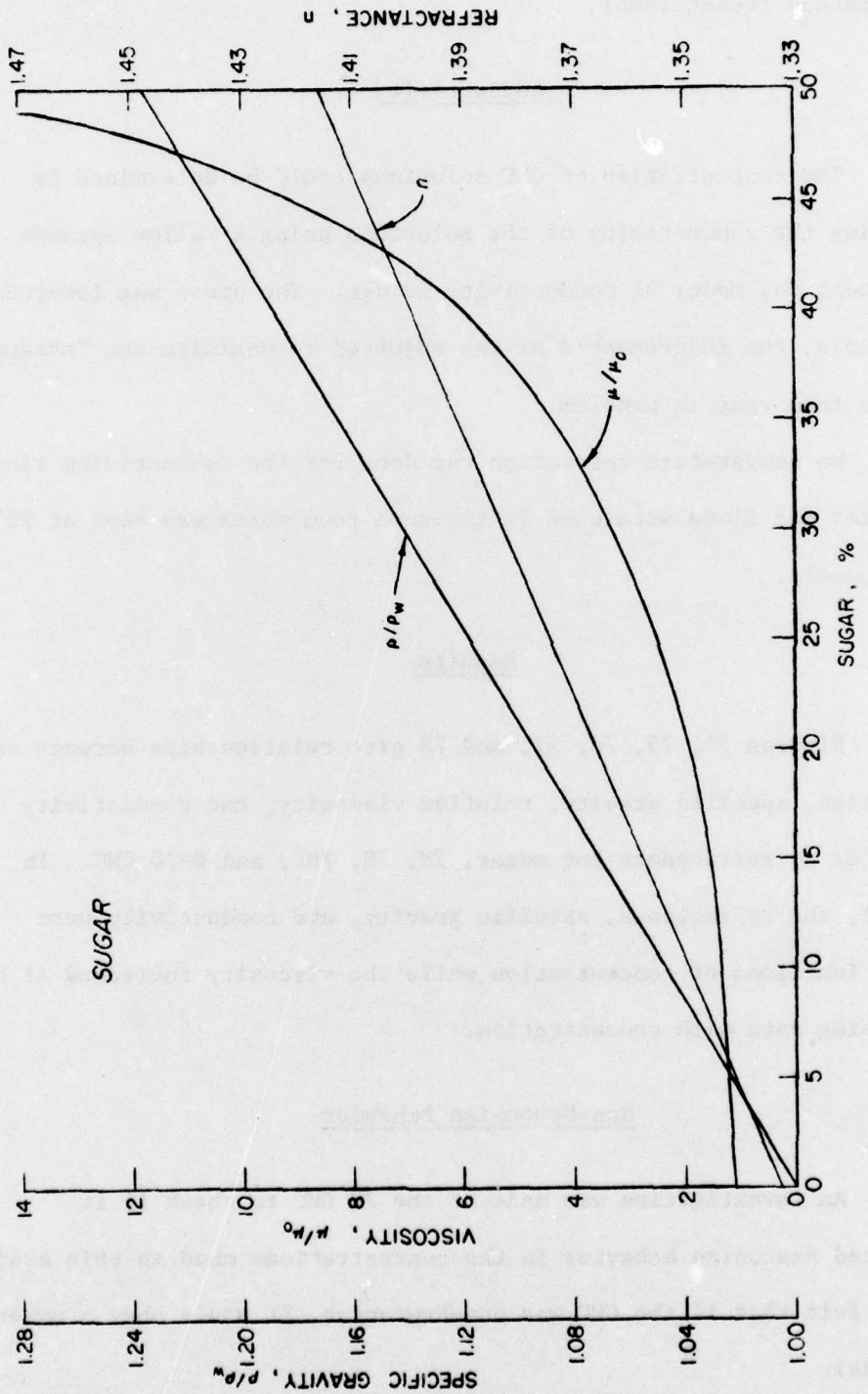

Fig. 74. Properties of sugar

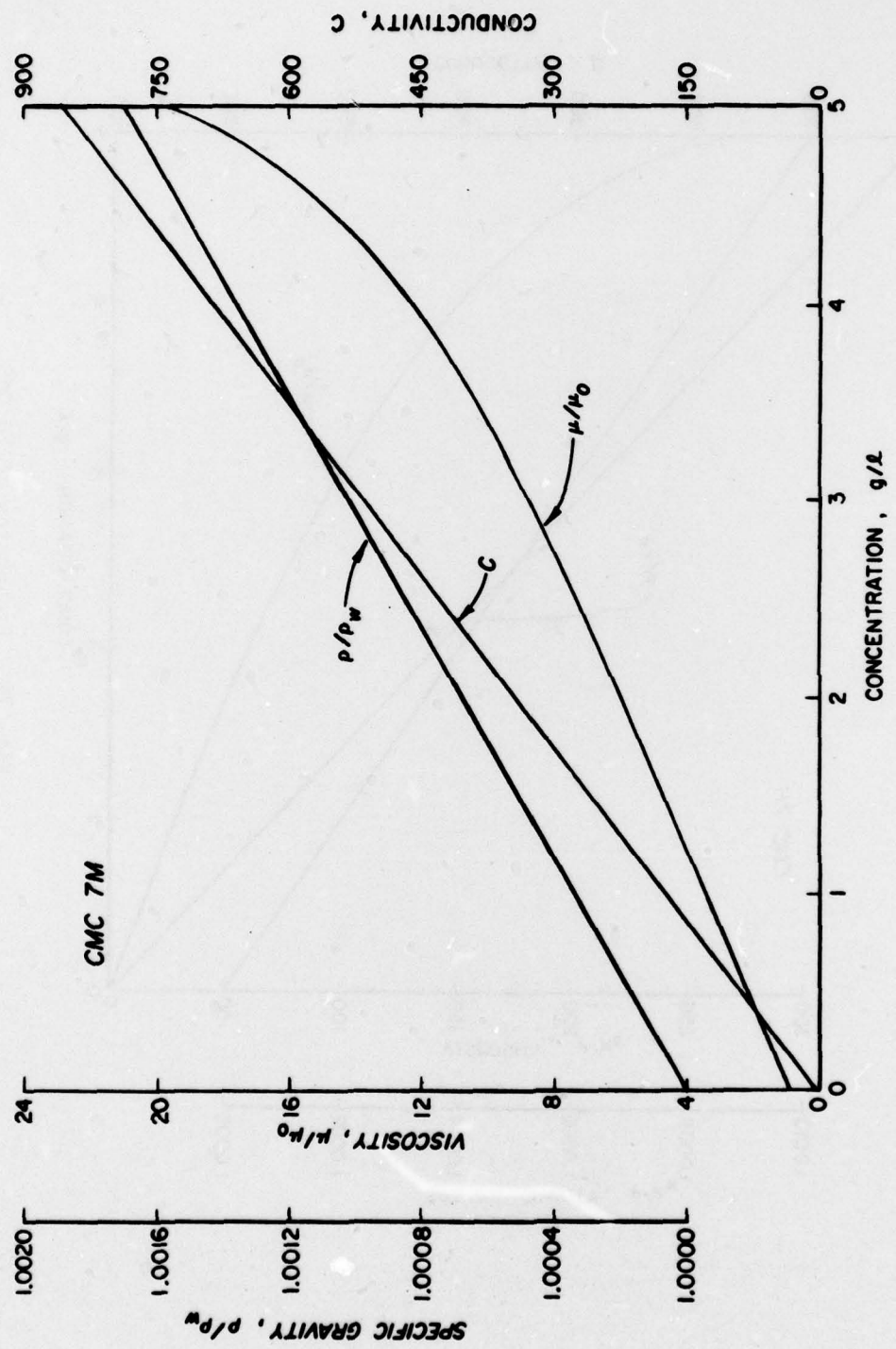

Fig. 75. Properties of 7M CMC

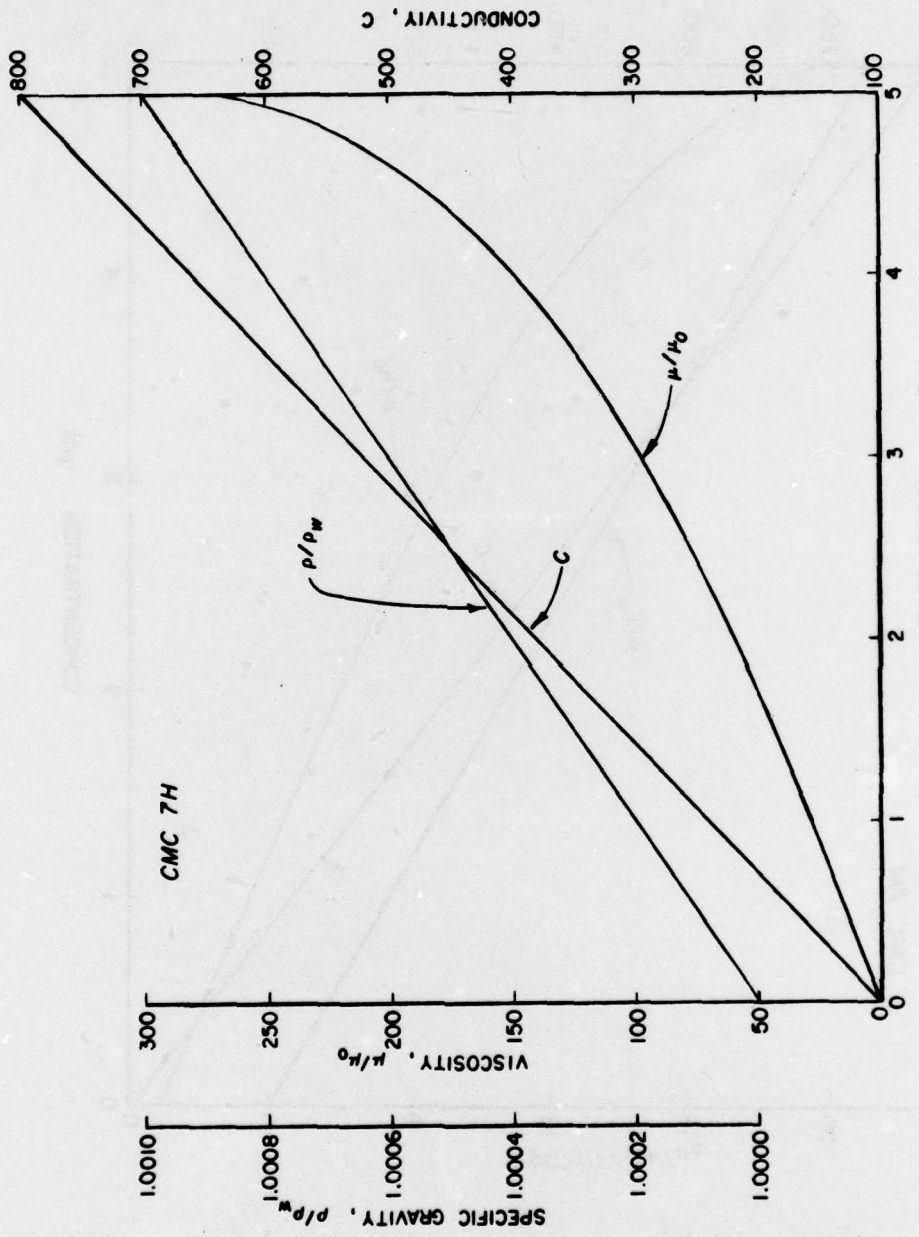

Fig. 76. Properties of 7H CMC

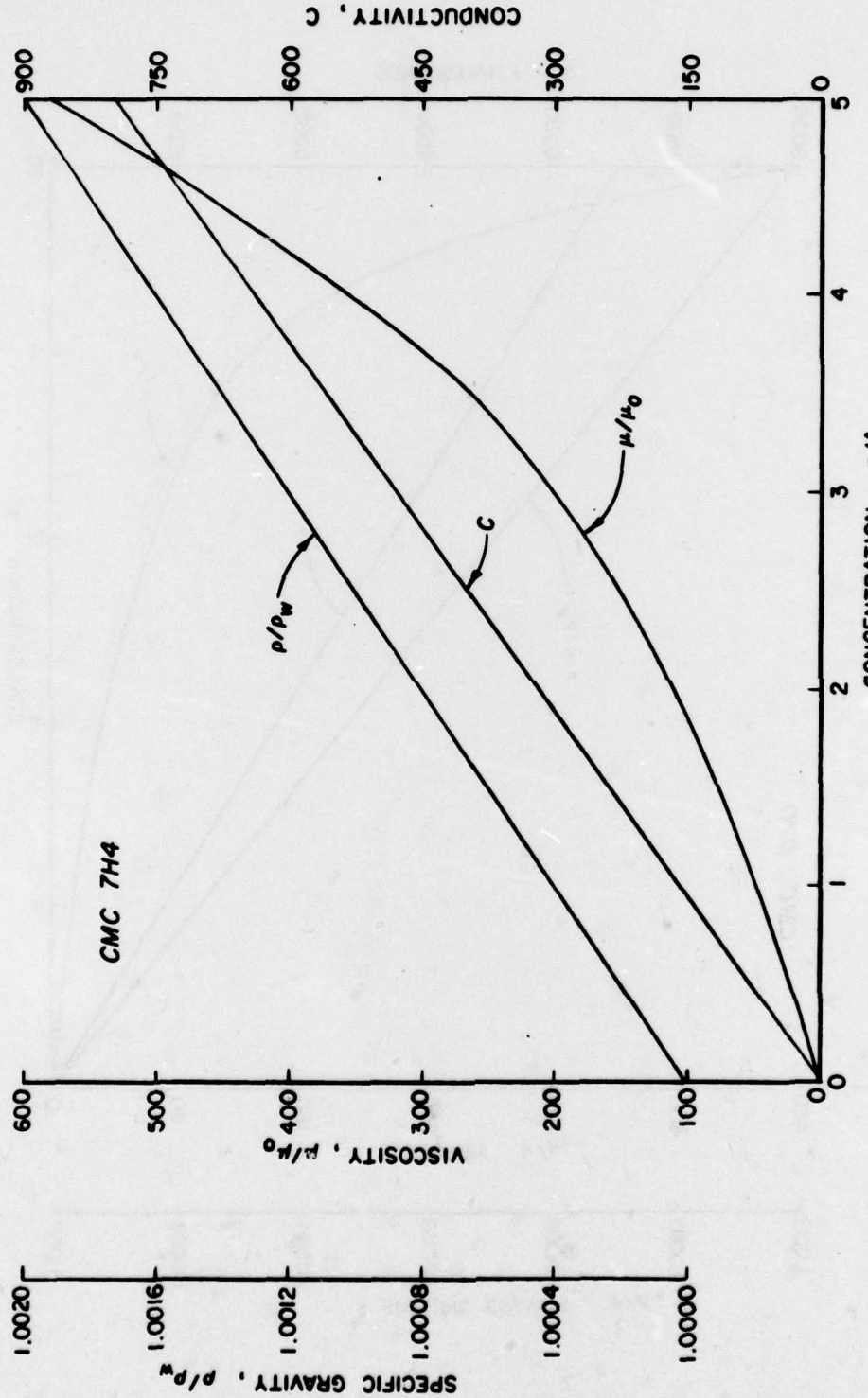

Fig. 77. Properties of 7H4 CMC

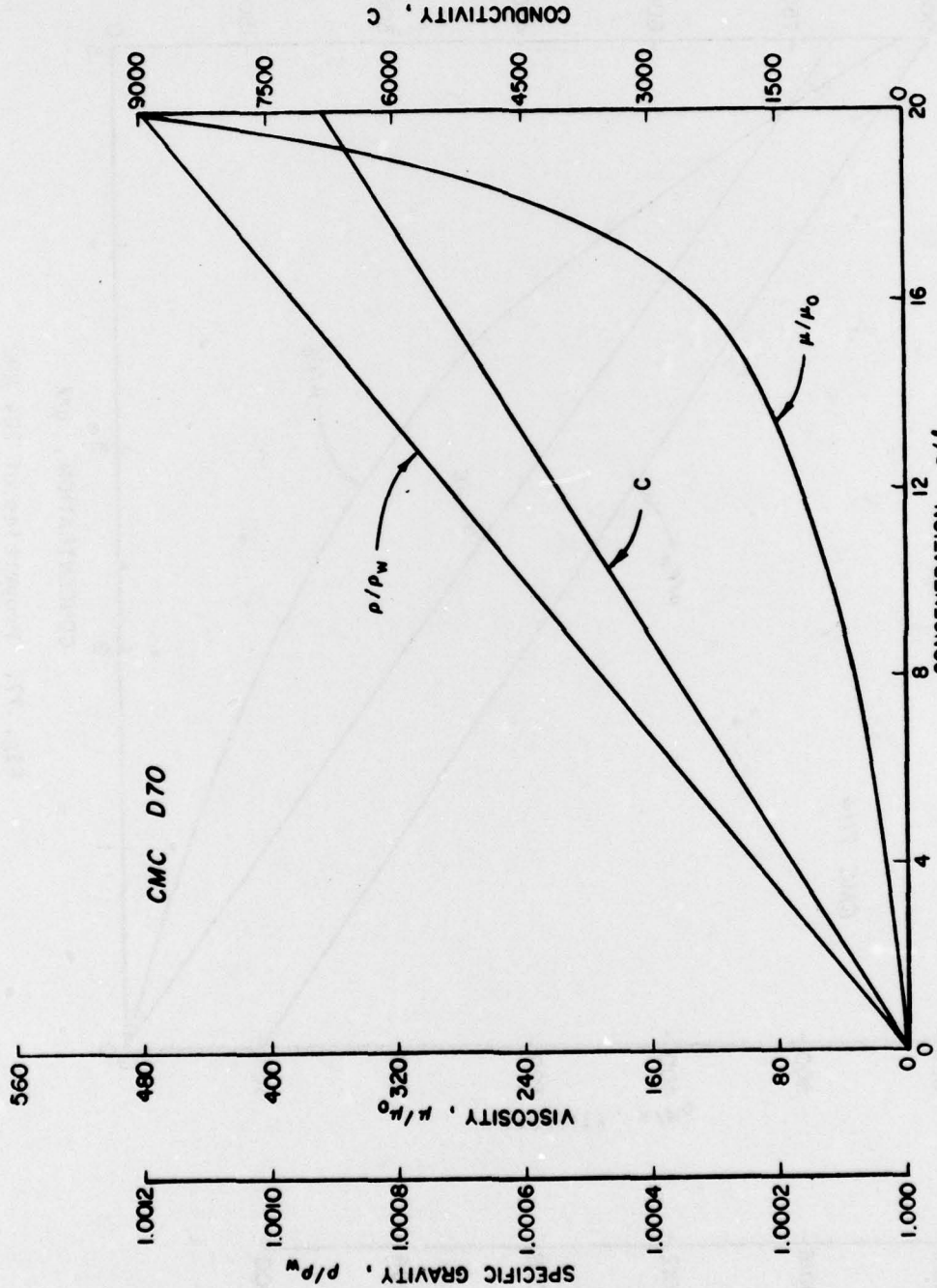

Fig. 78. Properties of D-70 CMC

The rotational speed (Ω) in radians/sec and shear stress at the bob (τ_b) in degrees/cm^2 were measured for an array of rotational speeds, cup sizes and bob sizes. Note that the bob is the part of the viscometer that rotates while the cup is the container holding the fluid. The data were reduced using the following method adopted from Van Wazer et al. (1963).

In a rotational viscometer the power law model can be given as

$$\tau_{r\theta} = m|-du/dr|^n \tag{172}$$

The shear stress $\tau_{r\theta}$ can be related to the torque of the viscometer by

$$\tau_{r\theta} = \frac{T}{2\pi r^2 h} \tag{173}$$

where T is torque, dyne-cm

h is effective length of spindle with end corrections

and shear rate can be given as

$$\frac{du}{dr} = r\,\frac{dw}{dr} \tag{174}$$

where w is angular velocity in radian/sec.

Substituting for du/dr in equation 174, and rearranging gives

$$-dw = \left(\frac{T}{2\pi\ hm}\right)^{1/n} r^{-(1+2n)}\ dr \tag{175}$$

Integrating with $w = 0$ at $r = R_c$ (cup reading) and $w = \Omega$ at R_B (bob radius) gives

$$\Omega = \left(\frac{T}{2\pi\ hm}\right)^{1/n}\left(\frac{n}{2}\right)\left(R_B^{-2/n} - R_c^{-2/n}\right) \tag{176}$$

Taking log of both sides and substituting

$$T = \tau_b 2\pi R_B^2 h \text{ for } T \tag{177}$$

where τ_b is shear at the bob

$$\ln\Omega = 1/n \ln(\tau_b) + \ln \frac{n}{2m} \left[1 - (RB/RC)^{2/n}\right] \quad (178)$$

Plotting $\ln\Omega$ vs. $\ln\tau_b$ allows n to be determined from the slope of the plots. A 5 g/ℓ solution of 7H type CMC was tested for a variety of rotational speeds and bob sizes. The data are shown in Figure 79.

A curve fit program was used to determine the slope and y-intercept for each of the lines. n was found to be 1.01, 1.04 and 1.01. Since these values of n were very close to 1, n will be considered 1 for 7H CMC.

m can be found from the y-intercept (y_o)

$$m = \frac{e^{-y_o}}{2} \left[1 - (R_a/R_c)^2\right] \text{ for } n = 1 \quad (179)$$

Since n = 1, m = μ = actual viscosity μ = 2.69 @28°C
The above value agrees with the values which would be obtained if the fluid were assumed to be Newtonian. When the value n is one, the power law model reduces to Newton's Law of Viscosity. It was concluded that 7H CMC was Newtonian at 5 g/ℓ or lower concentrations for shear stresses less than 625 dynes/cm^2 (full scale on viscometer).

A plot similar to Figure 79 was prepared for 7H4 CMC. It also proved to be Newtonian at 5 g/ℓ.

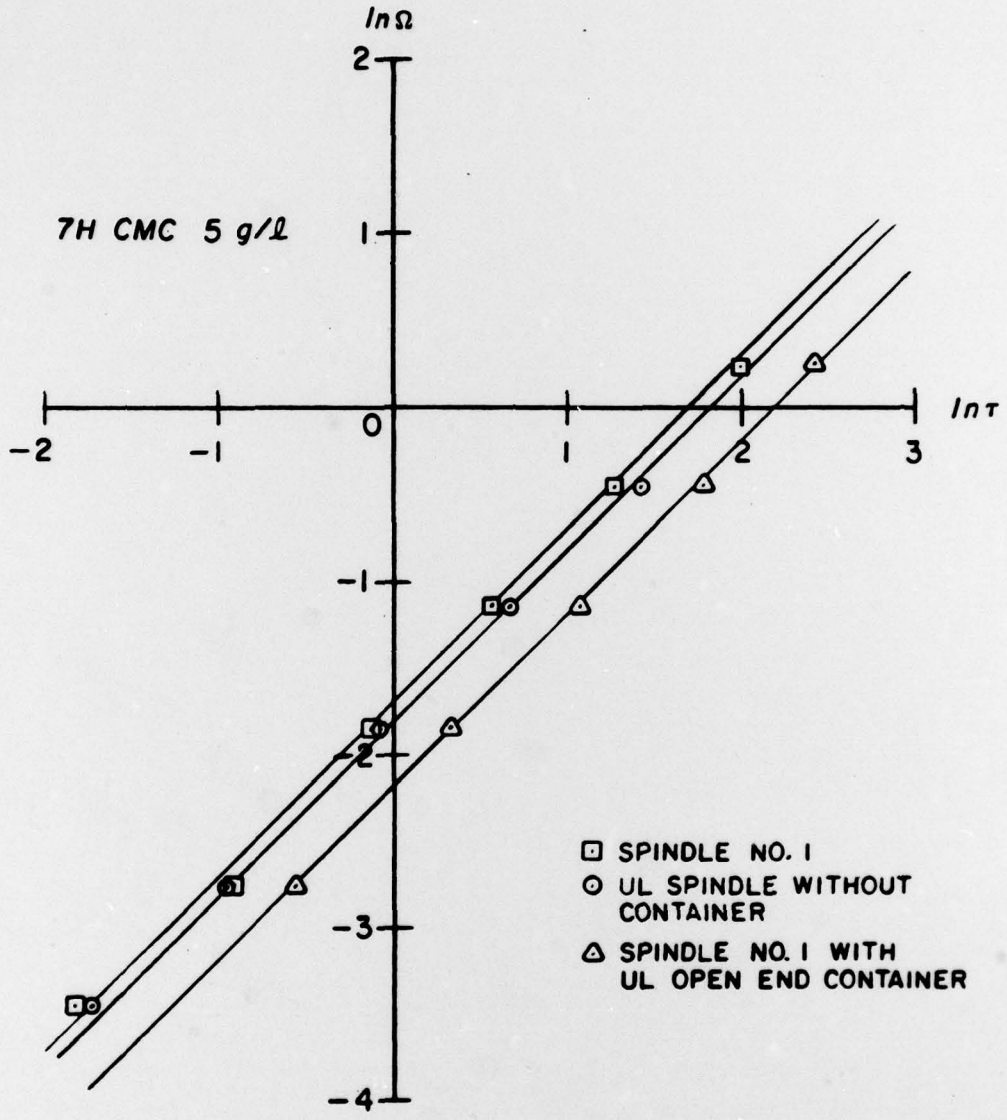

Fig. 79. Power law plot, 7H CMC

APPENDIX D: EFFECT OF SUSPENDED SOLIDS ON VISCOSITY

The viscosity of a suspension increases with an increase in the suspended solids concentration. This increase is a consequence of the perturbing of the flow of the liquid phase around the solid particle. The suspended particles can be viewed as inhibiting the transfer of momentum through the fluid.

Frisch and Simha (1956), Sardon (1953) and Jeffrey and Acrivos (1976) present numerous models to describe the dependence of viscosity on concentration. The models generally treat the liquid phase as a continuum as they are based on the assumption of high values of the Knudsen number (d/λ, where d is the linear dimension of the apparatus and λ is the mean free path).

The models can be divided into three categories based on the assumptions made in their derivation. The first category is "extremely dilute suspensions" in which the suspended particles do not interact with one another; the second is "dilute suspensions" in which there is some hydrodynamic interaction between particles; and the third is "concentrated suspension" in which reactions between particles become of primary importance.

In extremely dilute suspensions, the change in viscosity due to suspended particles is the sum of the changes caused by each particle. The concentration dependence of viscosity is linear in this range and can be given by the "intrinsic viscosity," $[\mu]$ where

$$[\mu] = \frac{1}{\mu_o} \frac{d\mu}{ds} \quad c \to o \tag{180}$$

$[\mu]$ = intrinsic viscosity, cm^3/gr

μ_o = viscosity of fluid phase without suspended particles, dynes-sec/cm^2

s = concentration, gr/cm^3

The models of extremely dilute suspensions can be developed by linearizing the Navier-Stokes equation using Stokes' or Oseen's approximation. Since there is no interaction between particles, the boundary condition on flow at an infinite distance from the particles can be specified. Assuming the particles to be non-interacting spheres, one can arrive at Einstein's solution

$$\mu_{rel} = \frac{\mu}{\mu_o} = 1 + 2.5\phi \tag{181}$$

where ϕ = volume concentration of particles.

The solution is somewhat different if one assumes dumbbell-shaped particles with length, L, and sphere radius, a.

$$\mu_{rel} = 1 + 1.5(L/a)^2\phi \tag{182}$$

A wide variety of relationships have been derived based on the assumptions used in constructing the models.

When the solid concentration becomes larger, the particles begin to exert hydrodynamic forces on one another. The particles will also begin to aggregate. This can be seen by the plotting relative viscosity vs. concentration as done by Roscoe (1953). At some point, the slope begins to increase with concentration. Models to describe the behavior of particles in this range have the form

$$\mu_{rel} = 1 + 2.5\phi + X\phi^2 \tag{183}$$

where

$$X = \begin{cases} 14.1 & \text{Gold} \\ 12.6 & \text{Simha} \\ 7.35 & \text{Vand} \\ 7.17 & \text{Vand} \\ 4.51 & \text{Vand} \\ 3.1 & \text{Vand} \\ 2.5 & \text{de Bruijn} \end{cases}$$

depending on the researcher. Where aggregation becomes important, the concentration dependence of viscosity can be written as

$$\frac{\mu}{\mu_o} = 1 + s\,[\mu]\,(1 + K_1\,[\mu]\,s + K_2\,[\mu]^2\,s^2 + \ldots) \tag{184}$$

where s = weight concentration, g/cm^3.

Researchers have found K_1 to be on the order of 0.33 to 1.25. The last equation can be rearranged in terms of "relative specific viscosity," μ/s

$$\frac{\mu_{sp}}{c} = [\mu]\,(1 + K_1\,[\mu]\,s + K_2\,[\mu]^2\,s^2 + \ldots) \tag{185}$$

where μ_{sp} = specific viscosity = $(\mu-\mu_o)/\mu_o$

Once the suspensions become highly concentrated, rational models can no longer be developed to describe the viscosity because of the complexity of interparticle interactions. The simplest models are of the form

$$\mu_{rel} = 1/(1-\phi)^{5/2} \tag{186}$$

Since suspensions tend to become non-Newtonian in this range, this type of model is of very little value.

Empirical studies by Krone (1963a, 1963b) and Migniot (1968) have shown that naturally occurring suspensions exhibit the behavior of Bingham plastics at high concentrations. At extremely high concentrations, (>500 g/ℓ), they may even become thixotrophic.

Several of the models relating concentrations and viscosity are compared with field data gathered by Migniot (1968), Tiederman and Reischman (1973), and Krone (1963b). These values are shown in Table 6. Mignoit's data are for a variety of sediments in estuaries and rivers. The data of Tiederman and Reischman are for dredged material. Krone's data are for San Francisco Bay sediments. These experimental values are compared with values calculated using models for extremely dilute, dilute, and concentrated suspensions. The models, taken from Frisch and Simha (1956), were

extremely dilute

$$\mu_{sp} = \mu_{rel} - 1 = 1 + 2.5\phi \tag{181}$$

dilute

$$\mu_{sp} = 2.5\phi + 14\phi^2 \tag{187}$$

concentrated

$$\mu_{sp} = \frac{1}{(1-\phi)^{2.5}} - 1 \tag{188}$$

It was assumed that the specific gravity of the particles was 2.67.

The theoretical models consistently predict extremely low specific viscosities. The models generally ignore electrical attraction and assume regular shape particles which is generally not the case in naturally occurring sediments. The low values reported by Migniot were

TABLE 6

THEORETICAL vs. EXPERIMENTAL SPECIFIC VISCOSITIES

$(\mu-\mu_o)/\mu_o$

Weight Concentration (g/ℓ)	Volume Concentration (cm^3/cm^3)	Specific Viscosity					
		Theoretical Models			Experimental Data		
		Extremely Dilute	Dilute	Concentrated	Krone	Migniot	Tiederman and Reischman
1	0.000374	0.001	0.001	0.001	---	0.0	---
10	0.00374	0.009	0.009	0.009	0.06	0.0-0.1	---
20	0.00748	0.018	0.019	0.019	0.12	0.0-0.3	---
50	0.0187	0.046	0.051	0.048	0.36	0.0-1.6	0.2-0.4
100	0.0374	0.093	0.112	0.010	0.96	0.1-9	9
200	0.0748	0.186	0.26	0.21	---	0.2-80	2-16

for powdered limestone. There is fairly good agreement between predicted viscosities and Migniot's low values.

As the concentration of the suspension increases, the viscosity becomes non-Newtonian. This will occur at different concentrations for different suspensions. The non-Newtonian model that best fits the suspension is the Bingham plastic model

$$\tau_{yx} = -\mu \frac{du}{dy} + \tau_y \quad , \quad |\tau_{yx}| > \tau_{oyx} \tag{124}$$

$$\frac{du}{dy} = 0 \quad , \quad |\tau_{yx}| < \tau_{oyx} \tag{125}$$

where

τ_{yx} = shear force in x direction in plane perpendicular to y, dyne/cm^2

u = velocity in x direction, cm/sec

μ = viscosity coefficient, dyne-sec/cm^2

τ_{oyx} = yield shear stress, dyne/cm^2

The yield shear stress (which Migniot calls "initial rigidity") is a function of material type and concentration and is an indicator of the plasticity of the suspension. Migniot (1968) gives the yield shear as

$$\tau_o = n\, s^4 \tag{189}$$

where

s = concentration, g/ℓ

n = factor depending on material type

According to this model every suspension has an initial rigidity but many are very low. The relationship is graphed in Figure 80, taken from Migniot (1968). Note that the yield stress is highest for

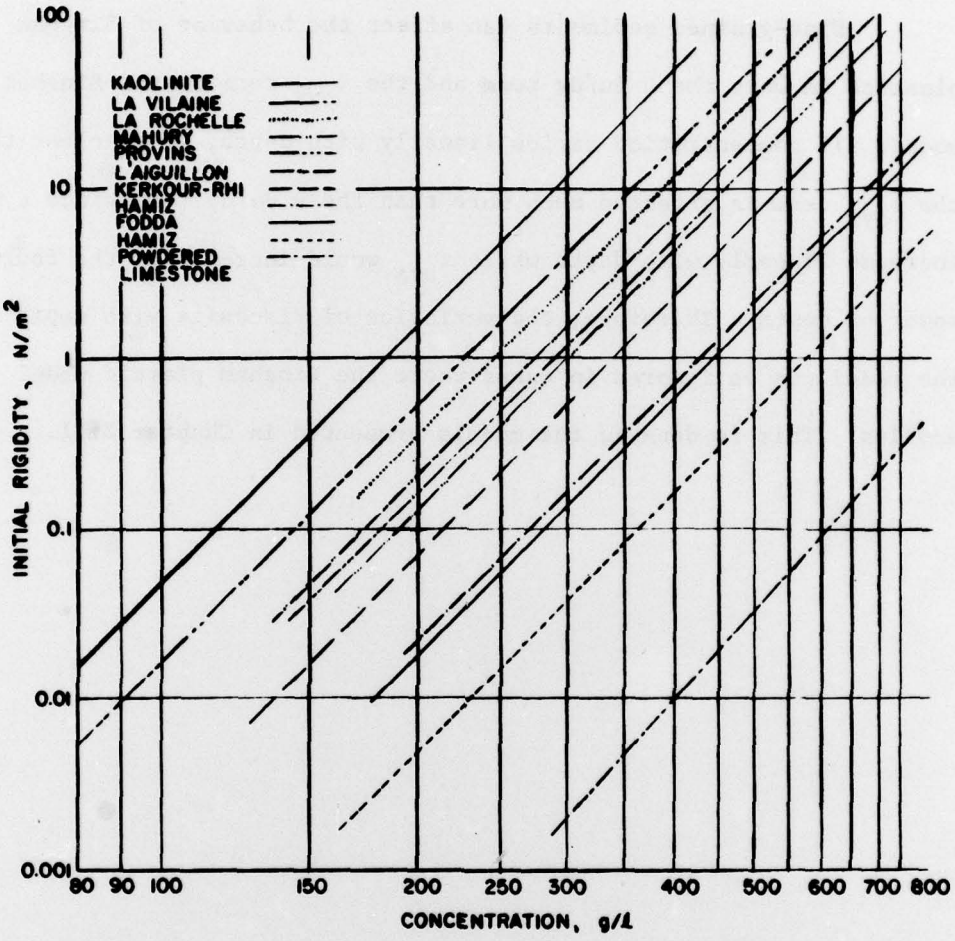

Fig. 80. Yield stress vs. suspended solids concentration

kaolinite and lowest for powdered limestone.

Fine-grained sediments can affect the behavior of Bingham plastics in both the μ du/dy term and the τ_{oyx} term in the Bingham model. If concentration varies linearly with depth, it is clear that the τ_{oyx} term is affected much more than the μ du/dy term since μ would increase linearly with depth while τ_{oyx} would increase as the fourth power of depth. Therefore, the variation of viscosity with depth in the model can be ignored in cases where the Bingham plastic model applies. This is done in the models presented in Chapter XIII.

APPENDIX E: NOTATION

a_1, a_2, a_3 = constants in one-dimensional solution with log viscosity gradient, 0

A = $\frac{2\ell}{\mu_o}\frac{\partial \mu}{\partial y}$, dimensionless linear viscosity gradient, 0

b = regression coefficient for slope

B = $\frac{g\ell^4 \varepsilon\rho_o}{q\,\mu_o}$, dimensionless ratio of buoyancy to viscous forces, 0

c_1 = slope of log viscosity gradient, 1/L

C = $c_1\,\ell$, dimensionless log viscosity gradient, 0

d = actual distance from point to position perpendicular to camera, cm

d_A = apparent value of d, cm

D = diffusion coefficient, L^2/T

f = constant in solution by Gehar and Mascalo, 1/LT

f_j = value of function f in jth interval in skewness calculation

F = $q/\ell^2\sqrt{\varepsilon g}$, densimetric Froude number, 0

g = 980 cm/sec^2, acceleration due to gravity, cm/sec^2

h = length of viscometer bob, cm

i = index on grid cell in x-direction, 0

j = index on grid cell in y-direction, 0

ℓ = characteristic length, cm

L = distance from camera to flume, cm

L = dimensionless depth of forward flowing layer (non-Newtonian), 0

L_a = dimensionless depth to interface, 0

m = number of grid cells in x-direction, 0

m = constant in power law model, M/LT

n = number of grid cells in y-direction, 0

n = exponent in power law model, 0

p = pressure, M/LT^2

P_x = $\partial p/\partial x$, pressure gradient, M/L^2T^2

P or P_x = $p_x \ell^3/q\mu_o$, dimensionless pressure gradient, 0

q = characteristic flow rate, cm^2/sec

q_x = flow at cross-sections x in tank, cm^2/sec

r = radial distance, cm

R = $q\rho_o/\mu_o$, Reynolds number, 0

R_B = radius of viscometer bob, cm

R_c = radius of viscometer cup, cm

s = concentration, M/L^3

s_e = effluent concentration, M/L^3

S = dimensionless concentration, s(Y)/s(1/2), 0

S_e = dimensionless effluent concentration, 0

S_e = standard error of the estimate, 0

S_x = standard deviation, 0

t = time to reach steady-state, sec

T = viscometer torque, dyne-cm

u = velocity in x-direction, cm/sec

U = $u\ell/q$, dimensionless velocity in x-direction, 0

U_j = dimensionless velocity in jth grid cell, 0

U_∞ = dimensionless velocity far from sink, 0

v = velocity in y-direction, cm/sec

V = $v\ell/q$, dimensionless velocity in y-direction, 0

V^* = dimensionless velocity at which tank surface drops, 0

w = angular velocity, radians/sec

W = width of flume, cm

x = horizontal distance, cm

x_A = apparent x location of point, cm

x_{max} = distance to back wall of tank, cm

X = x/ℓ, dimensionless horizontal distance, 0

$\overline{X}$ = x/x_{max}, 0

X = constant in formula for viscosity of suspension, 0

X_{max} = dimensionless distance to back wall of tank, 0

y = vertical distance, cm

y_o = intercept of Ω vs. τ_b plot, 0

Y_A = apparent location of point, cm

Y = y/ℓ, dimensionless vertical distance, 0

Y_o = point about which skew is calculated, 0

Y_j = dimensionless elevation of jth grid cell, 0

δ_s = thickness of withdrawal zone, cm

ε = $1/\rho_o \ d\rho_s/dy$, density gradient, 1/cm

θ_A = angle of incidence from air, radians

θ_c = corrected angle of incidence from air, radians

θ_W = angle of refractance in water, radians

λ = mean free path of molecules, L

μ = viscosity, M/LT

μ_o = characteristic viscosity or viscosity of fluid phase with no suspended particles (Appendix D), M/LT

μ_B = viscosity of bottom layer, M/LT

μ_R = $\Delta\mu/\mu_o$, 0

μ_T = viscosity of top layer, M/LT

μ_{sp} = $(\mu-\mu_o)/\mu_o$, specific viscosity, 0

μ_{rel} = μ/μ_o, relative viscosity, 0

$[\mu]$ = $1/\mu_o \; d\mu/dc$ intrinsic viscosity, cm^3/gr

ρ = density, gr/cm^3

ρ_o = characteristic density, gr/cm^3

ρ_s = density of fluid with no motion, gr/cm^3

τ = $\ell^2\tau_{yx}/q\mu$, dimensionless shear stress, 0

τ_o = $\ell^2\tau_{oyx}/q\mu$, dimensionless yield stress, 0

τ_b = shear stress at viscometer bob, $dyne/cm^2$

τ_{yx} = component of shear stress tensor (also viscous transport of x-momentum in y direction), M/LT^2

τ_{oyx} = yield stress, M/LT^2

ϕ = arc tan (y/x), parallax error correction, radius

ϕ = volume fraction of suspended material (Appendix D), 0

Ψ = dimensionless stream function, 0

Ω = angular velocity of viscometer bob, radians/sec

In accordance with letter from DAEN-RDC, DAEN-ASI dated 22 July 1977, Subject: Facsimile Catalog Cards for Laboratory Technical Publications, a facsimile catalog card in Library of Congress MARC format is reproduced below.

Walski, Thomas M
Properties of steady, viscosity-stratified flow to a line sink / by Thomas M. Walski. Vicksburg, Miss. : U. S. Waterways Experiment Station ; Springfield, Va. : available from National Technical Information Service, 1979.
xi, 202 p. : ill. ; 27 cm. (*Technical report* - U. S. Army Engineer Waterways Experiment Station ; EL-79-6)
Prepared for Assistant Secretary of the Army (R&D) Department of the Army, Washington, D. C., under Project No. 4A161101A91D, Task 02, Work Unit 112.
References: p. 160-164.

1. Bingham plastic. 2. Mathematical models. 3. Rheology. 4. Selective withdrawal. 5. Stratification. 6. Stratified flow. 7. Viscosity. 8. Viscous flow. 9. Weirs. I. United States. Assistant Secretary of the Army (Research and Development). II. Series: United States. Waterways Experiment Station, Vicksburg, Miss. Technical report ; EL-79-6.
TA7.W34 no.EL-79-6